

SHAFT AND BLADE LOAD MEASUREMENTS ON A  
HIGHLY SKEWED PROPELLER MODEL IN ICE

CENTRE FOR NEWFOUNDLAND STUDIES

---

**TOTAL OF 10 PAGES ONLY  
MAY BE XEROXED**

(Without Author's Permission)

CORWYN E.W. MOORES







## **INFORMATION TO USERS**

**This manuscript has been reproduced from the microfilm master. UMI films the text directly from the original or copy submitted. Thus, some thesis and dissertation copies are in typewriter face, while others may be from any type of computer printer.**

**The quality of this reproduction is dependent upon the quality of the copy submitted. Broken or indistinct print, colored or poor quality illustrations and photographs, print bleedthrough, substandard margins, and improper alignment can adversely affect reproduction.**

**In the unlikely event that the author did not send UMI a complete manuscript and there are missing pages, these will be noted. Also, if unauthorized copyright material had to be removed, a note will indicate the deletion.**

**Oversize materials (e.g., maps, drawings, charts) are reproduced by sectioning the original, beginning at the upper left-hand corner and continuing from left to right in equal sections with small overlaps.**

**Photographs included in the original manuscript have been reproduced xerographically in this copy. Higher quality 6" x 9" black and white photographic prints are available for any photographs or illustrations appearing in this copy for an additional charge. Contact UMI directly to order.**

**ProQuest Information and Learning  
300 North Zeeb Road, Ann Arbor, MI 48106-1346 USA  
800-521-0600**

**UMI<sup>®</sup>**

## **NOTE TO USERS**

**This reproduction is the best copy available.**

**UMI**



**National Library  
of Canada**

**Acquisitions and  
Bibliographic Services**

**385 Wellington Street  
Ottawa ON K1A 0N4  
Canada**

**Bibliothèque nationale  
du Canada**

**Acquisitions et  
services bibliographiques**

**385, rue Wellington  
Ottawa ON K1A 0N4  
Canada**

*Your file* *Votre référence*

*Our file* *Notre référence*

**The author has granted a non-exclusive licence allowing the National Library of Canada to reproduce, loan, distribute or sell copies of this thesis in microform, paper or electronic formats.**

**The author retains ownership of the copyright in this thesis. Neither the thesis nor substantial extracts from it may be printed or otherwise reproduced without the author's permission.**

**L'auteur a accordé une licence non exclusive permettant à la Bibliothèque nationale du Canada de reproduire, prêter, distribuer ou vendre des copies de cette thèse sous la forme de microfiche/film, de reproduction sur papier ou sur format électronique.**

**L'auteur conserve la propriété du droit d'auteur qui protège cette thèse. Ni la thèse ni des extraits substantiels de celle-ci ne doivent être imprimés ou autrement reproduits sans son autorisation.**

**0-612-62405-6**

**Canada**

**Shaft and Blade Load Measurements on a Highly Skewed  
Propeller Model in Ice**

**By**

**©Corwyn E. W. Moores, B. Eng.**

**A Thesis Submitted to the School of Graduate Studies  
as the Written Requirement for the Degree of  
Master of Engineering**

**Faculty of Engineering and Applied Science  
Memorial University of Newfoundland  
May 2001**

**St. John's, Newfoundland, Canada**

## **Abstract**

**Recent work pertaining to shipping traffic in Arctic and Sub Arctic regions has resulted in an increased understanding of the loading experienced by the propulsion systems of vessels equipped with highly skewed propellers. Testing completed on model propellers using conventional shaft load measurements indicates that the loading experienced in ice is substantially greater than that experienced in open water.**

**The research described herein was completed with the intention of determining the loading experienced by an individual highly skewed blade during the ice interaction process. It documents the results of a series of ice milling tests using a highly skewed propeller model. This 4-bladed model was designed to be tested in the ice tank at the National Research Council of Canada's Institute for Marine Dynamics (IMD). In this series of tests, loads experienced by an individual blade, as well as the conventionally measured shaft loads, were recorded. The blade loads were measured using a purpose built, hub-mounted dynamometer to which one propeller blade was mounted. Testing was completed over a range of pitch settings for the controllable pitch blades, including design, reduced and reverse settings. As well, tests at a range of ice cut depths and advance ratios were conducted to observe the effect of each of these on the blade loads.**

**Results from the ice milling tests indicated that during the ice milling event the blade attached to the dynamometer experienced maximum peak loads that were substantially higher than  $\frac{1}{4}$  of the maximum shaft loads. During the tests, the maximum loads in most cases were observed in the design condition. However, relative increases in load due to**

ice when compared to the open water loads were seen to rise as the pitch was reduced from the design case. Ice loading effects on the maximum resultant bending moment at the blade root, a common design criterion, were also observed to be significantly higher than the open water case. Based on these observations it is concluded that the regulations for propeller design based on the loading experienced during design pitch operation in open water, with allowances for ice interaction, should be reconsidered for a more detailed design based on ice loading tests.

In addition to the ice milling tests, a series of compression tests were also performed to determine the effect of temperature and strain rate on the model ice used for the model propeller tests. Results from these tests indicate that EG/AD/S model ice follows a similar stress versus strain rate pattern as fresh and salt water ice. This result lends credence to its use as the modeling medium for propeller ice interaction, where strain rates are higher than in other types of ice-structure interaction phenomena.

## **Acknowledgements**

**Thanks are extended to Dr. Brian Veitch and Dr. Neil Bose for the insight, support, and guidance they provided throughout the entirety of my Master of Engineering program. From the inception of this research project to the completion of this thesis and the papers included herein they have been supportive and invaluable as a source of assistance and information for which I am in their debt.**

**I would also like to acknowledge the financial and in-kind support for the research provided by Lloyd's Register through Mr. John Carlton, Transport Canada, Memorial University of Newfoundland and the Natural Sciences and Engineering Research Council of Canada.**

**Thanks for personal financial support is also extended to Memorial University of Newfoundland, the Natural Sciences and Engineering Research Council of Canada, and the Government of Newfoundland and Labrador.**

**Gratitude is also expressed to everyone at the National Research Council of Canada, Institute for Marine Dynamics, especially Stephen Jones, Austin Bugden, John Bell, Edward Kennedy, and Art Bowker and to Memorial University's Technical Services department for assistance and guidance during the construction of the testing apparatus, completion of the tests, and the analysis of the results.**

**Special thanks are extended to my parents, Nathaniel and Barbara Moores, and my brothers Justin and William for their moral support and encouragement during a time when other pressing concerns were occupying our minds. Finally, last but not least, sincerest thanks are extended to my wife Stephanie O'Brien whose moral and emotional support helped me through not only the completion of my masters' program but also the unexpected family strains which occurred in conjunction.**

# Table of Contents

<b>Abstract</b> .....	<b>ii</b>
<b>Acknowledgements</b> .....	<b>iv</b>
<b>List of Tables</b> .....	<b>ix</b>
<b>List of Figures</b> .....	<b>x</b>
<b>List of Abbreviations and Symbols</b> .....	<b>xix</b>
<b>List of Appendices</b> .....	<b>xxi</b>
<b>Introduction and Overview</b> .....	<b>1</b>
<b>1.1 Objective and Scope</b> .....	<b>1</b>
<b>1.2 Review of Work on Propeller-Ice Interaction</b> .....	<b>3</b>
<b>1.3 Review of Work on High Strain Rate Ice Compression Tests</b> .....	<b>6</b>
<b>Description of Papers</b> .....	<b>7</b>
<b>2.1 Effects of Strain Rate and Temperature on the Uniaxial Compressive Strength of Model Ice, 16<sup>th</sup> International Conference on Port and Ocean Engineering under Arctic Conditions 2001 (POAC '01), Ottawa, Canada</b> .....	<b>7</b>
<b>2.2 Blade Load Measurements on a Model Propeller in Ice, 20<sup>th</sup> Offshore Mechanics and Arctic Engineering Conference 2001 (OMAE '01), Rio de Janeiro, Brazil</b> .....	<b>9</b>
<b>2.3 Multi-Component Blade Load Measurements on a Propeller in Ice, Society of Naval Architects and Marine Engineers, 2001 Annual Meeting Transactions Volume 109, (SNAME '01), Orlando, USA</b> .....	<b>11</b>
<b>2.4 Co-Authorship Statement</b> .....	<b>13</b>
<b>Effects of strain rate and temperature on the uniaxial compressive strength of EG/AD/S CD model ice</b> .....	<b>19</b>
<b>3.1 Abstract</b> .....	<b>20</b>
<b>3.2 Symbols</b> .....	<b>20</b>
<b>3.3 Introduction</b> .....	<b>20</b>
<b>3.4 Apparatus and Method</b> .....	<b>22</b>

<b>3.5 Results and Discussion .....</b>	<b>25</b>
<b>3.6 Summary and Conclusions .....</b>	<b>32</b>
<b>3.7 Acknowledgements .....</b>	<b>33</b>
<b>3.8 References .....</b>	<b>33</b>
<b>Preliminary blade load measurements on a model propeller in ice .....</b>	<b>34</b>
<b>4.1 Abstract .....</b>	<b>35</b>
<b>4.2 Introduction .....</b>	<b>35</b>
<b>4.3 Test Setup .....</b>	<b>37</b>
<b>4.4 Method .....</b>	<b>48</b>
<b>4.5 Results .....</b>	<b>52</b>
<b>4.6 Summary and Conclusions .....</b>	<b>56</b>
<b>4.7 Acknowledgements .....</b>	<b>57</b>
<b>4.8 References .....</b>	<b>58</b>
<b>Multi-component blade load measurements on a propeller in ice .....</b>	<b>59</b>
<b>5.1 Abstract .....</b>	<b>60</b>
<b>5.2 Introduction .....</b>	<b>60</b>
<b>5.3 Method .....</b>	<b>62</b>
<b>5.4 Results .....</b>	<b>76</b>
<b>5.5 Conclusions .....</b>	<b>83</b>
<b>5.6 Acknowledgements .....</b>	<b>84</b>
<b>5.7 References .....</b>	<b>84</b>
<b>5.8 Figures .....</b>	<b>86</b>
<b>Summary .....</b>	<b>95</b>
<b>Appendix I – Propeller Blade Geometry .....</b>	<b>103</b>
<b>Appendix II – EG/AD/S Compression Test Error Analysis .....</b>	<b>105</b>

<b>Appendix III – Propeller-Ice Interaction Test Error Analysis .....</b>	<b>109</b>
<b>Appendix IV - Shaft Thrust and Torque Coefficients versus Advance Coefficient Charts .....</b>	<b>114</b>
<b>Appendix V - Blade Thrust and Torque Coefficients versus Advance Coefficient Charts .....</b>	<b>122</b>
<b>Appendix VI - Blade Bending Moments versus Advance Coefficient Charts .....</b>	<b>130</b>

## List of Tables

Table 3-1 Results of error analysis.....	32
Table 4-1 Test matrix for sheet number 2.....	49
Table 4-2 Test matrix for sheet number 3.....	49
Table 4-3 Test matrix for sheet number 4.....	50
Table 5-1 Test matrix for sheet number 2.....	73
Table 5-2 Test matrix for sheet number 3.....	74
Table 5-3 Test matrix for sheet number 4.....	74
Table 5-4 Maximum and minimum blade load table.....	83
Table II-1 Error Analysis Of EG/AD/S Compression Tests.....	106
Table III-1 Propeller-Ice Interaction Error Analysis.....	110

## List of Figures

Figure 2-1 Extrapolation of EG/AD/S compressive strength.....	8
Figure 3-1 Data traces for load and displacement at three strain rates .....	26
Figure 3-2 Typical stress-strain curve for three strain rates.....	28
Figure 3-3 Plot of peak stress against strain rate for three temperatures. ....	29
Figure 3-4 Peak stress versus strain rate for the low strain rates only. ....	30
Figure 4-1 Definition of blade depth.....	37
Figure 4-2 Test pass diagram; 2nd, 3rd, and 4th ice sheet .....	40
Figure 4-3 Propeller boat layout.....	41
Figure 4-4 Dimensions of blade dynamometer .....	43
Figure 4-5 Directions $x$ , $y$ , and $z$ on the propeller .....	45
Figure 4-6 Assembled model propeller.....	47
Figure 4-7 Average, Min, and Max $K_T$ Ice / OW .....	53
Figure 4-8 Average, Min, and Max $K_Q$ Ice / OW .....	53
Figure 4-9 Thrust coefficient on individual blade.....	55
Figure 4-10 $10 \times$ Torque coefficient on individual blade .....	55
Figure 5-1 Test pass diagram .....	64
Figure 5-2 Propeller boat layout.....	65
Figure 5-3 Dimensions of blade dynamometer .....	67
Figure 5-4 Directions $x$ , $y$ , and $z$ on the propeller .....	69
Figure 5-5 Assembled model propeller .....	71
Figure 5-6 a) $K_T - \Phi = 31.30^\circ - h_i = 34.0$ mm .....	86

Figure 5-6 b) $K_Q - \Phi = 31.30^\circ - h_i = 34.0 \text{ mm}$ .....	86
Figure 5-7 a) $K_T - \Phi = 24.07^\circ - h_i = 34.0 \text{ mm}$ .....	86
Figure 5-7 b) $K_Q - \Phi = 24.07^\circ - h_i = 34.0 \text{ mm}$ .....	86
Figure 5-8 a) $K_T - \Phi = - 20.93^\circ - h_i = 28.0 \text{ mm}$ .....	86
Figure 5-8 b) $K_Q - \Phi = - 20.93^\circ - h_i = 28.0 \text{ mm}$ .....	86
Figure 5-9 a) $K_T - \Phi = 31.30^\circ - \text{Range of } h_i$ .....	87
Figure 5-9 b) $K_Q - \Phi = 31.30^\circ - \text{Range of } h_i$ .....	87
Figure 5-10 a) $K_T - \Phi = 24.07^\circ - \text{Range of } h_i$ .....	87
Figure 5-10 b) $K_Q - \Phi = 24.07^\circ - \text{Range of } h_i$ .....	87
Figure 5-11 a) $K_T - \Phi = - 20.93^\circ - \text{Range of } h_i$ .....	87
Figure 5-11 b) $K_Q - \Phi = - 20.93^\circ - \text{Range of } h_i$ .....	87
Figure 5-12 a) Effect of Ice Strength vs. Cut Depth .....	88
Figure 5-12 b) Effect of Ice Strength vs. Advance Coefficient .....	88
Figure 5-13 a) $X$ - Force on Individual Blade .....	89
Figure 5-13 b) $X$ - Moment on Individual Blade.....	89
Figure 5-14 a) $Y$ - Force on Individual Blade.....	89
Figure 5-14 b) $Y$ - Moment on Individual Blade.....	89
Figure 5-15 a) $Z$ - Force on Individual Blade.....	89
Figure 5-15 b) $Z$ - Moment on Individual Blade.....	89
Figure 5-16 a) $K_{T\text{Blade}} - \Phi = 31.30^\circ - h_i = 34.0 \text{ mm}$ .....	90
Figure 5-16 b) $K_{Q\text{Blade}} - \Phi = 31.30^\circ - h_i = 34.0 \text{ mm}$ .....	90
Figure 5-17 a) $K_{T\text{Blade}} - \Phi = 24.07^\circ - h_i = 34.0 \text{ mm}$ .....	90

Figure 5-17 b) $K_{QBlade}$ - $\Phi = 24.07^\circ$ - $h_i = 34.0$ mm .....	90
Figure 5-18 a) $K_{TBlade}$ - $\Phi = - 20.93^\circ$ - $h_i = 28.0$ mm.....	90
Figure 5-18 b) $K_{QBlade}$ - $\Phi = - 20.93^\circ$ - $h_i = 34.0$ mm.....	90
Figure 5-19 a) $K_{TBlade}$ - $\Phi = 31.30^\circ$ - Range of $h_i$ .....	91
Figure 5-19 b) $K_{QBlade}$ - $\Phi = 31.30^\circ$ - Range of $h_i$ .....	91
Figure 5-20 a) $K_{TBlade}$ - $\Phi = 24.07^\circ$ - Range of $h_i$ .....	91
Figure 5-20 b) $K_{QBlade}$ - $\Phi = 24.07^\circ$ - Range of $h_i$ .....	91
Figure 5-21 a) $K_{TBlade}$ - $\Phi = - 20.93^\circ$ - Range of $h_i$ .....	91
Figure 5-21 b) $K_{QBlade}$ - $\Phi = - 20.93^\circ$ - Range of $h_i$ .....	91
Figure 5-22 a) $K_{TBlade}$ vs. $\Phi$ (17.6 mm Mean Cut) .....	92
Figure 5-22 b) $K_{QBlade}$ vs. $\Phi$ (17.6 mm Mean Cut) .....	92
Figure 5-23 a) $K_{TBlade}$ vs. $\Phi$ (31.0 mm Mean Cut) .....	92
Figure 5-23 b) $K_{QBlade}$ vs. $\Phi$ (31.0 mm Mean Cut) .....	92
Figure 5-24 a) $OOPBM$ - $\Phi = 31.30^\circ$ - $h_i = 34.0$ mm .....	93
Figure 5-24 b) $IPBM$ - $\Phi = 31.30^\circ$ - $h_i = 34.0$ mm .....	93
Figure 5-25 a) $OOPBM$ - $\Phi = 24.07^\circ$ - $h_i = 34.0$ mm .....	93
Figure 5-25 b) $IPBM$ - $\Phi = 24.07^\circ$ - $h_i = 34.0$ mm .....	93
Figure 5-26 a) $OOPBM$ - $\Phi = - 20.93^\circ$ - $h_i = 28.0$ mm .....	93
Figure 5-26 b) $IPBM$ - $\Phi = - 20.93^\circ$ - $h_i = 28.0$ mm.....	93
Figure 5-27 a) $OOPBM$ - $\Phi = 31.30^\circ$ - Range of $h_i$ .....	94
Figure 5-27 b) $IPBM$ - $\Phi = 31.30^\circ$ - Range of $h_i$ .....	94
Figure 5-28 a) $OOPBM$ - $\Phi = 24.07^\circ$ - Range of $h_i$ .....	94

Figure 5-28 b) <i>IPBM</i> - $\Phi = 24.07^\circ$ - Range of $h_i$ .....	94
Figure 5-29 a) <i>OOPBM</i> - $\Phi = - 20.93^\circ$ - Range of $h_i$ .....	94
Figure 5-29 b) <i>IPBM</i> - $\Phi = - 20.93^\circ$ - Range of $h_i$ .....	94
Figure 6-1 Illustration of tip loading.....	98
Figure I-1 Propeller Blade Geometry.....	104
Figure IV-1 a) $K_T$ : $\Phi = 31.30^\circ$ - $h_i = 20.5$ mm.....	115
Figure IV-1 b) $K_Q$ : $\Phi = 31.30^\circ$ - $h_i = 20.5$ mm.....	115
Figure IV-2 a) $K_T$ : $\Phi = 31.30^\circ$ - $h_i = 34.0$ mm.....	115
Figure IV-2 b) $K_Q$ : $\Phi = 31.30^\circ$ - $h_i = 34.0$ mm.....	115
Figure IV-3 a) $K_T$ : $\Phi = 31.30^\circ$ - $h_i = 43.0$ mm.....	115
Figure IV-3 b) $K_Q$ : $\Phi = 31.30^\circ$ - $h_i = 43.0$ mm.....	115
Figure IV-4 a) $K_T$ : $\Phi = 31.30^\circ$ - $h_i = 46.0$ mm.....	116
Figure IV-4 b) $K_Q$ : $\Phi = 31.30^\circ$ - $h_i = 46.0$ mm.....	116
Figure IV-5 a) $K_T$ : $\Phi = 31.30^\circ$ - $h_i = 60.0$ mm.....	116
Figure IV-5 b) $K_Q$ : $\Phi = 31.30^\circ$ - $h_i = 60.0$ mm.....	116
Figure IV-6 a) $K_T$ : $\Phi = 24.07^\circ$ - $h_i = 8.0$ mm.....	116
Figure IV-6 b) $K_Q$ : $\Phi = 24.07^\circ$ - $h_i = 8.0$ mm.....	116
Figure IV-7 a) $K_T$ : $\Phi = 24.07^\circ$ - $h_i = 18.0$ mm.....	117
Figure IV-7 b) $K_Q$ : $\Phi = 24.07^\circ$ - $h_i = 18.0$ mm.....	117
Figure IV-8 a) $K_T$ : $\Phi = 24.07^\circ$ - $h_i = 20.0$ mm.....	117
Figure IV-8 b) $K_Q$ : $\Phi = 24.07^\circ$ - $h_i = 20.0$ mm.....	117
Figure IV-9 a) $K_T$ : $\Phi = 24.07^\circ$ - $h_i = 28.0$ mm.....	117

Figure IV-9 b) $K_Q: \Phi = 24.07^\circ - h_i = 28.0 \text{ mm}$ .....	117
Figure IV-10 a) $K_T: \Phi = 24.07^\circ - h_i = 34.0 \text{ mm}$ .....	118
Figure IV-10 b) $K_Q: \Phi = 24.07^\circ - h_i = 34.0 \text{ mm}$ .....	118
Figure IV-11 a) $K_T: \Phi = 24.07^\circ - h_i = 40.0 \text{ mm}$ .....	118
Figure IV-11 b) $K_Q: \Phi = 24.07^\circ - h_i = 40.0 \text{ mm}$ .....	118
Figure IV-12 a) $K_T: \Phi = 24.07^\circ - h_i = 41.6 \text{ mm}$ .....	118
Figure IV-12 b) $K_Q: \Phi = 24.07^\circ - h_i = 41.6 \text{ mm}$ .....	118
Figure IV-13 a) $K_T: \Phi = 24.07^\circ - h_i = 51.0 \text{ mm}$ .....	119
Figure IV-13 b) $K_Q: \Phi = 24.07^\circ - h_i = 51.0 \text{ mm}$ .....	119
Figure IV-14 a) $K_T: \Phi = 16.03^\circ - h_i = 8.4 \text{ mm}$ .....	119
Figure IV-14 b) $K_Q: \Phi = 16.03^\circ - h_i = 8.4 \text{ mm}$ .....	119
Figure IV-15 a) $K_T: \Phi = 16.03^\circ - h_i = 18.6 \text{ mm}$ .....	119
Figure IV-15 b) $K_Q: \Phi = 16.03^\circ - h_i = 18.6 \text{ mm}$ .....	119
Figure IV-16 a) $K_T: \Phi = 16.03^\circ - h_i = 23.0 \text{ mm}$ .....	120
Figure IV-16 b) $K_Q: \Phi = 16.03^\circ - h_i = 23.0 \text{ mm}$ .....	120
Figure IV-17 a) $K_T: \Phi = -20.97^\circ - h_i = 8.0 \text{ mm}$ .....	120
Figure IV-17 b) $K_Q: \Phi = -20.97^\circ - h_i = 8.0 \text{ mm}$ .....	120
Figure IV-18 a) $K_T: \Phi = -20.97^\circ - h_i = 16.0 \text{ mm}$ .....	120
Figure IV-18 b) $K_Q: \Phi = -20.97^\circ - h_i = 16.0 \text{ mm}$ .....	120
Figure IV-19 a) $K_T: \Phi = -20.97^\circ - h_i = 24.5 \text{ mm}$ .....	121
Figure IV-19 b) $K_Q: \Phi = -20.97^\circ - h_i = 24.5 \text{ mm}$ .....	121
Figure IV-20 a) $K_T: \Phi = -20.97^\circ - h_i = 28.0 \text{ mm}$ .....	121

Figure IV-20 b) $K_Q$ : $\Phi = -20.97^\circ - h_i = 28.0$ mm .....	121
Figure V-1 a) $K_{TBlade}$ : $\Phi = 31.30^\circ - h_i = 20.5$ mm .....	123
Figure V-1 b) $K_{QBlade}$ : $\Phi = 31.30^\circ - h_i = 20.5$ mm.....	123
Figure V-2 a) $K_{TBlade}$ : $\Phi = 31.30^\circ - h_i = 34.0$ mm.....	123
Figure V-2 b) $K_{QBlade}$ : $\Phi = 31.30^\circ - h_i = 34.0$ mm.....	123
Figure V-3 a) $K_{TBlade}$ : $\Phi = 31.30^\circ - h_i = 43.0$ mm .....	123
Figure V-3 b) $K_{QBlade}$ : $\Phi = 31.30^\circ - h_i = 43.0$ mm.....	123
Figure V-4 a) $K_{TBlade}$ : $\Phi = 31.30^\circ - h_i = 46.0$ mm .....	124
Figure V-4 b) $K_{QBlade}$ : $\Phi = 31.30^\circ - h_i = 46.0$ mm.....	124
Figure V-5 a) $K_{TBlade}$ : $\Phi = 31.30^\circ - h_i = 60.0$ mm .....	124
Figure V-5 b) $K_{QBlade}$ : $\Phi = 31.30^\circ - h_i = 60.0$ mm.....	124
Figure V-6 a) $K_{TBlade}$ : $\Phi = 24.07^\circ - h_i = 8.0$ mm .....	124
Figure V-6 b) $K_{QBlade}$ : $\Phi = 24.07^\circ - h_i = 8.0$ mm.....	124
Figure V-7 a) $K_{TBlade}$ : $\Phi = 24.07^\circ - h_i = 18.0$ mm .....	125
Figure V-7 b) $K_{QBlade}$ : $\Phi = 24.07^\circ - h_i = 18.0$ mm.....	125
Figure V-8 a) $K_{TBlade}$ : $\Phi = 24.07^\circ - h_i = 20.0$ mm .....	125
Figure V-8 b) $K_{QBlade}$ : $\Phi = 24.07^\circ - h_i = 20.0$ mm.....	125
Figure V-9 a) $K_{TBlade}$ : $\Phi = 24.07^\circ - h_i = 28.0$ mm .....	125
Figure V-9 b) $K_{QBlade}$ : $\Phi = 24.07^\circ - h_i = 28.0$ mm.....	125
Figure V-10 a) $K_{TBlade}$ : $\Phi = 24.07^\circ - h_i = 34.0$ mm .....	126
Figure V-10 b) $K_{QBlade}$ : $\Phi = 24.07^\circ - h_i = 34.0$ mm.....	126
Figure V-11 a) $K_{TBlade}$ : $\Phi = 24.07^\circ - h_i = 40.0$ mm .....	126

Figure V-11 b) $K_{QBlade}$ : $\Phi = 24.07^\circ - h_i = 40.0$ mm.....	126
Figure V-12 a) $K_{TBlade}$ : $\Phi = 24.07^\circ - h_i = 41.6$ mm .....	126
Figure V-12 b) $K_{QBlade}$ : $\Phi = 24.07^\circ - h_i = 41.6$ mm.....	126
Figure V-13 a) $K_{TBlade}$ : $\Phi = 24.07^\circ - h_i = 51.0$ mm .....	127
Figure V-13 b) $K_{QBlade}$ : $\Phi = 24.07^\circ - h_i = 51.0$ mm.....	127
Figure V-14 a) $K_{TBlade}$ : $\Phi = 16.03^\circ - h_i = 8.4$ mm .....	127
Figure V-14 b) $K_{QBlade}$ : $\Phi = 16.03^\circ - h_i = 8.4$ mm.....	127
Figure V-15 a) $K_{TBlade}$ : $\Phi = 16.03^\circ - h_i = 18.6$ mm .....	127
Figure V-15 b) $K_{QBlade}$ : $\Phi = 16.03^\circ - h_i = 18.6$ mm.....	127
Figure V-16 a) $K_{TBlade}$ : $\Phi = 16.03^\circ - h_i = 23.0$ mm .....	128
Figure V-16 b) $K_{QBlade}$ : $\Phi = 16.03^\circ - h_i = 23.0$ mm.....	128
Figure V-17 a) $K_{TBlade}$ : $\Phi = -20.97^\circ - h_i = 8.0$ mm .....	128
Figure V-17 b) $K_{QBlade}$ : $\Phi = -20.97^\circ - h_i = 8.0$ mm .....	128
Figure V-18 a) $K_{TBlade}$ : $\Phi = -20.97^\circ - h_i = 16.0$ mm .....	128
Figure V-18 b) $K_{QBlade}$ : $\Phi = -20.97^\circ - h_i = 16.0$ mm .....	128
Figure V-19 a) $K_{TBlade}$ : $\Phi = -20.97^\circ - h_i = 24.5$ mm .....	129
Figure V-19 b) $K_{QBlade}$ : $\Phi = -20.97^\circ - h_i = 24.5$ mm .....	129
Figure V-20 a) $K_{TBlade}$ : $\Phi = -20.97^\circ - h_i = 28.0$ mm.....	129
Figure V-20 b) $K_{QBlade}$ : $\Phi = -20.97^\circ - h_i = 28.0$ mm .....	129
Figure VI-1 a) $OOPBM$ : $\Phi = 31.30^\circ - h_i = 20.5$ mm .....	131
Figure VI-1 b) $IPBM$ : $\Phi = 31.30^\circ - h_i = 20.5$ mm.....	131
Figure VI-2 a) $OOPBM$ : $\Phi = 31.30^\circ - h_i = 34.0$ mm .....	131

Figure VI-2 b) <i>IPBM</i> : $\Phi = 31.30^\circ - h_i = 34.0$ mm.....	131
Figure VI-3 a) <i>OOPBM</i> : $\Phi = 31.30^\circ - h_i = 43.0$ mm .....	131
Figure VI-3 b) <i>IPBM</i> : $\Phi = 31.30^\circ - h_i = 43.0$ mm.....	131
Figure VI-4 a) <i>OOPBM</i> : $\Phi = 31.30^\circ - h_i = 46.0$ mm .....	132
Figure VI-4 b) <i>IPBM</i> : $\Phi = 31.30^\circ - h_i = 46.0$ mm.....	132
Figure VI-5 a) <i>OOPBM</i> : $\Phi = 31.30^\circ - h_i = 60.0$ mm.....	132
Figure VI-5 b) <i>IPBM</i> : $\Phi = 31.30^\circ - h_i = 60.0$ mm.....	132
Figure VI-6 a) <i>OOPBM</i> : $\Phi = 24.07^\circ - h_i = 8.0$ mm .....	132
Figure VI-6 b) <i>IPBM</i> : $\Phi = 24.07^\circ - h_i = 8.0$ mm.....	132
Figure VI-7 a) <i>OOPBM</i> : $\Phi = 24.07^\circ - h_i = 18.0$ mm .....	133
Figure VI-7 b) <i>IPBM</i> : $\Phi = 24.07^\circ - h_i = 18.0$ mm.....	133
Figure VI-8 a) <i>OOPBM</i> : $\Phi = 24.07^\circ - h_i = 20.0$ mm .....	133
Figure VI-8 b) <i>IPBM</i> : $\Phi = 24.07^\circ - h_i = 20.0$ mm.....	133
Figure VI-9 a) <i>OOPBM</i> : $\Phi = 24.07^\circ - h_i = 28.0$ mm .....	133
Figure VI-9 b) <i>IPBM</i> : $\Phi = 24.07^\circ - h_i = 28.0$ mm.....	133
Figure VI-10 a) <i>OOPBM</i> : $\Phi = 24.07^\circ - h_i = 34.0$ mm .....	134
Figure VI-10 b) <i>IPBM</i> : $\Phi = 24.07^\circ - h_i = 34.0$ mm.....	134
Figure VI-11 a) <i>OOPBM</i> : $\Phi = 24.07^\circ - h_i = 40.0$ mm .....	134
Figure VI-11 b) <i>IPBM</i> : $\Phi = 24.07^\circ - h_i = 40.0$ mm.....	134
Figure VI-12 a) <i>OOPBM</i> : $\Phi = 24.07^\circ - h_i = 41.6$ mm .....	134
Figure VI-12 b) <i>IPBM</i> : $\Phi = 24.07^\circ - h_i = 41.6$ mm.....	134
Figure VI-13 a) <i>OOPBM</i> : $\Phi = 24.07^\circ - h_i = 51.0$ mm .....	135

Figure VI-13 b) <i>IPBM</i> : $\Phi = 24.07^\circ - h_i = 51.0$ mm.....	135
Figure VI-14 a) <i>OOPBM</i> : $\Phi = 16.03^\circ - h_i = 8.4$ mm .....	135
Figure VI-14 b) <i>IPBM</i> : $\Phi = 16.03^\circ - h_i = 8.4$ mm.....	135
Figure VI-15 a) <i>OOPBM</i> : $\Phi = 16.03^\circ - h_i = 18.6$ mm .....	135
Figure VI-15 b) <i>IPBM</i> : $\Phi = 16.03^\circ - h_i = 18.6$ mm.....	135
Figure VI-16 a) <i>OOPBM</i> : $\Phi = 16.03^\circ - h_i = 23.0$ mm .....	136
Figure VI-16 b) <i>IPBM</i> : $\Phi = 16.03^\circ - h_i = 23.0$ mm.....	136
Figure VI-17 a) <i>OOPBM</i> : $\Phi = -20.97^\circ - h_i = 8.0$ mm .....	136
Figure VI-17 b) <i>IPBM</i> : $\Phi = -20.97^\circ - h_i = 8.0$ mm .....	136
Figure VI-18 a) <i>OOPBM</i> : $\Phi = -20.97^\circ - h_i = 16.0$ mm .....	136
Figure VI-18 b) <i>IPBM</i> : $\Phi = -20.97^\circ - h_i = 16.0$ mm .....	136
Figure VI-19 a) <i>OOPBM</i> : $\Phi = -20.97^\circ - h_i = 24.5$ mm .....	137
Figure VI-19 b) <i>IPBM</i> : $\Phi = -20.97^\circ - h_i = 24.5$ mm .....	137
Figure VI-20 a) <i>OOPBM</i> : $\Phi = -20.97^\circ - h_i = 28.0$ mm .....	137
Figure VI-20 b) <i>IPBM</i> : $\Phi = -20.97^\circ - h_i = 28.0$ mm .....	137

# List of Abbreviations and Symbols

## Titles and Abbreviations

EG/AD/S	Ethylene Glycol, Aliphatic Detergent and Sugar (model ice)
IMD	Institute for Marine Dynamics
POAC	Port and Ocean Engineering Under Arctic Conditions
OMAE	Offshore Mechanics and Arctic Engineering
SNAME	Society of Naval Architects and Marine Engineers
OW	Open Water

## Nomenclature for POAC Paper

$t$	Mean sample thickness	[mm]
$w$	Mean sample width	[mm]
$l$	Length of the sample	[mm]
$v$	Compression speed	[m/s]
$\dot{\epsilon}$	Strain rate	[1/s]
$F$	Peak force	[N]
$\sigma_{\max}$	Peak stress	[kPa]

## Nomenclature for OMAE and SNAME Papers

$h_i$	Depth of cut into Ice	[mm]
$Q$	Propeller Torque	[Nm]
$T$	Propeller Thrust	[N]
$r$	Relative Radius	[m]
$R$	Propeller Radius	[m]
$D$	Propeller Diameter	[m]
$P$	Propeller Pitch	[m]
$\Phi$	Propeller Pitch Angle	[°]
$x$	X-Axis of Blade Dynamometer	[-]

<b><i>y</i></b>	<b>Y-Axis of Blade Dynamometer</b>	<b>[-]</b>
<b><i>z</i></b>	<b>Z-Axis of Blade Dynamometer</b>	<b>[-]</b>
<b><i>n</i></b>	<b>Rotational Speed of Propeller</b>	<b>[1/s]</b>
<b><i>V</i></b>	<b>Carriage Speed</b>	<b>[m/s]</b>
<b><i>J</i></b>	<b>Advance Coefficient</b>	<b>[-]</b>
<b><i>K<sub>T</sub></i></b>	<b>Thrust Coefficient</b>	<b>[-]</b>
<b><i>K<sub>Q</sub></i></b>	<b>Torque Coefficient</b>	<b>[-]</b>
<b><i>K<sub>TBlade</sub></i></b>	<b>Thrust Coefficient Based on Blade Load</b>	<b>[-]</b>
<b><i>K<sub>QBlade</sub></i></b>	<b>Torque Coefficient Based on Blade Load</b>	<b>[-]</b>
<b><i>OOPBM</i></b>	<b>Out of Plane Bending Moment</b>	<b>[Nm]</b>
<b><i>IPBM</i></b>	<b>In Plane Bending Moment</b>	<b>[Nm]</b>

## **List of Appendices**

<b>Appendix I – Propeller Blade Geometry .....</b>	<b>103</b>
<b>Appendix II – EG/AD/S Compression Test Error Analysis .....</b>	<b>105</b>
<b>Appendix III – Propeller-Ice Interaction Test Error Analysis.....</b>	<b>109</b>
<b>Appendix IV – Shaft Thrust and Torque Coefficients versus Advance Coefficient Charts .....</b>	<b>114</b>
<b>Appendix V – Blade Thrust and Torque Coefficients versus Advance Coefficient Charts .....</b>	<b>122</b>
<b>Appendix VI – Blade Bending Moments versus Advance Coefficient Charts .....</b>	<b>130</b>

# **Chapter 1**

## **Introduction and Overview**

### **1.1 Objective and Scope**

Loads due to a propeller contacting ice occur frequently on ships that navigate in Arctic and sub-Arctic regions. Ice can be pushed into the propeller of the ship during ramming, backing or just through normal navigation in ice covered waters. Loads resulting from these contacts can result in damage to the propulsion system and possibly in the failure of the ship to maintain operation.

Currently, propellers for vessels that navigate in ice are designed based on regulations in which an ice torque associated with a vessel's particular ice class is determined. This torque, along with the assumption that the blade behaves as a cantilever, is used to determine the required propeller blade dimensions, including section thickness. Inadequacies in this method can be seen since blade failures still occur. Furthermore, the ice torques on which these designs are based have been calculated based on model and full-scale data of current ice class propellers, the majority of which are of conventional design.

With the increased commercial shipping traffic in Arctic and Sub Arctic regions, all of the regulations pertaining to the design and classification of vessels that navigate in ice have come under review. To better understand the dynamics involved during the propeller-ice interaction, several research projects have been completed, again focusing

mainly on conventional propellers. As such, the design of highly skewed propellers for use in ice navigation has been regarded as a special case to be considered separately. To help address this gap in the current knowledge, an experimental program was devised consisting of tests of three highly skewed model propellers in the IMD ice tank.

The first of these highly skewed model propellers was tested by Searle et al. (1999a) in conjunction with a more conventional R-Class propeller. Shaft loads from these tests were analyzed to determine the effect of ice milling on the propulsion system. Based on the observed results from this set of experiments it was further determined that, in addition to the shaft loads, the loads experienced by an individual blade would be of interest. To measure blade loads, a new dynamometer was designed and built by IMD. The dynamometer is mounted inside the propeller hub and is capable of measuring the loads on a single blade. Using this and other more conventional propeller testing equipment, tests were conducted in the IMD ice tank. The shaft and blade loads on a highly skewed propeller model were measured over a range of pitch settings, depths of cut, and advance coefficients. Propeller blades details are included in Appendix I.

To support the experimental investigation of propeller-ice loads, a second series of experiments was conducted to determine for the first time the compressive strength properties of the EG/AD/S model ice at high strain rates. Comprised of a dilute aqueous solution of (e)thylene (g)lycol, (a)liphatic (d)etergent, and (s)ugar, this model ice is described in detail by Timco (1986). EG/AD/S model ice was collected from a number of ice sheets and tested to failure in a uniaxial compression test over a large range of strain

rates at three different temperatures. The compressive strength properties of the EG/AD/S ice at high strain rates were of interest to assist in scaling the results from the model ice milling tests, since ice failure occurs at high strain rates during milling.

## **1.2 Review of Work on Propeller-Ice Interaction**

Searle (1999) presented an up to date review of work performed in the field of propeller ice interaction in the past ten years, as well as referencing an extensive review by Veitch (1992). The work most relevant to ice milling of highly skewed propellers are those by Veitch (1995), Doucet et al. (1998) and Liu et al. (2000). These all discuss the use of numerical simulations to calculate the combined ice and hydrodynamic loads on a propeller interacting with ice.

Direct testing of model propellers in ice has also been conducted and discussed by a number of groups including Keinonen and Browne (1990), Browne et al. (1991), and Tamura et al. (1997). Walker et al. (1994) and Minchev et al (2001) also have reported on the effect of flow blockage by ice on blade cavitation.

Recent published work on propeller ice interaction include those of Searle et al. (1999a, 1999b), in which the shaft loads as a result of a model propeller interacting with a model ice sheet were recorded, and Doucet et al. (1999) in which the design of a propeller based on open water and ice loading was described and the resulting blade scantlings compared. Using both a conventional propeller model and a highly skewed propeller model Searle et al. (1999a) determined the thrust and torque coefficients for a series of operating

conditions and depths of cut. By comparing the loading patterns experienced by the highly skewed propeller model to a more conventional R-Class propeller, Searle et al. (1999a) concluded that while both propellers behaved similarly, the magnitude of the loading due to ice on the highly skewed propeller was more pronounced. As well the highest loads in the R-class propeller were observed during off design conditions. The propeller was tested in all four operating quadrants, that is, the cases of the propeller rotating both forward and backward combined with the vessel traveling both forward and backward. Based on results from these tests, it was concluded that the highest propeller loading condition did not occur in the first quadrant (propeller rotation positive, ship speed positive), as would normally be used for design, but rather in quadrant 2 where the blade rotation is positive and ship speed negative or in quadrant 3 where rotation is negative and ship speed is positive. The highly skewed propeller was not tested in these off design conditions.

During these tests the highly skewed propeller model was damaged. Subsequent inspection of the full scale propellers (the propeller was a model of the propellers fitted to the *MV Caribou*, one of the Marine Atlantic Gulf of St. Lawrence Ferries) during a dry-docking showed qualitatively similar damage.

In addition to recent model testing, work has been done on the design and development of numerical computer simulations that calculate the loading on a single blade during its contact with an ice feature. Doucet et al. (1998) described the use of a panel method code called PROPELLA that was modified to calculate the ice milling forces, as well as the

hydrodynamic forces encountered due to the water and presence of the ice. These simulations were completed using conventional ice class propeller geometry. It was noted that during the ice contact the blades experienced an out of plane bending moment that bent the blade backward. Spindle torque was also calculated and seen to increase by an order of magnitude from the open water case when the blade contacted the ice feature. Using the same base code PROPELLA, Liu et al. (2000) completed a series of open water and blocked flow simulations for a group of propellers including one highly skewed propeller shape. It was noted in this paper that the relative out of plane bending moment, as compared to the bollard or open water value, experienced by the highly skewed propeller was consistently higher than those of other ice class propellers in identical conditions. For example, when using an ice wall blockage the highly skewed propeller experienced out of plane ratios of approximately 4.1 while the remaining ice class propellers were at most 2.9 and the majority were around 2.0. Again, these ratios are all compared to the open water bollard bending moment. Measured shaft torque was also observed to increase relatively more for the highly skewed propeller when compared to the bollard or open water results with ratios of approximately 1.9 observed in the highly skewed case while the other propellers had ratios of between 0.6 and 1.3.

With the exception of Searle et al. (1999a, 1999b) and Liu et al. (2000) previous ice class propeller research has been concerned almost exclusively with traditional propeller geometry. To supplement the tests conducted by Searle et al. (1999a, 1999b) the results presented in this thesis involve the determination of the shaft and blade loads for a highly skewed propeller model. In addition to the measurement of blade loads, which is an

important novel feature of these tests, the inclusion of a range of pitch settings for the propeller blades also expands on Searle et al. (1999a, 1999b). Three pitch settings in the first quadrant (propeller blades pitched to provide forward thrust and vessel moving forward) and one setting in the fourth quadrant (propeller blades pitched to give negative thrust and ship moving in reverse) were tested. Note that controllable pitch propeller shafts do not actually reverse rotation but rather pitch is changed into the negative angle of attack region to perform reverse functions. Results of the actual loads experienced by an individual blade are intended to assist in the development of design methods for skewed propellers for ice navigation since blade structural design depends on blade loading rather than shaft loading.

### **1.3 Review of Work on High Strain Rate Ice Compression Tests**

The effect of temperature and strain rate on the uni-axial compressive strength of EG/AD/S model ice was also investigated to better understand the results from model tests conducted in model ice. Prior to this work some uni-axial compression tests on ice were conducted at high strain rates (above  $10^{-1} \text{ s}^{-1}$ ). These included tests on polycrystalline ice by Jones (1982), and Meglis (1998) and tests on simulated Baltic Sea ice by Jones (1997). All of these data sets indicated an increase in the compressive strength of the ice at higher strain rates, regardless of the type of ice. While low strain rate compressive strength of model EG/AD/S ice was discussed in Timco (1986), the effect of higher strain rates was not known prior to the completion of this work.

## **Chapter 2**

### **Description of Papers**

#### **2.1 Effects of Strain Rate and Temperature on the Uniaxial Compressive Strength of Model Ice, 16<sup>th</sup> International Conference on Port and Ocean Engineering under Arctic Conditions 2001 (POAC '01), Ottawa, Canada.**

POAC bi-annually holds an international conference where researchers, engineers and scientists meet to discuss research and developments in their fields. Before being presented at the POAC conferences independent researchers in the field first review the papers. Accepted authors are then invited to present their work at the conference and subsequently have it published in the conference proceedings. These are then distributed for reference purposes. At the time of writing the paper included in this thesis has been accepted by this review process and the version included herein will be submitted for printing with only minor modifications, if any.

The paper describes a series of compression tests conducted by varying the temperature and strain rates at which a series of EG/AD/S ice samples were tested. From this data a pattern for the peak stress versus strain rate was developed. An error analysis of these tests is included in Appendix II of this thesis. The testing range for strain rate was  $10^{-8}$  to  $10^1 \text{ s}^{-1}$ , which incorporated strain rates at higher speeds than previously tested for model ice. Using the data recorded from the compression tests of EG/AD/S ice at each temperature, a general pattern was developed relating the failure stress to the strain rate. This pattern was seen to be similar for each of the three temperatures tested. As well, the

pattern appears to be consistent with those recorded by previous researchers for other types of ice. Based on the similarity of this pattern between various ice types and conditions it may be reasonable to extrapolate that the same pattern exists during the conditions present during propeller-ice interaction.

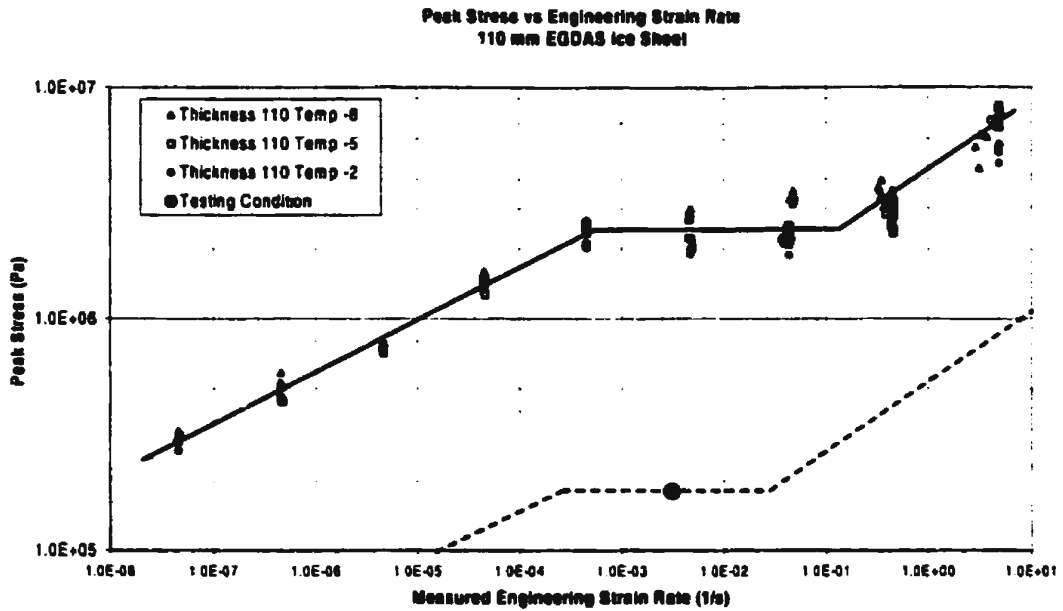


Figure 2-1 Extrapolation of EG/AD/S compressive strength

Making the projection that the peak failure stress follows the same pattern versus strain rate, a value for the failure stress at the high strain rates observed during propeller-ice interactions (approximately  $10^{-1} \text{ s}^{-1}$ ) can be estimated using a compressive strength and strain rates of approximately  $3 \times 10^{-2} \text{ s}^{-1}$  recorded during the test program.

Approximate compressive strengths of 100 to 180 kPa recorded during the propeller-ice interaction tests therefore can be plotted as shown in Figure 2-1. In this plot the solid line shows the pattern recorded during the compression tests of the EG/AD/S ice at various strain rates and temperatures. Plotting a general trend line (dashed line in Figure 2-1) parallel to the compression test line leads to an extrapolated value of compressive strength of approximately  $1 \times 10^6$  Pa (1 MPa) at the  $10^{-1} \text{ s}^{-1}$  strain rate. To verify this assumption compressive tests of the EG/AD/S ice at high strain rates (approximately  $10^1 \text{ s}^{-1}$ ) need to be conducted while the ice is at the ice milling test condition. No attempt to use this extrapolation has been made in the analysis of the blade loads discussed here since no full scale extrapolation has been conducted.

## **2.2 Blade Load Measurements on a Model Propeller in Ice, 20<sup>th</sup> Offshore Mechanics and Arctic Engineering Conference 2001 (OMAE '01), Rio de Janeiro, Brazil.**

A subgroup of the American Society of Mechanical Engineers International, the Ocean, Offshore and Arctic Engineering Division, which organizes the OMAE conferences, is a collection of engineers and scientists who design and develop vessels and structures for marine operations. Divided into a series of symposia based on marine topics, the OMAE Conference is held annually to facilitate the exchange of research and knowledge. Papers submitted to the various symposiums for the OMAE conferences are subject to technical review by two independent experts in the field before being accepted for final presentation and publication in the OMAE conference proceedings. The paper included in

**this thesis has been reviewed and accepted by reviewers and will be the version submitted for printing with minimal editorial changes.**

**Results from a subset of the propeller-ice interaction test program were examined in detail in this paper to demonstrate the validity of the results from the blade dynamometer. This subset was comprised of a series of tests conducted during a single carriage run. This means that the pitch angle, depth of cut and the strength of the ice did not change significantly over the entire data set. Consequently, the ice loads on the propeller shaft and blade can be examined as a function of advance coefficient from 0.2 to 0.6, independently of the ice strength, pitch, and depth of cut. The conditions for this run involved a pitch angle of  $24.07^\circ$ , depth of cut of 45 mm, and an estimated ice strength of approximately 30 kPa in flexure, approximately 90 kPa in compression.**

**The shaft loads were seen to hold relatively constant over the lower advance coefficients (0.2 to 0.4) but then to drop substantially at 0.6. Thrust at this value was seen to drop below the open water value. Torque drops as well, but remains above the open water value at all advance coefficients. As well, the torque loads were observed to show more response to the ice milling event (1 to 2 times greater response) than the thrust loads. Blade load measurements show similar results, with the thrust load on a single blade increasing up to 3 to 4 times the open water value, while torque is seen to be 5 to 6 times higher.**

Loading was observed to be cyclic, as was expected of ice milling. As the advance coefficient increased, the thrust and torque coefficients decreased, due to the changing location and magnitude of the resultant force of the ice milling (Searle et al., 1999a and Mintchev et al., 2001). This indicates that the individual blade during milling experienced a load of the same magnitude as the remainder of the propeller in total, or approximately three times the load experienced during open water operation.

### **2.3 Multi-Component Blade Load Measurements on a Propeller in Ice, Society of Naval Architects and Marine Engineers, 2001 Annual Meeting Transactions Volume 109, (SNAME '01), Orlando, USA**

The main journal of SNAME and a premier journal in the field, the annual meeting transactions are comprised of a collection of papers documenting advancements in a wide range of topics related to marine vessels, systems, safety and testing. Papers intended for the SNAME annual meeting are required to undergo two separate reviews by experts in the topic area. The first of these reviews is conducted to review technical content. If the paper is deemed acceptable the author(s) is/are informed and revisions to the paper suggested. The requested revisions are then completed and the revised paper is again submitted for review. The second review again examines the technical content of the paper. Written discussions of accepted papers are solicited by SNAME from experts in the field. Authors reply in writing to the advance written discussions and to oral discussions at the annual meeting. Written questions and responses form a part of the final published paper.

In the SNAME paper included here the results of the propeller-ice interaction experiments conducted at IMD are presented, including the shaft loads and blade loads observed at each of four different pitch settings over a range of milling cut depths from approximately 8 mm to 60 mm. A subset of shaft loads are presented as the confidence interval that contains 95% of the data points from the shaft dynamometer. This subset included an upper and lower bound as well as the mean recorded value at each of a range of advance ratios. The remaining shaft loads are shown as mean values only. The blade loads resulting from 3 of the 89 cases tested are also presented against the open water data using a 98% confidence interval for the maximum and minimum points to avoid loss of extreme maxima; mean results are included for the remainder of the 86 test cases.

The results recorded from the blade load dynamometer in the direction of vessel travel and the moment about the shaft axis are reduced into the non-dimensional coefficients for thrust and torque. As in the case of the shaft loads, a maximum, mean and minimum cycle value for each of the coefficients was calculated and compared to both the open water and shaft coefficients, both reduced by 75% to account for a single blade. In addition to these non-dimensional coefficients the moment loads experienced by the blade are also resolved into the in-plane and out-of-plane bending moments and the spindle torque exerted on the blade. Again the values are non-dimensionalized, using the bollard pull value for the particular pitch setting and the diameter of the propeller. Results are again compared to similar cases involving open water testing. An error analysis of the results recorded and calculated during these tests is included in Appendix III of this thesis.

In addition to the charts submitted to the SNAME '01 journal paper a complete set of charts documenting the maximum, mean and minimum values of shaft load, blade load and blade bending moments are included in Appendix IV, V, and VI respectively.

At the time of printing the SNAME paper include herein was past due for acceptance into the SNAME '01 conference. Should it be subsequently rejected for this conference it is the authors intention to re-submit it for the SNAME '02 conference.

## **2.4 Co-Authorship Statement**

### **Effects of Strain Rate and Temperature on the Uniaxial Compressive Strength of Model Ice, POAC '01**

A series of compression tests on the EG/AD/S ice used to model real ice at propeller scale was conducted to better understand the results from ice milling experiments. These were arranged and conducted by the author, Dr. Brian Veitch, Dr. Neil Bose, Varma Gottumukkala, and Chris Woodford from Memorial University and Dr. Stephen Jones, and Austin Bugden from IMD. Details of the specific tasks in the implementation of this test program follow.

**Concept Development:** In preparation for the interpretation of results from propeller-ice interaction experiments Dr. Neil Bose, Dr. Stephen Jones and Dr. Brian Veitch developed the concept to test the compressive strength of EG/AD/S ice at high strain rate.

**Experimental Program Development:** Once the concept for the experiments was derived Dr. Neil Bose, Dr. Stephen Jones, Dr. Brian Veitch, Varma Gottumukkala, Austin Bugden and the author met and developed a testing plan to test EG/AD/S ice over a range of strain rates, including both high and low strain rates. Dr. Brian Veitch and the author then revised the testing plan to give the most viable test results in the region of interest with the fewest number of tests possible.

**Sample Collection and Storage:** After revision of the test program the author developed a collection sequence to gather EG/AD/S ice samples from a prepared sheet of EG/AD/S ice. The author, Varma Gottumukkala, Austin Bugden, and Chris Woodford then collected the required ice samples and stored them in the IMD cold room until testing facilities became available.

**Experimental Testing:** When compression testing facilities became available Austin Bugden, Varma Gottumukkala, Chris Woodford and the author began preparing and testing ice samples. This involved the milling of samples into uniform prisms and then compressing them to failure. A total of 142 tests were completed over the course of two weeks during which time the author provided updates to Dr. Brian Veitch, and Dr. Stephen Jones concerning the progress and results of the experiments.

**Data Analysis:** After completion of the test program the author and Dr. Stephen Jones both began working on analysis of the data independently. In addition, the author undertook an error analysis to determine the significance of minor variations observed in

the results. Once analyzed results were available from both the author and Dr. Stephen Jones, the findings were presented to Dr. Brian Veitch and Dr. Neil Bose. This group then discussed the results and decided to present the results at the POAC '01 conference in Ottawa.

**Paper Preparation and Submission:** The author proceeded to prepare the first draft of the paper for presentation at the conference. Once prepared the preliminary paper was circulated through the co-authors, Dr. Brian Veitch, Dr. Stephen Jones, Dr. Neil Bose and Austin Bugden, for comments. These were then incorporated into the draft paper by the author along with the authors' own revisions and the revised draft re-circulated through the authors. Minor changes were again made by the author and the prepared draft was forwarded to the POAC '01 review committee by Dr. Brian Veitch.

**Blade Load Measurements on a Model Propeller in Ice, OMAE '01 and Blade Load Measurement on a Model Propeller in Ice, SNAME Transactions '01**

Noting a lack of model and full scale data pertaining to the blade loads experienced by highly skewed ice-class propellers, researchers from Memorial University and IMD in collaboration with Lloyd's Register and Transport Canada undertook the examination of loading on an individual blade of a model highly skewed propeller during the ice milling interaction. The project team members were Neil Bose, Brian Veitch and the author from Memorial University, Stephen Jones, John Bell, Edward Kennedy, Brian Hill, Austin Bugden and Chris Meadus from IMD, and John Carlton from Lloyd's Register.

**Concept Development:** Based on tests conducted by Shawn Searle in 1999, Dr. Neil Bose, Dr. Brian Veitch, Dr. Stephen Jones, John Carlton, John Bell, Don Spencer, and Carl Harris developed the concept of testing a highly skewed propeller in ice and recording the loads experienced by an individual blade in some manner. After some discussion it was decided that a six component dynamometer built or installed in the hub of the propeller should be possible, which could record the six components of load experienced by a blade while milling into ice.

**Physical Components:** John Bell and Art Bowker designed a six-component dynamometer capable of mounting in the hub of a highly skewed propeller model and measuring the expected loads during ice milling. The dynamometer was fabricated by NRC and outfitted with a series of strain gages by Ed Kennedy in close cooperation with Art Bowker. During this time John Bell also supervised the construction of a new ice propeller boat and propeller hub for use in the test program. Blades for the propeller model were specified and supplied by John Carlton based on the required scale decided during the preliminary discussions. The propeller blades were supplied without the required mounting facilities. The author then performed a quality assurance on the blades and developed a system for mounting the blades and adjusting the pitch for various tests.

**Calibration:** Once fabricated and strain gauged the new dynamometer required calibration. The author was responsible for applying various combined loads to the dynamometer and recording the resulting output. The applied loads and resulting outputs were analyzed by Art Bowker, the author and John Bell to develop a calibration matrix

that could convert the voltage readings from the dynamometer into forces and moments. This included a program developed by the author to perform the non-linear iterative calibration calculations. Other equipment, including the shaft dynamometer, also required calibration, which was completed by the author and Austin Bugden prior to the start of testing.

**Experimental Program Development:** Dr. Brian Veitch and the author jointly developed a test program for the propeller tests including both open water and ice milling tests. During the actual tests the author modified the test matrix slightly to account for delays and difficulties encountered during testing.

**Experimental Setup:** Shaft alignment and physical assembly of the test setup was performed by the author and Austin Bugden. The ice-propeller boat was mounted to the ice tank carriage along with the required data acquisition hardware. Immediately prior to the commencement of testing the author mounted the blades in the correct pitch position and confirmed that the blade depth of submergence was correct for the particular test.

**Testing:** In collaboration with Brian Hill, Austin Bugden, Chris Meadus, Blair Parsons, and Don Spencer, the author assisted during the tests by ensuring the correct pitch settings and depth of cut was performed. In addition the author performed preliminary data analysis of the various measurements between tests to ensure all of the sensors were performing as expected. The author was also responsible for deciding which changes to make to the test plan in the interest of time, ice remaining, and result validity.

**Data Analysis:** Once testing had been completed the author performed a preliminary analysis of the results from both the shaft and blade dynamometers. This involved determining which data was valid and removing electronic data spikes from the recorded time traces. Once spikes were removed the data was plotted into a readable format and analyzed by the author for apparent patterns. Theories explaining of these patterns were then formulated and distributed to Dr. Brian Veitch, Dr. Neil Bose, Dr. Stephen Jones and John Carlton for comments and discussion. Based on these comments the theories were re-examined and revised until all parties were confident they accurately represented the observed phenomena.

**Paper Preparation and Submission:** During and following the revision of the theories the author also wrote papers for the OMAE '01 Conference and the SNAME '01 annual meeting based on the results of these experiments. Once preliminary drafts of these two papers were prepared they were circulated to the co-authors Dr. Brian Veitch, Dr. Neil Bose, Dr. Stephen Jones, John Bell, and John Carlton for review and comments. Comments from the co-authors and revision to the analysis of the results were then incorporated, by the author, in new drafts of these papers. The new drafts were re-circulated to the co-authors and comments integrated into the draft papers submitted for review. At the time of writing, comments from the reviewers of the OMAE '01 paper had been received by the author and a response incorporated into the paper for final submission.

## **Chapter 3**

**Paper Prepared for Port and Ocean Engineering under Arctic  
Conditions 2001 Conference**

**Title:**

**Effects of strain rate and temperature on the uniaxial  
compressive strength of EG/AD/S CD model ice**

**Authors:**

**Corwyn Moores, Brian Veitch, and Neil Bose**  
*Faculty of Engineering and Applied Science, Memorial University of Newfoundland,  
St. John's, NF A1B 3X5, Canada*

*and*

**Stephen J. Jones and Austin Bugden**  
*Institute for Marine Dynamics, National Research Council of Canada, P.O. Box 12093,  
Stn. A, St. John's, NF A1B 3T5, Canada*

### **3.1 Abstract**

Results of a series of uniaxial compression tests with EG/AD/S correct density model ice are presented. A wide range of strain rates ( $10^{-8} < \dot{\epsilon} < 10^1 \text{ s}^{-1}$ ) was covered at three temperatures,  $-2^\circ$ ,  $-5^\circ$ , and  $-8^\circ\text{C}$ . The temperatures chosen are typical of those encountered in propeller-ice interaction tests. Results reported here are for samples taken from a 110 mm thick ice sheet. Each test specimen was machined into a rectangular prism before testing. Multiple tests at nominally identical strain rates and temperatures were conducted. The failure behaviour of the model ice was found to be similar to other ice, as were the stress/strain rate and stress-temperature relationships.

### **3.2 Symbols**

$t$	Mean sample thickness
$w$	Mean sample width
$l$	Length of the sample
$v$	Compression speed
$\dot{\epsilon}$	Strain rate
$F$	Peak force
$\sigma_{\max}$	Peak stress

### **3.3 Introduction**

The interpretation of results from propeller-ice interaction tests conducted in the ice tank at the National Research Council's Institute for Marine Dynamics (IMD) with EG/AD/S

Correct Density (CD) model ice requires knowledge of the compressive strength of the ice. At the strain rates involved in propeller-ice model tests,  $1-10 \text{ s}^{-1}$  or so, there were no data available on the strength of the ice. Therefore, a series of tests were conducted to measure the uniaxial compressive strength at these strain rates. It was not possible to measure the strength in-situ with the equipment available, so the tests were run using material testing equipment in one of the cold rooms at IMD. In the course of the work the strain rate range was extended to lower values, ultimately covering a range from  $4.6 \times 10^{-8}$  to  $4.6 \times 10^0 \text{ s}^{-1}$ , at three temperatures, -2, -5 and -8°C. These temperatures were chosen as typical of the temperatures encountered in the propeller-ice interaction experiments. The results reported here are for samples taken from an ice sheet with a nominal thickness of 110 mm.

The majority of compressive strength results that exist for both model and real ice are comprised of mainly low strain rates ( $< 10^1 \text{ s}^{-1}$ ). Some results from high strain rate tests of fresh water and artificially grown Baltic sea ice have been presented by Jones (1997). These results indicated an increase in the strength at the highest strain rates tested (approximately  $1 \times 10^1 \text{ s}^{-1}$ ) as opposed to the stabilization of the strength projected by other literature (Jones 1997). The current tests were conducted to determine the behavior of EG/AD/S CD ice.

### **3.4 Apparatus and Method**

#### **3.4.1 General Overview**

Model ice of a nominal thickness of 110 mm was initially collected from the ice tank at the IMD and stored at  $-15^{\circ}\text{C}$  until such time as testing was ready to begin. Testing took place in a temperature-controlled room where two Material Test Systems (MTS) machines were used to conduct uniaxial compressive strain rate tests on the samples by controlling the crosshead velocity of the MTS machines.

The sample dimensions were measured and the strain rate was calculated based on the crosshead velocity and undeformed length of the sample. The strain rate was then combined with the peak load, which was converted into a peak stress by dividing by the measured cross-sectional area, to give a relationship between strain rate and compressive strength. The tests were completed at 10 strain rates and 3 temperatures. Temperatures were chosen to be in the range expected in the ice tank while performing propeller-ice model tests, that is approximately  $-2^{\circ}\text{C}$  to  $-8^{\circ}\text{C}$ .

#### **3.4.2 Sample Preparation**

EG/AD/S CD model ice used at IMD is composed of 0.39% Ethylene Glycol, 0.036% Aliphatic Detergent and 0.04% Sugar (Timco, 1986). CD refers to the corrected density of the ice. By infusing the freezing ice with air bubbles the resulting density of the ice sheet can be controlled to give the desired ice density (Spencer and Timco, 1990). The ice was initially collected from the ice tank from a 110 mm thick ice sheet. Blocks of frozen EG/AD/S CD model ice with rough dimensions of 280mm  $\times$  360mm were cut

from the ice sheet using an electric chain saw. These blocks were all removed less than 12 hours after the tempering process of the ice had begun, to ensure that melting of the original ice sheet was kept to a minimum and to allow the ice to be handled with minimal risk of damage. Once the blocks had been cut, they were placed on wooden strips for a few minutes to allow the unfrozen EG/AD/S mixture contained in the ice to drain. This was done to eliminate additional freezing, which would occur in the blocks after they were stored. The blocks were then placed in plastic bags, numbered and dated, and stacked on shelves in the IMD small cold room where they were stored at  $-15^{\circ}\text{C}$  until testing.

At least 24 hours before testing was scheduled to start, the ice samples were moved into the large cold room to stabilize at the testing temperature (either  $-2^{\circ}\text{C}$ ,  $-5^{\circ}\text{C}$  or  $-8^{\circ}\text{C}$ ). This was done to ensure that the ice was at a uniform temperature. A thermistor inserted in a hole bored into the ice was used to ensure that the temperature was actually uniform. Once the blocks had stabilized at the testing temperature they were cut to size first using a bandsaw, and then using a milling machine and planer to give parallel ends and sides. The final sample size was 110mm thick  $\times$  110mm wide  $\times$  330mm long. The actual thickness of the samples varied since thickness was unmodified from the original sheet thickness, which showed some variation. Some samples were also weighed to determine ice density.

The samples' ends were wiped clean of ice fragments using a soft bristle paintbrush and the samples were either placed on the MTS platen for testing, or sealed in

plastic bags to prevent sublimation while waiting to be tested. Once the ends were milled, samples were not left more than 3 hours before being tested.

### **3.4.3 Equipment Preparation**

Two Material Testing Systems (MTS) machines were used: a high speed system for crosshead speeds between 0.15 m/s and the machines' upper limit of 1.5 m/s, and a low speed system setup for crosshead speeds between  $1.5 \times 10^{-2}$  m/s and  $1.5 \times 10^{-8}$  m/s. These are described in detail by Jones (1997). For a sample length of 330 mm, these speeds corresponded to a minimum strain rate of  $4.6 \times 10^{-8}$  s<sup>-1</sup> and a maximum of  $4.6 \times 10^0$  s<sup>-1</sup>. Tests were done at strain rate orders of magnitude increments of 10. For a given target strain rate, the crosshead speed was determined and used to program the MTS control system.

Both the low and high speed MTS machines were equipped with LVDT systems to measure displacement. A linear regression through the crosshead displacement versus time plot was used to verify the crosshead speed.

At the lower strain rates the applied loads were measured with a standard strain gage load cell (maximum load of 250 kN). This gage was mounted between the upper section of the test system and the upper platen. At higher strain rates (with the high speed MTS) a dynamic piezoelectric force link load cell with a 250 kN capacity was used to increase the response time of the measurement. Again the force link was mounted between the upper section of the test frame and the upper platen.

After the completion of a test the destroyed sample was cleared from between the platens of the MTS machine. The upper and lower platens were then brushed clean and inspected for residual freezing. If this existed the platens were cleaned with kerosene before the next test. The next sample was then mounted and the test process repeated.

### **3.5 Results and Discussion**

Qualitatively the ice was seen to go through three distinct failure modes. At lower strain rates, from about  $4.6 \times 10^{-8} \text{ s}^{-1}$  to  $4.6 \times 10^{-4} \text{ s}^{-1}$ , the ice failed in ductile creep, slowly deforming at an almost constant stress level. At the intermediate strain rates,  $4.6 \times 10^{-3} \text{ s}^{-1}$  to  $4.6 \times 10^{-2} \text{ s}^{-1}$ , the ice was observed to fail through a shear plane mechanism whereby the load increased to some level and then failure started. The load was then observed to drop and the ice failed completely on a shear plane at an angle of between  $30^\circ$  to  $60^\circ$ . Finally, at the highest strain rates,  $4.6 \times 10^{-1} \text{ s}^{-1}$  to  $4.6 \times 10^0 \text{ s}^{-1}$ , the ice was seen to fail in a totally brittle manner. The load increased to some peak value at which time the entire sample shattered explosively.

The measured displacements and loads for three typical samples at different strain rates of  $4.6 \times 10^0 \text{ s}^{-1}$ ,  $4.6 \times 10^{-3} \text{ s}^{-1}$ , and  $4.6 \times 10^{-6} \text{ s}^{-1}$  are shown in time traces in Figure 3-1 a, b, and c. The stress/strain curves shown in Figure 3-2 correspond to these same examples.

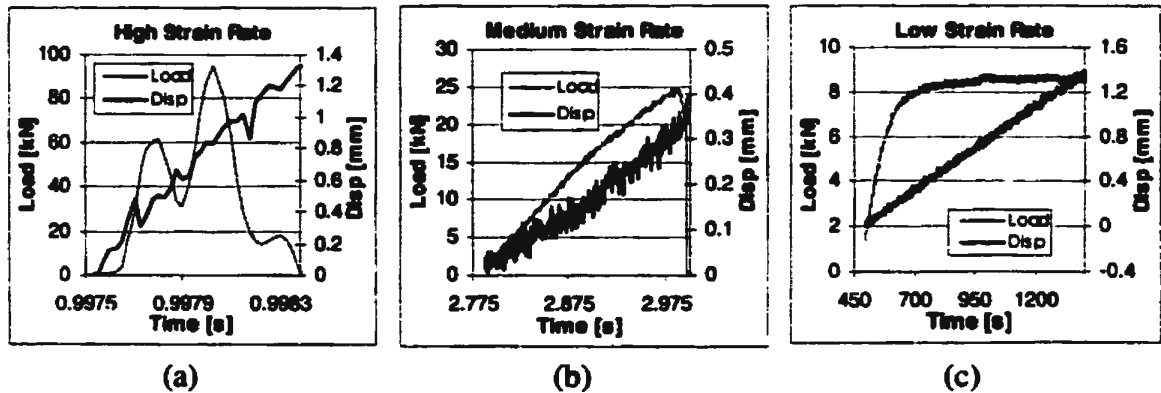


Figure 3-1 Data traces for load and displacement at three strain rates

Figure 3-2 shows that as the strain rate increases there is a larger variation in the measured loads, which shows up as scatter in the points making up the stress/strain curves. At the highest strain rate the sample was observed to fail in about  $5 \times 10^{-4}$  s, which is approximately two times the test system's response time. 10 times is preferred (ASM Handbook, 2000). When the load versus time trace was examined for this strain rate an intermediate peak was observed, (see Figure 3-1 a). After this peak the load is seen to drop before rising to a maximum. The piezoelectric load cell used for the high speed test is designed to respond to rate of change of the load applied. As the test frame system response to the initial impact of the ice was such that the system vibrated, at close to the resonance the maximum load recorded by the load cell may be the combined result of the motion of the sample being forced into the load cell and the response of the test frame to the initial impact. While the test frame response was not as large as the load applied by the sample, as evidenced by the load not reaching zero in the intermediate peak, it was large enough to make the value of the peak test load unreliable. At worst the maximum load to failure can be found to lie somewhere between the intermediate and

maximum peak loads. While it is likely the actual value is nearer the upper end of this range there is no way of proving exactly where. As such the peak stress for this strain rate in Figure 3-3 is shown with an estimate of error based on this range.

Due to the scatter no curve fit to the data was attempted here for the stress/strain resultant at a strain rate of  $4.6 \times 10^0 \text{ s}^{-1}$ . However, the general trend of the stress-strain curve at high strain rate is apparent, and can be assumed to be unaffected by the dynamic response. At low values of strain the stress is observed to be much lower than at the lower strain rates, a trend which continues up to strains between  $7.5 \times 10^{-4} \text{ mm/mm}$  and  $1.0 \times 10^{-3} \text{ mm/mm}$ . As the strain increases past this point the stress increases rapidly with the increase in strain up to a final failure point at higher stress levels than at the lower strain rates.

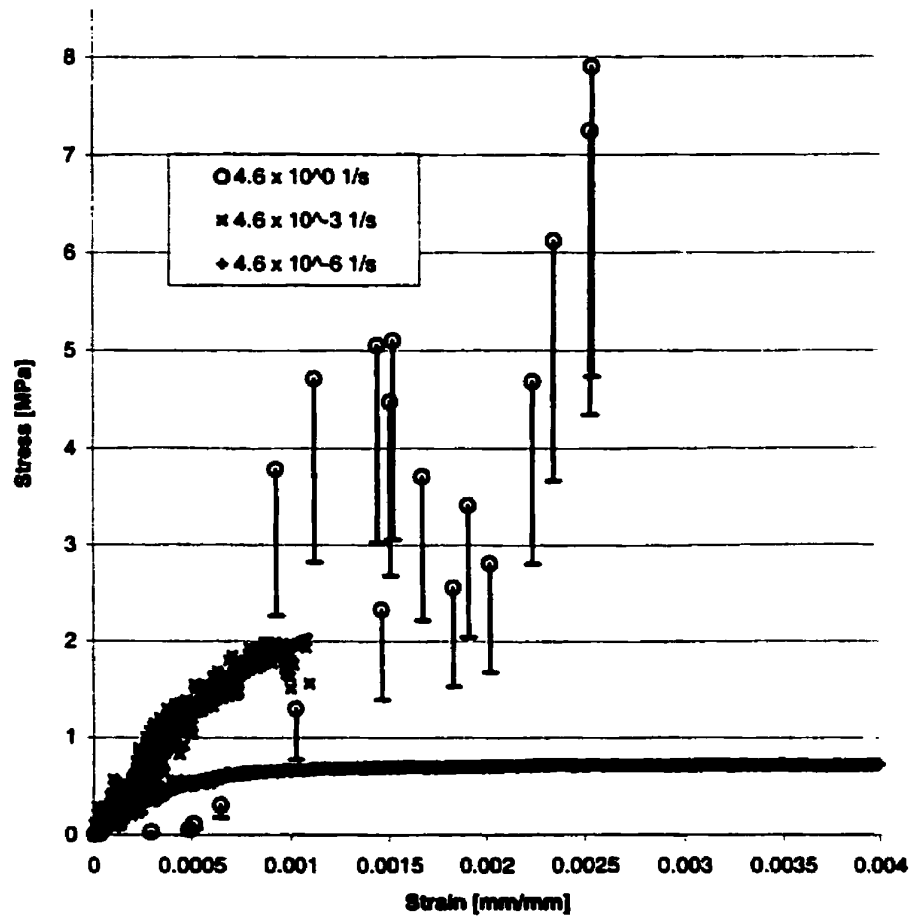


Figure 3-2 Typical stress-strain curve for three strain rates

Based on the peak load, the mean width ( $w$ ) and thickness ( $t$ ) of the individual samples, the peak stress was calculated. This was plotted against the strain rate defined as the crosshead speed ( $v$ ) divided by the undeformed length of the sample ( $l$ ). Crosshead speed was determined from a linear regression of the displacement curve for each test. Peak stress was then plotted against strain rate on a log/log scale, as shown in Figure 3-3. Also included on this chart are the results from tests by Jones (1982) and Meglis (1998) for poly crystalline ice and by Jones (1997) for Baltic Sea ice.

It can be seen that the Baltic Sea ice data are very close to the EG/AD/S CD data. This is believed to be because the EG/AD/S model ice contains “brine pockets” in a similar way to sea ice, but of different chemical composition. The pure polycrystalline data (Jones, 1982) is about a factor of 5 higher than the EG/AD/S data but of similar slope in the ductile range. The Meglis (1998) data are somewhat higher than the EG/AD/S data in the brittle range, by a factor of approximately 2.

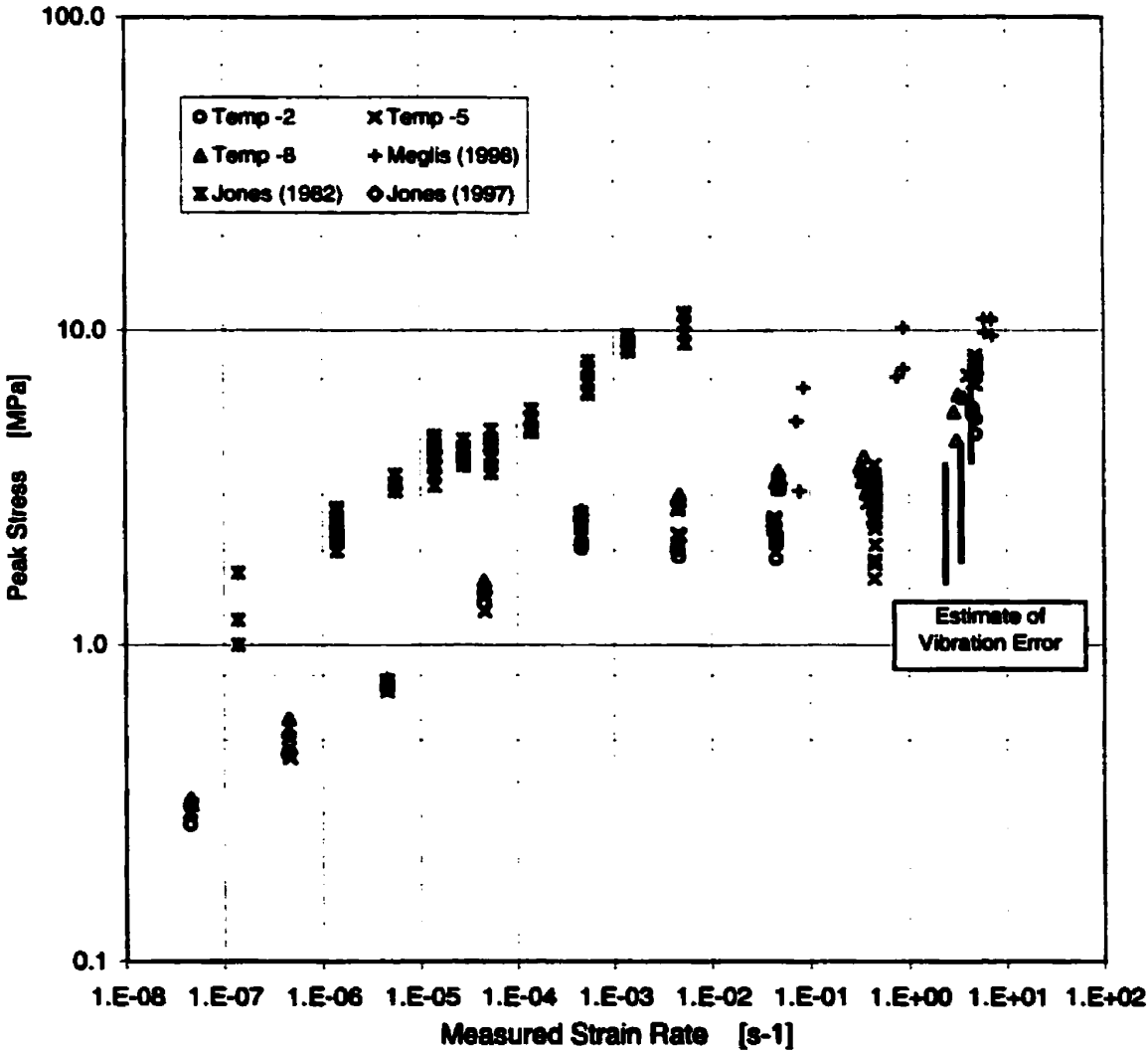


Figure 3-3 Plot of peak stress against strain rate for three temperatures.

A close-up of the lower strain rate range,  $4.6 \times 10^{-8} \text{ s}^{-1}$  to  $4.6 \times 10^{-4} \text{ s}^{-1}$ , is shown in Figure 3-4, also on a log/log scale. The data for the three temperatures fall on three distinct lines of similar slope. This shows that the peak stress can be related to strain rate by an equation

$$\sigma = A\dot{\epsilon}^m \quad [3.1]$$

where  $m$  is the slope of the lines in Figure 3-4 and  $A$  is a constant of proportionality.

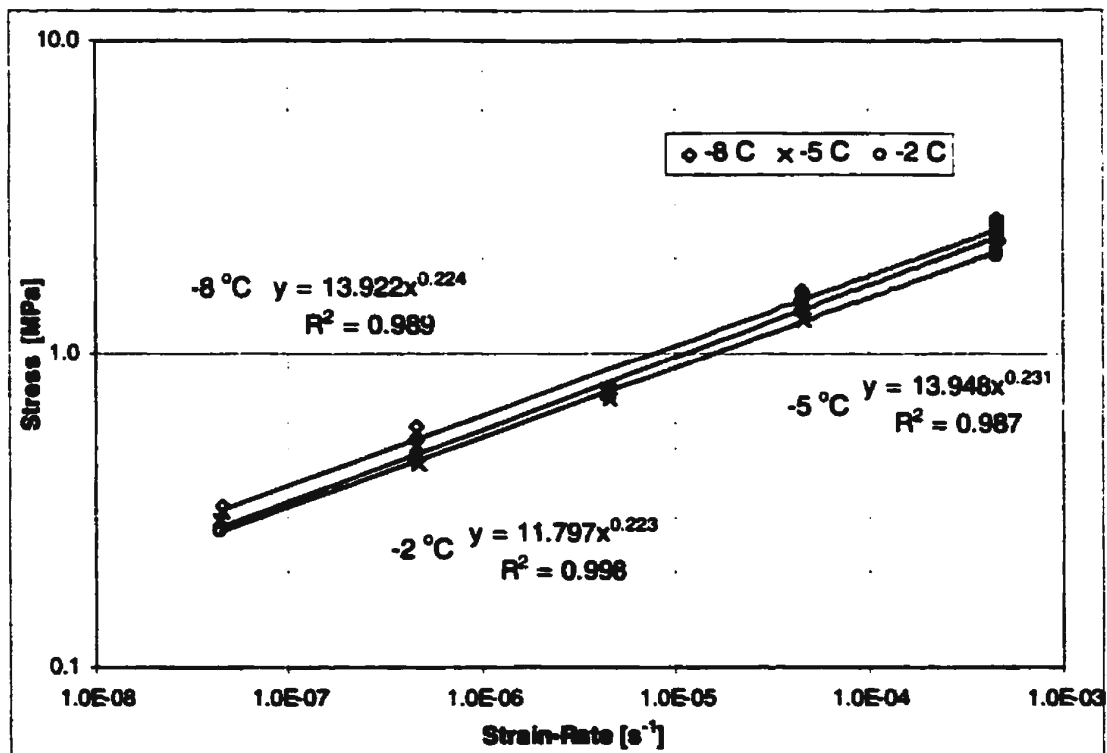


Figure 3-4 Peak stress versus strain rate for the low strain rates only.

The mean slope from Figure 3-4 is  $0.226 \pm 0.004$ , and the reciprocal of this, which is the flow law commonly used for ice, is 4.4. This implies

$$\sigma^n \propto \dot{\epsilon} \quad [3.2]$$

where  $n = 4.42 \pm 0.08$ . This value is similar to that found for polycrystalline ice in the same strain rate range. Jones (1982) found  $n = 5.04$  for unconfined, random polycrystalline ice, and 3.95 when confined, over a slightly higher strain rate range than used here.

Returning to Figure 3-3, the trend in the results with strain rate is similar for each of the three temperatures. Below strain rates of approximately  $1 \times 10^{-4} \text{s}^{-1}$  the strength - strain rate relationship is linear and there is very little scatter. Between  $1 \times 10^{-4} \text{s}^{-1}$  and about  $5 \times 10^{-1} \text{s}^{-1}$  the relationship between strain rate and strength is weak and there is a lot of scatter in the results. Above  $5 \times 10^{-1} \text{s}^{-1}$  the results continue to show a lot of scatter, but there is an apparent increase in the strength at the highest strain rates. The existence or magnitude of this increase is difficult to determine with certainty due to the effect of the vibration previously described. The range of possible values for peak load corresponds to possible peak stresses at the highest strain rate of approximately 1.5 MPa to 8.0 MPa.

These three regions reflect the different failure mechanisms observed: ductile creep at the lowest rates; brittle fracture at the highest rates; and a transition between ductile and brittle behavior in between. This increase in strength at the highest strain rates is in agreement with results obtained with freshwater columnar grained ice, and low salinity (2.4 ppt) ice (Jones, 1997).

### 3.5.1 Error Analysis

An error analysis of the results of the compression tests was completed for four representative strain rates. The results are shown in Table 3-1. The large error in peak stress at the  $4.6 \text{ s}^{-1}$  strain rate is a result of the dynamic effects described above. The remaining errors can be seen to be relatively small and when plotted on a log-log plot they are almost imperceptible.

Table 3-1 Results of error analysis

Desired Strain Rate [ $\text{s}^{-1}$ ]	Error in Strain Rate [%]	Error in Peak Stress [%]
$4.6 \times 10^{-7}$	1.6	3.4
$4.6 \times 10^{-3}$	2.6	3.4
$4.6 \times 10^{-1}$	1.1	3.4
$4.6 \times 10^0$	4.8	30.2

### 3.6 Summary and Conclusions

The uniaxial compressive strength of EG/AD/S CD model ice has been determined over a wide strain rate range and at three temperatures close to the melting point. At low strain rates, the strength follows a power law relationship with strain rate with an exponent of  $0.226 \pm 0.004$ . At strain rates around  $10^{-3} \text{ s}^{-1}$ , the failure changes to one of fracture with failure occurring on well defined shear planes. Finally, at the highest rates tested, the strength increases again. The results are shown to be to be highly accurate and consistent with data on freshwater and saline ice.

### **3.7 Acknowledgements**

We thank Chris Woodford and Varma Gottumukkala for their help with these experiments. The authors acknowledge with gratitude the financial support of this work from the Natural Sciences and Engineering Research Council of Canada and the National Research Council of Canada, Institute of Marine Dynamics.

### **3.8 References**

ASM Handbook, 2000. Volume 8, Mechanical Testing and Evaluation, Materials park, Ohio, p430-431.

Jones, S.J., 1982. The confined compressive strength of polycrystalline ice. *J. Glaciol.* Vol. 28, No. 98, p.171- 177.

Jones, S.J., 1997. High strain rate compression tests on ice. *J. Physical Chemistry B*, Vol. 101, No. 32, p. 6099-6101.

Meglis, I., Melanson, P. and Jordaan, I., 1998. High speed testing of freshwater granular ice, NRC/TMD Report CR-1998-02.

Spencer, D.S., Timco, G.W., 1990. CD model ice – A technique to produce controllable density model ice, IAHR Ice Symposium 90, Espoo, Finland.

Timco, G.W., 1986. EG/AD/S: A new type of model ice for refrigerated towing tanks, *Cold Science and Technology*, 12, p.175-195.

Woodford, C. 2000. Compressive strength of EGADS model ice over a range of strain rates. *OERC-2000-002*, Ocean Engineering Research Centre, Memorial University of Newfoundland.

## **Chapter 4**

**Paper Prepared for 20<sup>th</sup> International Conference on Offshore  
Mechanics and Arctic Engineering 2001  
Paper No. OMAE-01-6102**

**Title:**

**Preliminary blade load measurements on a model propeller in  
ice**

**Authors:**

**Corwyn Moores, Brian Veitch, and Neil Bose**  
*Faculty of Engineering and Applied Science, Memorial University of Newfoundland,  
St. John's, NF A1B 3X5, Canada*

*and*

**Stephen J. Jones and John Bell**  
*Institute for Marine Dynamics, National Research Council of Canada, P.O. Box 12093,  
Stn. A, St. John's, NF A1B 3T5, Canada*

*and*

**John Carlton**  
*Lloyd's Register, 71 Fenchurch Street, London, EC3M 4BS, United Kingdom*

## **4.1 Abstract**

Preliminary results of a series of model scale propeller experiments are presented. A large ( $\text{\O}270\text{mm}$ ) model of a highly skewed controllable pitch propeller was tested in both open water and ice covered water in the ice tank at the Institute for Marine Dynamics. Both the open water and ice experiments were done at four different pitch settings, each over a range of advance coefficient. The ice strength and the depth cut into the ice by the propeller were varied in the ice tests. The main aim of the experiments was to measure the effects of these variables on blade loads, in addition to their effects on shaft loads. Shaft loads were measured using conventional dynamometry. Loads and their locations on one blade were measured using a hub-mounted blade dynamometer designed and built for these tests. The blade dynamometer is described and some preliminary shaft and blade load measurements are presented and discussed.

## **4.2 Introduction**

Propellers on ships that navigate in ice covered waters routinely contact large pieces of ice. These contacts greatly increase the loading on the ships' propulsion system and as a result can cause severe damage to an under designed system. At present these systems are designed using rule formulae based on ice torque, which is linked to the ice-class of the particular vessel. However, propeller failures still occur indicating that a revision to the design guidelines is required.

To assist in determining the extent of additional loading that needs to be accounted for in propellers designed for ice navigation, various model and full-scale experiments have

been conducted. Much of model propeller-ice interaction work conducted in the last 10 years has been done on conventional (non-skewed) model propellers, both with and without ducts, (Minchev et al. 2001, Keinonen and Browne 1990, Browne et al. 1991, and Tamura et al. 1997). Results of tests with this style of propeller may apply to conventional propellers, but not to the highly skewed propellers used in passenger ferries and other vessels operating in ice.

To address this gap in knowledge, Searle et al. (1999a) did ice milling experiments with both a highly skewed model propeller and a conventional ice-class propeller model in model EG/AD/S ice. During these tests the thrust and torque on the shaft (total propeller load) were recorded as the model propellers milled into a sheet of EG/AD/S ice, (a mixture of water, (e)thylene (g)lycol, (a)liphatic (d)etergent and (s)ugar), in the ice tank at the National Research Council of Canada's Institute for Marine Dynamics (NRC-IMD) in St. John's, Newfoundland. One of the interesting findings of these experiments was that the ice loads were very sensitive to the operating conditions, in terms of angle of incidence, or alternatively advance coefficient. The magnitude and direction of the ice loads responded more dramatically to changes in operating conditions than did the hydrodynamic loads; further, this sensitivity was more pronounced for the highly skewed propeller than the more conventionally designed ice-class propeller. During the experiments, the model propeller blades bent – damage that corresponded qualitatively to damage experienced on the full-scale propeller, (Searle et al. 1999b).

A new set of experiments was designed to investigate ice loading on propeller blades in more detail, using Searle et al. (1999a) as a starting point. The experiments, which are the subject of this paper, incorporated a new hub mounted blade dynamometer to measure the blade loads and blade load location. As before, experiments were done over a range of advance coefficients, ice strengths and cut depths (see Figure 4-1). Further, tests were done at several pitch settings.

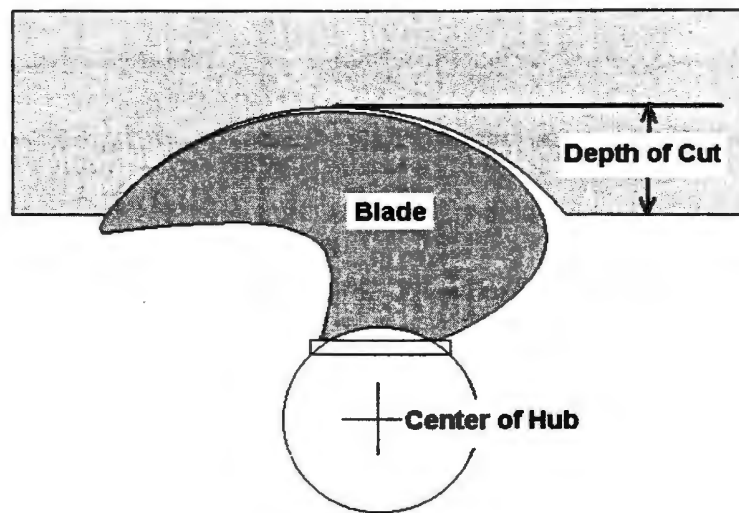


Figure 4-1 Definition of blade depth

## 4.3 Test Setup

### 4.3.1 Description of Test Tank and Ice Conditions

The tests were conducted in the IMD ice tank, Jones (1987). The useable area of this tank for ice testing is 76 m long and 12 m wide. It is 3 m deep. In addition a 15 m long setup area is separated from the ice sheet by a thermal door to allow equipment preparation while the ice sheet is growing. The carriage on this tank weighs approximately 80 tonnes

and is capable of velocities of up to 4.0 m/s. The carriage is designed with a central testing area where a test frame, mounted to the carriage frame, allows the experimental setup to move transversely across the entire width of the tank. In these experiments the test setup restricted the usable width to 6 m from the 3 m to the 9 m locations.

Model ice known as EG/AD/S was used as the ice in these experiments. EG/AD/S ice is specifically designed to provide the scaled flexural failure strengths of real ice (Timco 1986). The ice sheet is grown by first cooling the tank room to approximately  $-20^{\circ}\text{C}$  and then “seeding” the tank by spraying warm water into the cold air in a thin mist, allowing it to form ice crystals before it contacts the surface of the tank. The ice is then allowed to grow at approximately  $-20^{\circ}\text{C}$  until it has reached the desired thickness. The temperature of the room is then raised to above freezing and the ice is allowed to warm up and soften, a process called tempering, until the target ice strength is reached.

Four separate ice sheets were used. The first sheet was intentionally soft to ensure that the entire system was operating correctly and loads were within the expected ranges to prevent damage to the propeller, boat and dynamometer. The strength of the remaining three sheets was increase to better model the ice strength properties.

The first sheet was used to examine the testing procedure; it had a relatively weak target flexural strength of 30 kPa and nominal design thickness of 60 mm. The measured flexural strengths at the beginning and end of the test program for the first sheet were

27.4 kPa and 16.0 kPa, respectively, while average thickness was measured to be 59.0 mm and 58.4 mm at the same times.

The initial testing procedure involved placing longitudinal cuts approximately 0.75 m apart and 10 mm deep along the length of the ice. Transverse cuts were then made at approximately 0.5 m spacing and 10 mm depths, as illustrated in Figure 4-2. These were provided to allow the ice to break when the propeller boat plow contacted it thus preventing the ice from rising off the propeller. The cut pattern also caused the ice to break easily, preventing cracks from proceeding across the remaining ice sheet. The next test pass was then run alongside the previous one thus requiring only one longitudinal cut (the opposite edge being now open water).

This method was used for the entire first sheet and resulted in a total of five separate tracks down the tank. Unfortunately, due to the near presence of the free surface on the second through fifth runs, the propeller experienced ventilation at all but the highest advance ratios and as such the results were not considered valid. Also, the depth of cut was not possible to measure after a test because the ice was so soft the ice sheet remaining above the propeller did not have enough integrity to maintain its milled shape.

The second ice sheet had a target nominal thickness of 60 mm, and a target starting flexural strength of 40 kPa. The entire sheet was used; at the end the ice had a final strength of 20 kPa. To prevent the ventilation observed during the first ice sheet, the

number of tracks was reduced from five to three 0.75 m tracks, whose centerlines were 3 meters apart. This left a minimum of approximately 2.5 m of ice sheet on the tank surface on either side of the propeller boat, which proved sufficient to prevent ventilation. Once again longitudinal and transverse cuts were made in the ice to facilitate controlled breaking and clearing. Depth of cut targets were verified by slowly advancing the propeller into the ice sheet then backing off to retrieve the milled section. This procedure worked well until the ice reached approximately 30 kPa in strength at which time the ice was too soft to maintain its milled shape.

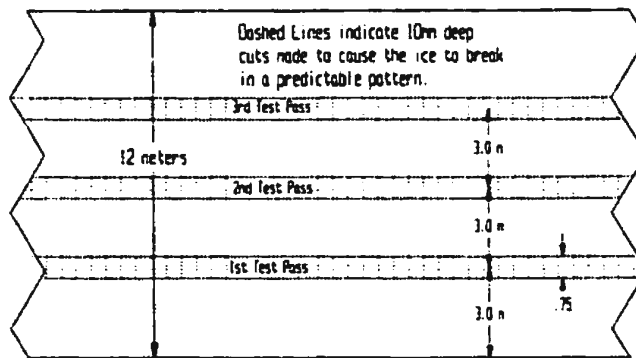


Figure 4-2 Test pass diagram; 2nd, 3rd, and 4th ice sheet

The remaining two ice sheets were prepared and tested in the same manner as the second with the target strength and thickness being 55 kPa at 60 mm and 55 kPa at 80 mm, respectively. Measured start and finish values for these sheets were 54 kPa and 40 kPa at 57 mm and 60 mm for the third sheet and 56 kPa and 35 kPa at 81 mm and 83 mm for the last sheet.

### 4.3.2 Propeller Boat

A new propeller boat was constructed for the tests. The design incorporated an ice plow attached after the propeller, but forward of the housing as illustrated in Figure 4-3.

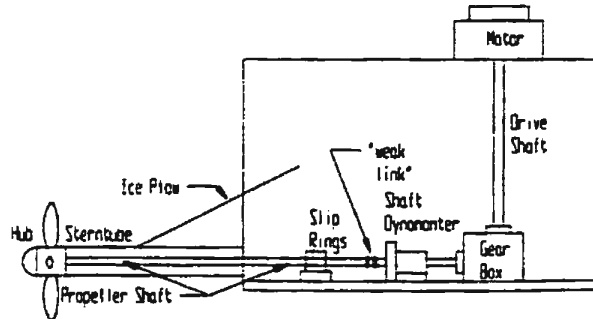


Figure 4-3 Propeller boat layout

Attached to the upper part of the housing, a 3 kW, 3000-rpm electric motor was used to drive a vertical shaft into a 90° 3:1 reduction gearbox. The output shaft of this gearbox was connected to a shaft dynamometer through a flexible coupling. The opposite end of the shaft dynamometer was then connected to the propeller drive shaft through a “weak link” solid connection, designed to fail before the maximum load of either the dynamometer or the gearbox was reached. The drive shaft was supported at the propeller end of the stern tube by a water-cooled brass bearing and sealed with a rubber stern tube seal. The aft end of the drive shaft was supported by the in-line shaft dynamometer.

Access to the components in the housing was possible from both the top and side of the propeller boat through Lexan covers, though the side cover offered better access to most components.

During open water tests, wave deflectors were fitted forward and aft to avoid swamping of the boat due to overtopping bow or following waves. The top cover was installed to keep water spray and waves out. For operation in the ice sheet the ice itself prevented the formation of a significant bow wave and the bow wave deflector was removed to allow the installation of the ice plow.

#### **4.3.3 Hub / Blade Dynamometer**

The loads experienced by a single blade were measured through the use of a newly designed hub mounted blade dynamometer. NRC-IMD designed and fabricated a stainless steel cylindrical dyno that was fitted inside the hub of the propeller and to which one of the propeller blades was mounted. Through a series of strain gauges mounted on the top and bottom of the dynamometer cylinder, the dynamometer was capable of measuring the full six components of load. Before calibration, the dynamometer was waterproofed and mounted inside the hub to eliminate mounting variation as a source of error. Dimensions of the dyno are shown in Figure 4-4.

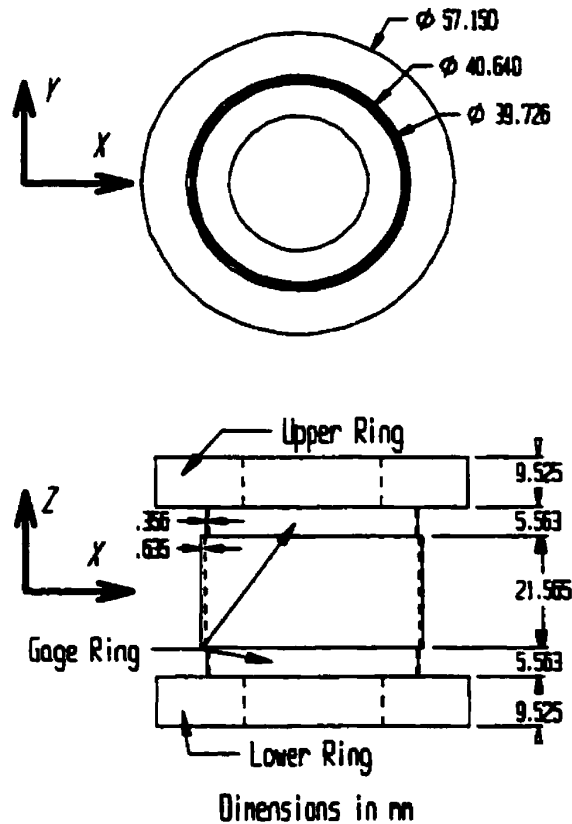


**Figure 4-4 Dimensions of blade dynamometer**

As the propeller being modeled had controllable pitch, it would have been ideal to change the pitch while the model propeller was moving, as in the full-scale system. This was not practical and instead a series of tapped holes were milled into the hub in the three blade mounting locations on the hub. Holes in the blade allowed it to be lined up at positions corresponding to design pitch of  $31.3^\circ$ , a reduced pitch  $7.2^\circ$  below design, a reduced pitch  $15.2^\circ$  below design and a reverse pitch  $52.2^\circ$  below the design pitch. The blade dynamometer was also required to provide the same mounting pattern. This was accomplished by attaching a pitch ring, with the correct hole sequence, to the blade side of the dynamometer. All mating of the dyno parts was conducted with stainless steel bolts

or grade eight bolts sealed with waterproofing to prevent rusting. The blades themselves were mounted with two stainless steel bolts each.

In an attempt to reduce the amount of noise picked up by the strain gauges they were outfitted with an electrical pre-amplification of approximately 100 times, thereby reducing the amount of amplification required at the output. Wiring for the blade dynamometer was then run through the hub back through the drive shaft to a small circuit board, which connected it to a power supply through a set of slip rings. The same slip ring set was used to convey the resulting six outputs to the signal-conditioning box where further electrical amplification was conducted to increase the output values to a substantial portion of the voltage required for full-scale deflection. Due to the high rotational speed and the requirement of a large number of data points over each blade-ice contact, each of these channels was sampled at 5000 Hz.

The design load limits of the blade dynamometer were as follows: maximum forces in  $x$  and  $y$  directions were both 800 N, maximum force in  $z$  was 600 N. Moment maximums were 85 Nm about both  $x$  and  $y$  and 50 Nm about  $z$ . Figure 4-4 shows the definitions of  $x$ ,  $y$ , and  $z$  directions with respect to the dynamometer; Figure 4-5 shows the orientation of these directions with respect to the propeller. Note that in this picture the propeller would be rotating counter clockwise and progressing forward out of the page.

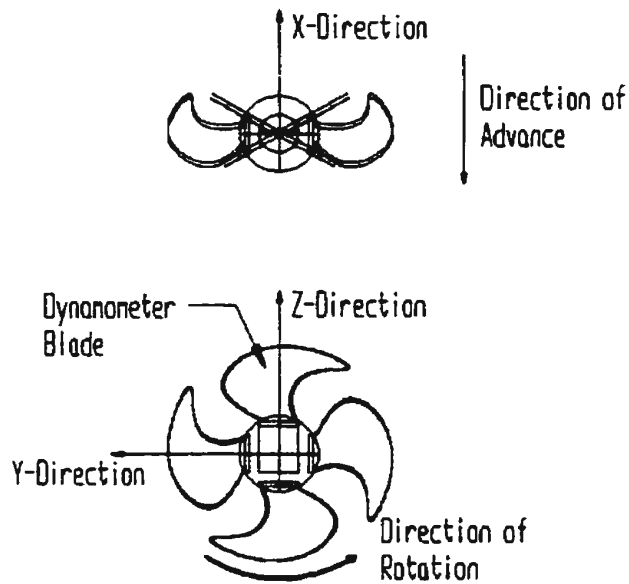


**Figure 4-5 Directions x, y, and z on the propeller**

Calibration of the blade dynamometer was conducted by securely mounting the hub, containing the dynamometer inside, in a known position and applying known loads and moments to the blade end of the dynamometer. These loads were applied in such a way that the dynamometer was exercised so that each of its six components were excited in both the positive and negative directions. To determine interaction effects, the relative magnitude of forces and moments were varied for different calibration setups. The data was then analyzed to produce a calibration matrix, which was then confirmed using 45 linearly independent loading conditions designed to simulate the expected operating range of the dynamometer during ice interactions. Once the tests were complete an abbreviated calibration was also conducted to ensure that no damage was done to the dynamometer during the tests. This showed that, with only very minor differences, the dynamometer maintained its original calibration properties.

A miscommunication during the blade fabrication resulted in the bases of the propeller blades being larger than intended; as such they protruded above the hub in a manner that was considered unacceptable from a hydrodynamic point of view. To fair the blade and hub together, Delrin fairing pieces were attached to the hub to increase its diameter to that represented by the blade bases. These pieces were then attached using a modeling sealer. To prevent the fairing from interfering with the dynamometer blade, the spacing for this blade was cut oversized by 30/1000ths of an inch on the diameter. The maximum deflection of the dynamometer was calculated to be 7/1000ths of an inch through FEA analysis. It was subsequently demonstrated that this oversizing was sufficient.

#### **4.3.4 Description of the Blades**

Provided by Lloyd's Register, the model propeller blades tested were 1:19.259 scale models of a propeller design from Lloyd's Register identified as model number 6603. The blades were highly skewed with a  $P/D$  at 0.7 radius of 1.337, and a skew of  $50^\circ$ . The model is a four bladed controllable pitch propeller, 270 mm diameter, similar in design to various propellers used on passenger ferries in Canada and Europe. Figure 4-6 shows a photo of the assembled propeller.

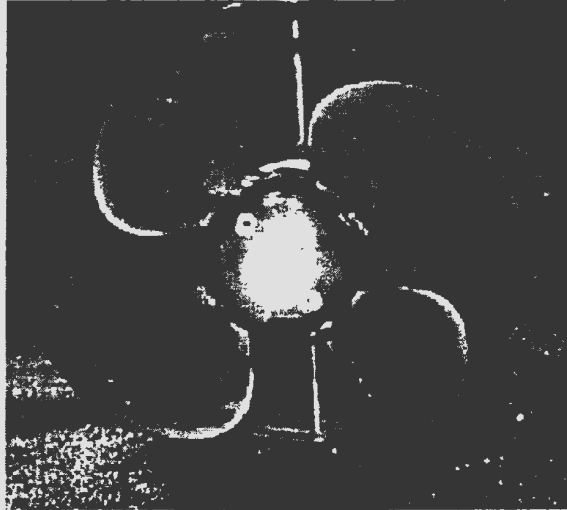


Figure 4-6 Assembled model propeller

#### **4.3.5 Other Sensor Equipment**

Other sensors were used to measure the shaft load, shaft speed, propeller depth, and carriage speed.

Shaft loads were measured using an in-line dynamometer manufactured by Sensor Development Inc. that had a maximum thrust load rating of 890 N and maximum torque load rating of 110 Nm. The dynamometer had 100% overload capacity and maximum rotational speed of 20 rps. These two channels were also sampled at 5000 Hz.

Shaft speed was measured by a tachometer built into the 3kW motor. The motor tachometer was calibrated using a laser tachometer. The motor was run through a series of settings and the rotational speed on the propeller side of the gearbox was measured using the laser tachometer. The settings for the correct motor speeds were then

determined. Since the rotational speed was not expected to vary greatly in the ice it was sampled at 100 Hz to conserve memory space.

Propeller depth was measured using a potentiometer, in which the base unit was mounted to the carriage and the end of the wire attached to the test frame holding the propeller boat. The zero value for this potentiometer was set at the point where the upper edge of the propeller circle just failed to break the surface of the water. Once set, the vertical position of the test frame did not change and as such it was sampled at only 50 Hz.

Carriage speed was recorded from a tachometer built into the drive motors of the carriage. Carriage speed does not vary greatly with the propeller interaction event; it was sampled at 100 Hz as well.

In addition to the sensors, three above water cameras were used to record the ice milling event. These recorded each test looking from the bow, starboard side and directly above the propeller.

#### **4.4 Method**

The following tables describe the total test matrix performed for these experiments. Tests whose results are discussed in this paper are shaded. In the legends pitches are defined as the pitch at the 0.7 radius. For example a pitch of  $24.07^\circ$  indicates a test performed at a 0.7R pitch setting of  $24.07^\circ$ , or  $7.23^\circ$  below design pitch of  $31.30^\circ$ . All tests were performed at a shaft speed of 10 rps. Below the pitch designation for each test are two ice strength values. These are the compressive and flexural strengths respectively of the ice

in kPa. The values stated are estimated by linearly interpolating between the two measured values nearest the test case.

Table 4-1 Test matrix for sheet number 2

Sheet 2		P-Ratio	
A indicates a Test at Pitch Setting =		31.30°	1.3371
F indicates a Test at Pitch Setting =		24.07°	0.9923
B indicates a Test at Pitch Setting =		16.03°	0.6318
C indicates a Test at Pitch Setting =		-20.93°	-0.8428

h <sub>i</sub>	Advance Ratio							
[mm]	0.1	0.2	0.3	0.4	0.5	0.6	0.7	
8	F 90   26		F 90   26		F 90   26			
16		F 104   32	F 104   32	F 103   32		F 103   32	F 103   32	
20	F 90   25		F 90   25		F 90   25			
28	F 90   25		F 90   25		F 90   25			
34		F 99   31	F 98   31	F 97   30		F 97   30		
40		F 93   29	F 93   29	F 93   29		F 93   29		
50	F 90   24		F 90   24		F 90   24			

Table 4-2 Test matrix for sheet number 3

Sheet 3		P-Ratio	
A indicates a Test at Pitch Setting =		31.30°	1.3371
F indicates a Test at Pitch Setting =		24.07°	0.9923
B indicates a Test at Pitch Setting =		16.03°	0.6318
C indicates a Test at Pitch Setting =		-20.93°	-0.8428

h <sub>i</sub>	Advance Ratio							
[mm]	0.1	0.2	0.3	0.4	0.5	0.6	0.7	
8	C B 85   37	C B 86   37	B 86   37					
16	C B 84   36	C B 84   36	B 84   36					
24.5	C B 84   36	C B 84   36	B 84   36					
34					F 146   48	F 146   48		
40		F 133   46	F 127   46	F 121   46		F 112   45	F 107   45	
50	F 71   31	F 71   31	F 71   31	F 71   31	F 71   31	F 71   31		
64.4		F 87   40	F 87   40	F 87   40		F 87   40		

Table 4-3 Test matrix for sheet number 4

Sheet 4		P-Ratio					
A indicates a Test at Pitch Setting =		31.36°					
F indicates a Test at Pitch Setting =		24.87°					
B indicates a Test at Pitch Setting =		16.83°					
C indicates a Test at Pitch Setting =		-28.93°					
h, (mm)	Advance Ratio						
	0.1	0.2	0.3	0.4	0.6	0.7	0.8
8			C				
			188   36				
16			C				
			188   36				
20.8	A		CA	A	A	A	A
	183   68		183   68	183   68	183   68	183   67	183   37
28	C	C	C				
	188   28	188   28	188   28				
34	A		A	A	A	A	A
	184   68		184   68	184   68	184   68	184   64	177   36
43	A		A	A	A	A	A
	188   82		188   82	188   48	188   48	188   48	183   33
46	A		A	A	A	A	A
	187   48		187   48	188   48	188   44	188   44	173   36
60	A		A	A	A	A	A
	183   42		183   41	181   39	188   38	187   38	188   26

Prior to the ice tests, the propeller was also tested in open water at each pitch setting over a range of advance ratio from 0.05 to 1.5. All open water tests were performed at a shaft immersion of 1.5D or 405 mm below the surface. Once the open water tests were completed the following procedure was then used to conduct the tests in ice.

#### 4.4.1 Blade Preparation

Blade pitch was verified to ensure the blades were all at the correct pitch for the particular set of tests. After placing each blade in the correct pitch setting the entire propeller boat was lowered to its zero position. The propeller was then raised out of the water and run through a series of shaft speeds from 8 rps to 14.5 rps in order to determine the frictional torque loads exerted on the system from the bearings and the slip ring. These loads were then used as the zero loading offsets to determine the load exerted on

the blade due to the ice and water. By performing these friction tests the centrifugal force exerted on the blade dynamometer could also be removed from the measured loads.

After completion of the friction run, the propeller was lowered into the water such that the blade would cut into the ice at the target depth. To ensure this depth was correct the propeller was slowly advanced into the ice sheet at slow rotational speed to prevent disturbing the ice and the resulting cut depth.

#### **4.4.2 Test Run**

Once blade depth had been verified the test was ready to commence. The carriage was programmed to run for at least 3 seconds at the target constant speed. The data collection system was started and the propeller held at zero rps for 3 seconds to establish a baseline. The propeller speed was then increased to 10 rps and a bollard pull recorded for 3 seconds. The bollard was used between runs to ensure the blade dynamometer was not drifting. After the bollard pull, the carriage was started and the propeller was run into the ice for the programmed distance. As soon as the carriage was stopped the data collection was stopped and the carriage backed off so that the actual cut depth could be examined. It was found that as the ice softened it became impossible to measure cut depth after the test run since the ice path was totally destroyed. In these cases the measurement taken at the start of the run was taken as the cut depth.

After all of the tests at a particular pitch were completed a friction test was run again.

## **4.5 Results**

The following results are from a single ice milling run performed at a pitch setting of  $24.07^\circ$ , and a single depth of cut, measured to be approximately 45 mm. This run was comprised of four carriage velocities at a constant rotational speed of 10 rps. Corresponding to advance ratios of 0.20, 0.30, 0.40 and 0.60 all four of these runs were completed within one minute of each other. As such the results presented here show no ice strength or cut depth effects. Results in Figures 4-7 and 4-8 were calculated using the loads measured by the in-line shaft dynamometer; Figures 4-9 and 4-10 show results from the blade dynamometer measurements.

Figure 4-7 shows the maximum, average, and minimum thrust coefficient for the ice milling test (as calculated from the in-line shaft dynamometer) versus the advance ratio. The mean thrust coefficient for the open water test is also plotted. Figure 4-8 illustrates the maximum, average and minimum torque coefficient (multiplied by 10) for each of the advance ratios for ice milling, and the mean torque coefficient from the open water test. The maximums and minimums were defined as the points at which 2.5% of the data points lie above and below these values, respectively.

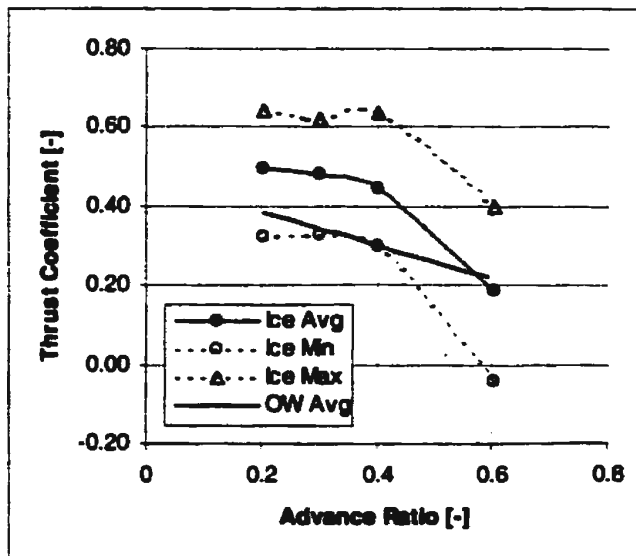


Figure 4-7 Average, Min, and Max  $K_T$  Ice / OW

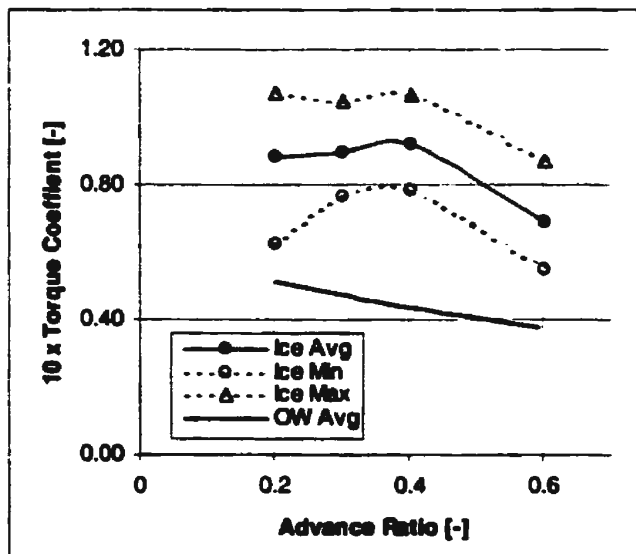


Figure 4-8 Average, Min, and Max  $K_Q$  Ice / OW

As the propeller enters the ice at low advance ratios the thrust is augmented over that experienced in open water. As the advance ratio increases the amount of augmented thrust is reduced until at some value of advance ratio, depending on the pitch and depth of cut, the ice load causes a reduction in the thrust. As illustrated in Figure 4-7, this point occurred at an advance ratio of just under 0.6 for this particular configuration.

To prevent damage to the model blade tips, which results from negative resultant thrust being applied at the tips, the advance ratios were not allowed to increase to the point where total thrust reached the negative region. This response of thrust can be explained if one considers the mechanics involved. As the propeller advances into the ice sheet slowly each successive blade enters the ice and behaves as a screw, pulling that particular blade forward, the result is an overall increase in the total thrust. As the speed of advance increases (increasing the advance ratio for constant shaft speed) the relative entry speed of the blades into ice increases, which makes "screwing" into the ice more difficult. Rather the blades are increasingly pressed into the sheet, causing loading on the suction side of the blade, which opposes the direction of travel, i.e. a negative thrust.

The increase in thrust and torque can also be seen in the loads on an individual blade. Figure 4-9 shows the thrust coefficient for both the ice milling and open water conditions at an advance ratio of 0.4.

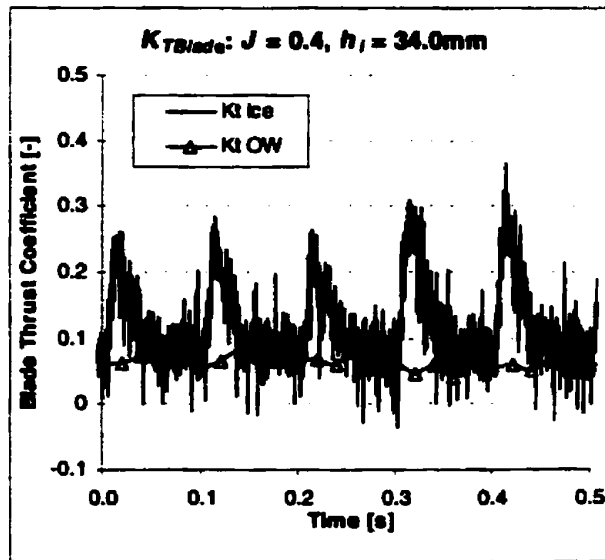


Figure 4-9 Thrust coefficient on individual blade

As can be seen the increase in loading due to the ice interaction can be three to four times the load experienced by the blade while operating in open water. A plot of  $10 \times$  torque coefficient versus time for the same case is shown in Figure 4-10.

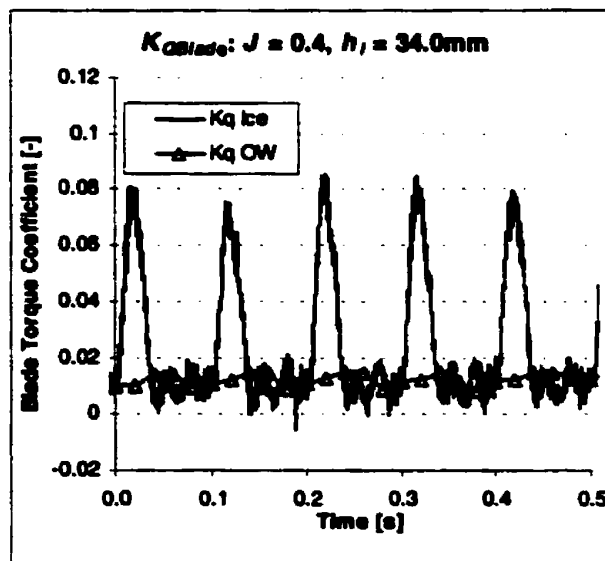


Figure 4-10  $10 \times$  Torque coefficient on individual blade

Again, large increases in the torque are associated with the blade interaction with the ice sheet. Torque loads on the order of 5 times the open water torque load are observed for this particular case.

Similar results to those illustrated here were observed for the 0.2 and 0.3 advance ratios. It was noted that the blade thrust loads increased with the decrease in advance ratio as in the thrust coefficient plot shown in Figure 4-7. At the 0.6 advance ratio, added thrust on the blade due to the ice was minimal, again as expected from the shaft load data. Torque on the blade showed little variation between the lower three advance ratios, but begins to drop off at the 0.6 advance ratio.

#### **4.6 Summary and Conclusions**

A new blade load dynamometer was described and the preliminary results from an experimental program designed to investigate the effects of propeller-ice interaction on a highly skewed model propeller have been presented. The results correspond to a pitch configuration reduced from that of the propeller's design pitch. The loads experienced on the shaft were presented for four advance ratios and were compared to open water propeller performance at the same advance ratios. As well, the thrust and torque components exerted on an individual blade during the ice milling interaction were discussed.

The magnitudes of the added loading in both thrust and torque indicate that ice loads are critically important design issues when considering propellers for ice navigation. The

**cyclic nature of this loading, coupled with the high loading experienced indicates that fatigue considerations should also be seriously considered in the design process.**

**Further work on the remainder of the tests described here is ongoing to determine effects of cut depth, pitch setting and advance ratio on the loads experienced by an individual blade during the propeller-ice interaction event and whether this can be used to improve the design and operation of highly skewed propellers for ice navigation.**

#### **4.7 Acknowledgements**

**This research was funded primarily through a joint project between Transport Canada, Lloyd's Register, and the National Research Council Canada. The first author acknowledges with gratitude the financial support of the Natural Sciences and Engineering Research Council (Canada) and the Government of Newfoundland & Labrador.**

**Thanks are due to the people from Oceanic Consulting Corporation, Art Bowker Inc, and Memorial University's Technical Services Department for their help in the experimental work. Special thanks are extended to the ice tank crew at IMD for their assistance in conducting the experiments. Finally, we acknowledge the valuable contribution that Mr. John Bell and Mr. Ed Kennedy made to the research, particularly their role in the blade dynamometer design, fabrication and calibration.**

## **4.8 References**

- Browne, R.P., Keinonen, A.J., and Semery, P., 1991, Ice Loading on Open and Ducted Propellers, *Proceedings of 1<sup>st</sup> ISOPE, Edinburgh.***
- Jones, S.J. 1987. Ice tank Test Procedures at the Institute for Marine Dynamics. *Institute for Marine Dynamics Report No. LM-AVR-20.***
- Keinonen, A.J., and Browne, R.P. 1990. Ice Propeller Interaction Forces. *Transport Canada Publication 10401E Vol.1.***
- Minchev, D., Bose, N., Veitch, B., Atlar, I., Paterson, I., 2001, *Some analyses of propeller ice milling experiments*, Submitted, Canadian Marine Hydromechanics and Structures Conference '01.**
- Searle, S., Veitch, B., and Bose, N., 1999a, Ice-Class Propeller Performance in Extreme Conditions, To appear, *Trans. Society of Naval Architects and Marine Engineers Vol 107.***
- Searle, S., Veitch, B., and Bose, N., 1999b, Experimental Investigation of a Highly Skewed Propeller in Ice, *Proceedings, OMAE-99-1130*, 8pp.**
- Tamura, K., Kato, H., and Yamaguchi, H., 1997, Experimental Approach to the Interaction between Nozzle-Propeller and Ice-Block, *Joint OMAE/POAC Conference, Yokohama, Japan.***
- Timco, G.W. 1986. EG/AD/S: A New Type of Model Ice for Refrigerated Towing Tanks. *Cold Regions Science and Technology*. Vol. 12: pages 175-195.**

## **Chapter 5**

**Paper Prepared for the Society of Naval Architects and Marine  
Engineers, 2001 Annual Meeting Transactions Volume 109,  
Orlando, USA**

**Title:**

**Multi-component blade load measurements on a propeller in  
ice**

**Authors:**

**Corwyn Moores, Brian Veitch, and Neil Bose**  
*Faculty of Engineering and Applied Science, Memorial University of Newfoundland,  
St. John's, NF A1B 3X5, Canada*

*and*

**Stephen J. Jones**  
*Institute for Marine Dynamics, National Research Council of Canada, P.O. Box 12093,  
Stn. A, St. John's, NF A1B 3T5, Canada*

*and*

**John Carlton**  
*Lloyd's Register, 71 Fenchurch Street, London, EC3M 4BS, United Kingdom*

## **5.1 Abstract**

**A model of a highly skewed controllable pitch propeller was tested in both open water and ice covered water in an ice tank. Both the open water and ice experiments were done at four different pitch settings, each over a range of advance coefficients. The ice strength and the depth cut into the ice by the propeller were varied in the tests. The main aims of the experiments were to measure the effects of these variables on blade loads, in addition to their effects on shaft loads. Shaft loads were measured using conventional dynamometry. Loads on one blade were measured using a six component hub-mounted blade dynamometer designed and built for these tests. The blade dynamometer is described and shaft and blade load measurements are presented and discussed. It was discovered that in certain conditions the individual blade experienced bending moments, thrust and torque loads that were on the order of ten times the mean cycle load during the ice milling event.**

## **5.2 Introduction**

**Navigation of ships in ice covered waters around the world is increasing with a number of cruise ships and ferries making regular trips in ice covered waters. Propulsion systems on these vessels are exposed to loading from ice contact. The resulting loading can greatly increase the demands on the propeller and propulsion system and as a result can cause severe damage to an under designed system. Presently, these systems are designed using rule formulae based on ice torque, which is linked to the ice-class of the particular vessel. A revision of these rules is required since propeller designs based on them still**

experience damage and failure. Bose et al. (1998) and Doucet et al. (1999) have proposed a new method for ice class propeller design and analysis, as have Katsman and Andruishin (1997) and Koskinen et al. (1996). The matter is currently the subject of a joint international effort under the IACS banner.

Various model and full-scale tests have been completed to help determine the extra loading caused by propeller interaction with ice. To date, however, the majority of this work has been completed on the more conventional propeller blade geometries, both with and without ducts, fitted to icebreaker designs. While the results of these investigations may be applicable to other conventional propellers, their extension to the highly skewed propellers used on passenger ferries and other vessels navigating in ice is questionable and requires additional investigation.

With the intention of addressing this gap in knowledge, Searle et al. (1999) completed a series of ice-milling tests with both highly skewed and conventional propeller models. During the tests in EG/AD/S model ice, the shaft loads resulting from propeller-ice interaction were recorded for a highly skewed propeller model and a more conventional icebreaker propeller model. Perhaps the most interesting result from these tests was that the ice loading was more highly dependent on operating condition, in terms of advance coefficient and hence blade angle of attack, than the hydrodynamic loads. Furthermore, this sensitivity to blade angle of attack was more apparent for the highly skewed propeller than for the conventional ice class propeller.

To assess the effect of ice loads on a single propeller blade when operating in ice the experiments described in this paper were conducted. A new propeller blade dynamometer was designed and built to measure the six components of load on an individual blade. The loads on a single blade during the propeller-ice interaction event were recorded for a range of operating conditions, including various advance coefficients and pitch settings, as well as a series of depths of cut into the ice.

## **5.3 Method**

### **5.3.1 Description of Ice Tank and Ice Conditions**

The tests were conducted in the National Research Council of Canada's Institute for Marine Dynamics (IMD) ice tank. The useable area of this tank for ice testing is 76 m long and 12 m wide. It is 3 m deep. In addition, a 15 m long setup area is separated from the ice sheet by a thermal door to allow equipment preparation while the ice sheet is growing. The carriage on this tank is capable of velocities from 0 to 4.0 m/s. The carriage is designed with a central testing area where a test frame, mounted to the carriage frame, allows the experimental setup to move transversely across the entire width of the tank. In these experiments the test setup restricted the usable width to 6 m across the middle of the tank. More information on the IMD can be found in Jones (1987).

Model EG/AD/S ice was used in these experiments. A mixture of water, (e)thylene (g)lycol, (a)liphatic (d)etergent and (s)ugar, EG/AD/S is specifically designed to provide the scaled flexural failure strengths of real sea ice (Timco 1986). The ice sheet is grown by first cooling the tank room to approximately  $-20^{\circ}\text{C}$  and then "seeding" the tank by

spraying warm water into the cold air in a thin mist, allowing it to form ice crystals before falling to the surface of the tank. The ice is then allowed to grow at approximately  $-20\text{ }^{\circ}\text{C}$  until it has reached the desired thickness. The temperature of the room is then raised to above freezing and the ice is allowed to warm up and soften, a process called tempering, until the target ice strength is reached.

Four ice sheets were used. The first sheet was used to examine the testing procedure; it had a relatively weak target flexural strength of 30 kPa and a target thickness of 60 mm. The remaining sheets were stronger with flexural strengths of 50 kPa. The second and third sheets were 60 mm thick, and the last sheet was 80 mm thick.

The initial testing procedure involved placing longitudinal cuts approximately 0.75 m apart and 10 mm deep along the length of the ice. Transverse cuts were then made at approximately 0.5 m spacing and 10 mm depths, as illustrated in Figure 5-1. These were provided to allow the ice to break when the propeller boat plow contacted it, thus preventing the ice from rising off the propeller. The cut pattern also caused the ice to break easily, preventing cracks from proceeding across the remaining ice sheet. The next test pass was then run alongside the previous one, thereby requiring only one longitudinal cut (the opposite edge being open water).

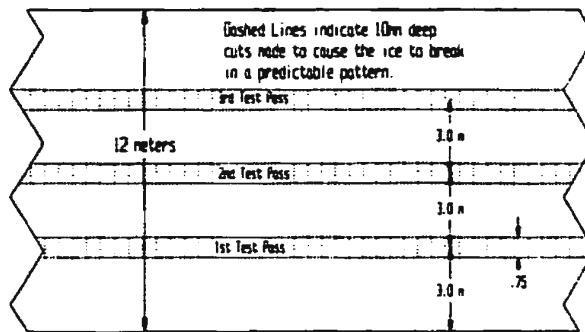


**Figure 5-1 Test pass diagram**

This method was used for the entire first sheet and resulted in a total of five separate tracks down the tank. Due to the close proximity of the free surface on the second through fifth runs, the propeller experienced ventilation at all but the highest advance ratios and as such the results were not considered valid. Also, the depth of cut was not possible to measure after a test because the ice was so soft the ice sheet remaining above the propeller did not have enough integrity to maintain its milled shape.

The second ice sheet had a target nominal thickness of 60 mm, a target starting flexural strength of 40 kPa and a compressive strength of approximately 120 kPa. The entire sheet was used; at the end of the test period, the ice had a flexural strength of 20 kPa. To prevent the ventilation observed during tests in the first ice sheet, the number of tracks was reduced from five to three, whose centerlines were 3 meters apart, as shown in Figure 5-1. This left a minimum of 2.5 m of ice on the tank surface on either side of the propeller boat, which proved sufficient to prevent ventilation. Once again, longitudinal and transverse cuts were made in the ice to facilitate controlled breaking and clearing. Depth of cut targets were verified by slowly advancing the propeller into the ice sheet,

then backing off to retrieve the milled section. This procedure worked well until the ice dropped to approximately 30 kPa in strength at which time the ice was too soft to maintain its milled shape.

The remaining two ice sheets were prepared and tested in the same manner as the second, with the target flexural strength and thicknesses of 55kPa and 60mm and 80mm. Measured start and finish values for these sheets were 54 kPa and 30 kPa at 51 mm and 60.4 mm for the third sheet, and 65 kPa and 25 kPa at 74.4 mm and 81 mm for the last sheet.

### 5.3.2 Propeller Boat

A new propeller boat was constructed for the tests. The design incorporated an ice plow attached after the propeller, but forward of the housing as illustrated in Figure 5-2.

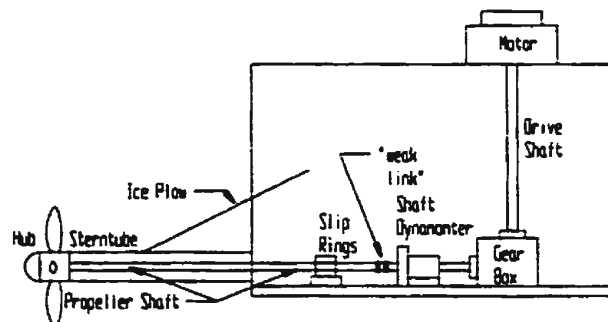


Figure 5-2 Propeller boat layout

A 3 kW, 3000-rpm electric motor attached to the upper part of the housing was used to drive a vertical shaft into a 90° 3:1 reduction gearbox. The output shaft of this gearbox

was connected to a shaft dynamometer through a flexible coupling. The opposite end of the shaft dynamometer was then connected to the propeller drive shaft through a “weak link” solid connection, designed to fail before the maximum load of either the dynamometer or the gearbox was reached. The drive shaft was supported at the propeller end of the stern tube by a water-cooled brass bearing and was sealed with a rubber stern tube seal. The aft end of the drive shaft was supported by the in-line shaft dynamometer.

Access to the components in the housing was possible from both the top and side of the propeller boat through Lexan covers, but the side cover offered better access to most components.

During open water tests, wave deflectors were fitted forward and aft to avoid swamping of the boat due to overtopping bow or following waves. The top cover was installed to keep water spray and waves out. For operation in the ice sheet, the ice itself prevented the formation of a significant bow wave and the bow wave deflector was removed to allow the installation of the ice plow.

### **5.3.3 Hub / Blade Dynamometer**

The loads experienced by a single blade were measured through the use of a specially designed hub mounted blade dynamometer. NRC designed and fabricated a stainless steel cylindrical dynamometer, with varying wall thickness, that was fitted inside the hub of the propeller and to which one of the propeller blades was mounted. It was capable of measuring the six components of load through a series of strain gauges mounted on two

gage rings, see Figure 5-3, which were designed with thinner walls (0.356 mm) to ensure peak stress was concentrated in these areas. Strain differences between corresponding gages in the upper and lower gage rings were used to calculate the applied  $x$  and  $y$  forces and moments. A separate set of gages attached to the lower gage ring only was used to measure  $z$  force and moment loads. Some main dimensions of the dynamometer are shown in Figure 5-3.

Before calibration, the dynamometer was waterproofed and mounted inside the hub to eliminate mounting variation as a source of error.

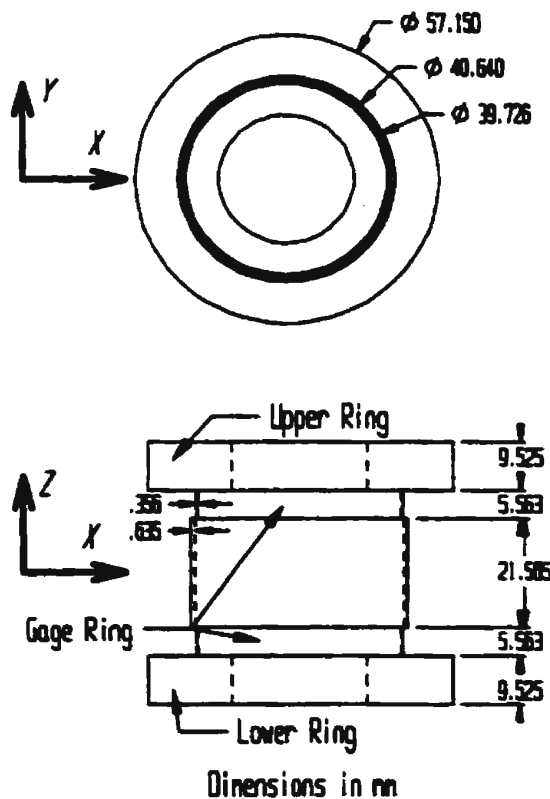


Figure 5-3 Dimensions of blade dynamometer

As the propeller being modeled had controllable pitch, it would have been ideal to change the pitch while the model propeller was moving as in the full-scale system. This was not practical and instead a series of tapped holes were milled into the hub in the three blade mounting locations on the hub. Holes in the blade allowed it to be lined up at positions corresponding to the design pitch of  $31.3^\circ$ , a reduced pitch  $7.2^\circ$  below design, a reduced pitch  $15.2^\circ$  below design and a reverse pitch  $52.2^\circ$  below the design pitch. The blade dynamometer was also required to provide the same mounting pattern. This was accomplished by attaching a pitch ring, with the correct hole sequence, to the blade side of the dynamometer. All mating of the dynamometer parts was conducted with stainless steel machine screws or grade eight machine screws sealed with waterproofing to prevent rusting. The blades themselves were mounted with two stainless steel bolts each.

In an attempt to reduce the amount of noise picked up by the strain gauges, they were outfitted with an electrical pre-amplification of approximately 100 times, thereby reducing the amount of amplification required at the output and allowing higher voltages to be transmitted over the slip rings. Wiring for the blade dynamometer was then run through the hub back through the drive shaft to a small circuit board, which connected it to a power supply through a set of slip rings. The same slip ring set was used to convey the resulting six outputs to the signal conditioning box where further electrical amplification was conducted to increase the output values to approximately 75% of the voltage required for full-scale deflection. Due to the high rotational speed and the requirement of a large number of data points over each blade-ice contact, each of these channels was sampled at 5000 Hz.

The design load limits of the blade dynamometer were as follows: maximum forces in the  $x$  and  $y$  directions were both 800 N, maximum force in the  $z$  direction was 600 N. Moment maximums were 85 Nm about both  $x$  and  $y$  axes and 50 Nm about  $z$  axis. Figure 5-4 shows the definitions of  $x$ ,  $y$ , and  $z$  directions with respect to the dynamometer. It also shows the orientation of these directions with respect to the propeller. Note that in this picture the propeller would be rotating counter clockwise and progressing forward out of the page.

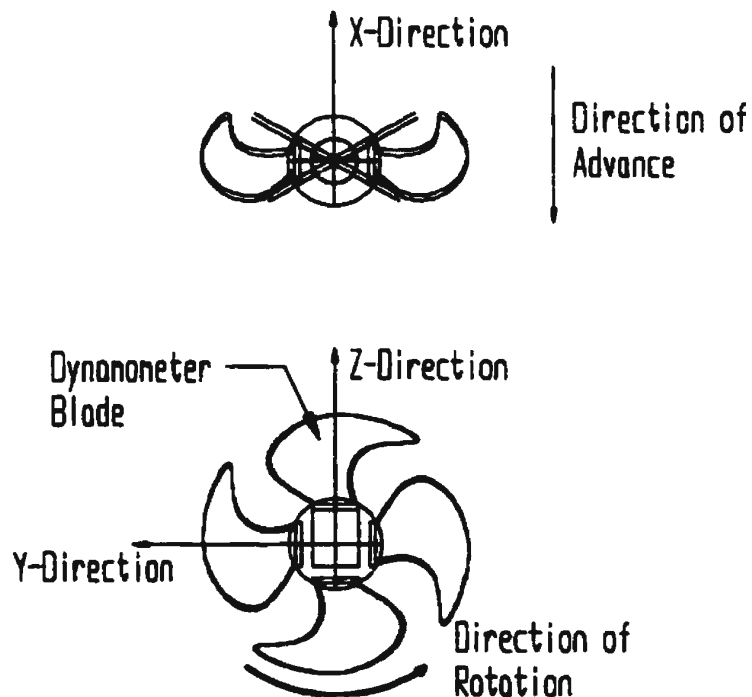


Figure 5-4 Directions  $x$ ,  $y$ , and  $z$  on the propeller

Calibration of the blade dynamometer was conducted by securely mounting the hub, containing the dynamometer inside, in a known position and applying known loads and moments to the blade end of the dynamometer. These loads were applied in such a way that the dynamometer was excited in the positive and negative directions of all six components. To determine interaction effects, the relative magnitude of forces and moments were varied for different calibration setups. The data was then analyzed to produce a calibration matrix, which was then confirmed using 45 linearly independent loading conditions designed to simulate the expected operating range of the dynamometer during ice interactions. Once the tests were complete an abbreviated set of calibration loads was also applied to the dynamometer to ensure that no damage was done during the tests. This showed that, with only very minor differences, the dynamometer maintained its original calibration properties.

#### **5.3.4 Description of the Blades**

The model propeller blades were provided by Lloyd's Register. They were 1:19.259 scale models of a propeller design identified as model number 6603. The blades were highly skewed with a  $P/D$  at the 0.7 radius fraction of 1.337, and a skew of  $50^\circ$ . Expanded area ratio of the blade was 0.542 and the projected area ratio was 0.449. The model was a four bladed adjustable pitch propeller, 270 mm in diameter, similar to that described by Searle et al. (1999) and similar in design to various propellers used on passenger ferries in Canada and Europe. Figure 5-5 shows a photo of the assembled propeller.

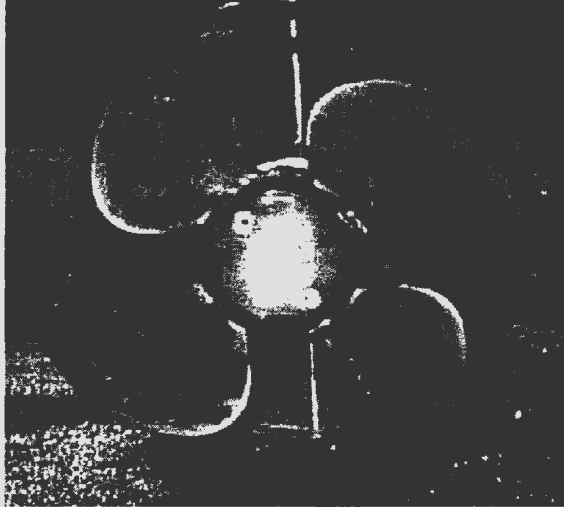


Figure 5-5 Assembled model propeller

### **5.3.5 Blade Quality Control**

To ensure that the blades provided were of a quality high enough to remove hydrodynamic variation as a source of error all four blades were checked. To complete this quality check a mounting stand for the blade was first designed and constructed. This mounting block was designed to attach to a rotary table and rotate about the shaft axis location. At the same time the blade being tested was mounted at the correct radius to simulate the actual propeller radius. Positions on the blade could then be measured using a milling machine and a touch probe, and the angular location of the rotary table to give an accuracy of within  $\pm 0.001''$ .

### **5.3.6 Other Sensor Equipment**

Other sensors were used to measure the shaft load, shaft speed, propeller submergence, and carriage speed.

Shaft loads were measured using an in-line dynamometer manufactured by Sensor Development Inc. that had a maximum thrust load rating of 890 N and maximum torque load rating of 110 Nm. The dynamometer had 100% overload capacity and maximum rotational speed of 20 rps. These two channels were also sampled at 5000 Hz.

Shaft speed was measured by a tachometer built into the 3kW motor. The motor tachometer was calibrated using a laser tachometer. The motor was run through a series of settings and the rotational speed on the propeller side of the gearbox was measured using the laser tachometer. The settings for the correct motor speeds were then determined. As the rotational speed was not expected to vary greatly in the ice it was sampled at 100 Hz to conserve memory space.

Propeller submergence was measured using a potentiometer, in which the base unit was mounted to the carriage and the end of the wire was attached to the test frame holding the propeller boat. The zero value for this potentiometer was set at the point where the upper edge of the propeller circle just failed to break the surface of the water. Once set, the vertical position of the test frame did not change and as such it was sampled at only 50 Hz.

Carriage speed was recorded from a tachometer built into the drive motors of the carriage. Carriage speed did not vary greatly during the propeller interaction event. It was sampled at 100 Hz as well.

In addition to the sensors, three above water cameras were used to record the ice milling event. These recorded each test looking from the bow, starboard side and directly above the propeller.

### 5.3.7 Test Matrix

The following tables (Tables 5-1, 5-2, and 5-3) describe the test matrix used to guide these experiments. In the legends charts pitches are defined from zero pitch, i.e. the design pitch is 31.30°. All tests were performed at a shaft speed of 10 rps. Below the pitch designation for each test are two ice strength values. These are the compressive and flexural strengths respectively of the ice in kPa. The values stated are estimated by linearly interpolating between the two measured values nearest the test case.

Table 5-1 Test matrix for sheet number 2

Sheet 2									
A indicates a Test at Pitch Setting =					31.30°				
F indicates a Test at Pitch Setting =					24.07°				
B indicates a Test at Pitch Setting =					18.03°				
C indicates a Test at Pitch Setting =					- 28.93°				
h <sub>i</sub> [mm]	Advance Ratio								
	0.1	0.2	0.3	0.4	0.5	0.6	0.7		
0	F		F		F				
	90	28		90	28		90	28	
10	F		F		F		F		F
		104	32	104	32	103	32		103
20	F		F		F				
	90	25		90	25		90	25	
30	F		F		F				
	90	25		90	25		90	25	
34	F		F		F		F		
		90	31	90	31	97	30		97
40	F		F		F		F		
		93	29	93	29	93	29		93
50	F		F		F				
	90	24		90	24		90	24	

Table 5-2 Test matrix for sheet number 3

Sheet 3									
A indicates a Test at Pitch Setting =					31.30°				
F indicates a Test at Pitch Setting =					24.67°				
B indicates a Test at Pitch Setting =					18.03°				
C indicates a Test at Pitch Setting =					-20.93°				
$r_h$	Advance Ratio								
(mm)	0.1	0.2	0.3	0.4	0.5	0.6	0.7		
6	CB	CB	B						
	85   37	86   37	86   37						
16	CB	CB	B						
	84   38	84   38	84   38						
24.5	CB	CB	B						
	84   38	84   38	84   38						
34					F	F			
					148   48	148   48			
40		F	F	F		F	F		
		133   48	127   48	121   48		112   48	107   48		
50	F	F	F	F	F	F			
	71   31	71   31	71   31	71   31	71   31	71   31			
54.4		F	F	F		F			
		87   40	87   40	87   40		87   40			

Table 5-3 Test matrix for sheet number 4

Sheet 4									
A indicates a Test at Pitch Setting =					31.30°				
F indicates a Test at Pitch Setting =					24.67°				
B indicates a Test at Pitch Setting =					18.03°				
C indicates a Test at Pitch Setting =					-20.93°				
$r_h$	Advance Ratio								
(mm)	0.1	0.2	0.3	0.4	0.5	0.7	0.8		
6			C						
			160   30						
16			C						
			160   30						
20.6	A		CA	A	A	A	A		
	183   60		183   50	183   58	183   50	183   57	183   37		
28	C	C	C						
	160   28	160   28	160   28						
34	A		A	A	A	A	A		
	194   38		194   38	194   38	194   38	194   54	177   38		
43	A		A	A	A	A	A		
	188   32		188   32	188   48	188   48	188   48	188   33		
48	A		A	A	A	A	A		
	167   48		167   48	168   48	168   44	168   44	173   38		
60	A		A	A	A	A	A		
	188   42		188   41	181   38	188   38	187   38	188   29		

5.3.8 Blade Preparation

Blade pitch was first verified to ensure the blades were all at the correct pitch for the particular set of tests. After placing each blade in the correct pitch setting the entire

propeller boat was lowered to its zero position and then raised out of the water and run through a series of shaft speeds from 8 rps to 14.5 rps in order to determine the frictional torque loads exerted on the system. These loads were then used as the zero loading offsets to determine the load exerted on the blade due to the ice and water. By performing these friction tests the centrifugal force exerted on the blade dynamometer could also be removed from the measured loads.

After completion of the friction run, the propeller was lowered into the water such that the blade would cut into the ice at the target depth. To ensure this depth was correct the propeller was slowly advanced into the ice sheet at slow rotational speed to prevent disturbing the ice and the resulting cut depth.

### **5.3.9 Test Run**

Once blade submergence had been verified the test was ready to commence. The carriage was programmed to run for at least 3 seconds at the target constant speed. The data collection system was started and the propeller held at zero rps for 3 seconds to establish a baseline. The propeller speed was then increased to 10 rps and a bollard pull recorded for 3 seconds. The bollard pull result was used between runs to ensure the blade dynamometer was not drifting. After the bollard pull test, the carriage was started and the propeller was run into the ice for the programmed distance. As soon as the carriage was stopped the data collection was stopped and the carriage backed off so that the actual cut depth could be examined. It was found that as the ice softened it became impossible to

measure cut depth after the test run as the ice path was totally destroyed. In these cases the measurement taken at the start of the run was taken as the cut depth.

After all of the tests at a particular pitch were completed a friction test was run again.

## **5.4 Results**

The following graphs, Figures 5-6 to 5-8 show the maximum, mean and minimum values for thrust and torque coefficient at three pitches,  $31.30^\circ$ ,  $24.07^\circ$ , and  $-20.93^\circ$ . These are shown for a similar depth of cut of approximately 34 mm for the first two pitch settings and a depth of cut of 28 mm for the  $-20.93^\circ$  pitch setting. The following three figures (Figure 5-9 to 5-11) show the mean values for the remaining depths of cut at these same pitch settings. Four additional depths of cut are presented for the design pitch ( $31.30^\circ$ ), seven at the reduced pitch of  $24.07^\circ$ , and three at the reverse pitch setting of  $-20.93^\circ$ . (To maintain standard propeller coefficient convention, torque coefficient is multiplied by a factor of 10).

Based on the thrust and torque coefficients, it was shown that in general as the depth of cut increases the additional shaft loading as a result of the ice is more pronounced on the torque than on thrust. This is shown in the graphs by comparing the average thrust and torque curves for both a low and high depth of cut to the open water curves for the same pitch setting. For example, in Figure 5-9, at the design pitch and depth of cut of 20.5 mm the thrust coefficient is approximately 0.05 higher than the open water curve. Similarly, the  $10 \times$  torque coefficient curve for the same depth of cut is up to about 0.2 above the

open water curve. In the same figure at a depth of cut of 60.0 mm the thrust coefficient curve is up to 0.4 above the open water curve, while the  $10 \times$  torque coefficient curve is over 1.0 higher than the open water case. Similar results can be seen at the other pitch settings and cut depths.

It was also found that the increase in loading on shaft loads occurred at progressively lower cut depths as the pitch was reduced from the design pitch. That is, conditions farther from the design conditions increase the amount of ice loading. For example, at the reverse pitch setting of  $-20.93^\circ$ , Figure 5-11, the average thrust and torque coefficients are larger at the lowest cut depth of 8.0 mm than in the open water case. However, at a reduced pitch of  $24.07^\circ$  and a cut depth of 18.0 mm, Figure 5-10, thrust and torque coefficient curves are only marginally different from the open water values. At the design pitch of  $31.30^\circ$  and cut depth of 20.5 mm, Figure 5-9, these curves are slightly higher than those for open water, but not as much as in the reverse pitch of  $-20.93^\circ$ .

As the cut depth increased from open water to 60mm for the design pitch, shaft loading was observed to increase. At advance coefficients less than 0.3 this increase was less pronounced than at advance coefficients between 0.3 and 0.6, where the increase was seen to be on the order of the original open water thrust and torque values. As the advance coefficient increased beyond about 0.6 the thrust and torque values were seen to begin to drop quickly.

At the reduced pitch of  $24.07^\circ$ , the increase in thrust with advance ratio and cut depth seen in the design pitch data was observed (Figure 5-10), but was not as marked as in the design case. The torque load, however, did show the same near 2 times increase in load between advance coefficients of 0.2 and 0.5. The drop in shaft load observed above an advance coefficient of 0.6 in the design case was seen at a lower advance coefficient in the reduced case, starting at a value of around 0.5.

Below the graphs for thrust and torque coefficients are two graphs that illustrate the effect of two different ice strengths, 29.7 kPa and 40.9 kPa flexural strength, on the thrust and torque coefficients. In the first, Figure 5-12(a), the effect of the depth of cut at a constant advance ratio of 0.3 is illustrated. It can be seen that at the lower cut depth the softer ice appears to cause more thrust load. At the higher ice strengths the torque is higher than at the lower ice strength.

Figure 5-12(b) shows the effect of ice strength on the thrust and torque coefficients over a range of advance ratios. As noted previously, the thrust coefficient was influenced less by ice strength than the torque. This is shown in the percentage increase in thrust coefficient. The higher ice strength resulted in about a 10% increase in thrust at higher advance ratios ( $J > 0.4$ ) where it appears to result in a nearly constant difference. In the same region the torque coefficient was approximately 30 to 50% higher. At lower advance ratios the thrust coefficient shows little change with change in ice strength, while the torque continues to increase significantly at the higher ice strength.

Following the results from the shaft dynamometer are a series of charts depicting the loads recorded by the blade dynamometer. The first three figures, Figure 5-13 to Figure 5-15, illustrate the resultant blade loads as a result of ice milling for two complete blade cycles, at a pitch setting of  $24.07^\circ$ , an advance coefficient of 0.2 and a depth of cut of 34.0 mm. These loads include the hydrodynamic effects on the blade but have the centrifugal loads removed through the taring process. Mean open water loads for the same pitch setting and advance coefficient are also shown. The orientations of the blade loads are defined using the axis convention shown in Figure 5-4.

The blade load results are seen to follow patterns similar to those calculated numerically by Doucet et al. (1998), where ice milling and hydrodynamic loads on several conventional, non-skewed, propellers were calculated. Liu et al. (2000) published results that show a decrease in both the thrust and torque experienced by the blade immediately before the blade contacted the ice feature. This was followed by a subsequent increase as a result of the ice interaction. A similar dip can be observed in both the thrust (negative  $X$ -Force) and torque ( $X$ -Moment) directions, Figure 5-13(a) and Figure 5-13(b) at a time of 0.09 seconds. While there was no method provided in these experiments to determine exactly when the instrumented blade entered the ice sheet, the similarity between the physical model results and numerical predictions lends credence to the assumption that the entry occurs at the point where the loads begin to increase, i.e. at a time of 0.1 seconds. Based on the shaft loads observed for this situation, Figure 5-7(a) and (b), the thrust and torque were both seen to increase above the open water value. This is also shown in the blade load data in that the  $x$  force and  $x$  moment see increases in load. Note

that an increase in thrust loading results in the value of  $x$ -force becoming more negative in the blade dynamometer loads as a result of the dynamometer axis orientation.

Figures 5-16 to 5-18 show the maximum, mean and minimum thrust and torque coefficients experienced by the single blade. In this case the maximum and minimum loads are defined as the average of the top (bottom) 1% of the data points from five consecutive milling cycles, or approximately the highest (lowest) 25 points in a series of approximately 2500 data points.

In Figures 5-16 to 5-18, blade thrust and torque coefficients are plotted as a function of advance ratio at the same pitch settings and cut depths as in the previously discussed shaft loads. These figures illustrate how the load experienced by a single blade is affected by the milling process, including the measured maximum and minimum loading. The following charts, Figures 5-19 to 5-21, show the mean blade loads observed for the other cut depths at these same blade pitches. Also included on all these charts are the mean open water curves divided by four to account for an individual blade.

It is shown that as the depth of cut increases the mean as well as the maximum load experienced by the blade increases from the open water load. For example, at the design pitch and a depth of cut of 20.5 mm the mean thrust and torque coefficients were approximately 50% and 25% higher, respectively, than the corresponding open water values. At a depth of cut of 60mm these same values were approximately 100% and 150% higher (Figure 5-19).

Figures 5-22 and Figure 5-23 show the minimum, mean and maximum individual blade results of thrust and torque coefficients plotted against the pitch angle for two depths of cut, mean depths of 17.6 mm and 31.0 mm, at advance coefficients of 0.2 and 0.3 respectively. These charts illustrate the off design concerns discussed previously. In the off design conditions, such as reverse pitch, large percentage changes in open water loads occur at low advance ratios and depths of cuts. These same relative changes are not observed at pitch angles closer to the design pitch until the propeller is operated at higher advance ratios or deeper depths of cut. These charts also support the observed occurrence of maximum loads, which can be several times greater than the open water or mean cycle loads.

The final set of plots, Figures 5-24 to 5-29, shows the out of plane and in plane bending moments that were recorded about the base of the blade. In this case the blade plane is defined as the plane containing the root section pitch line (pitch angle of  $42.3^\circ$  when the blade is at the design pitch).

When the mean value of the out of plane bending moment is calculated and compared to the open water curve for the design pitch, Figure 5-24(a), the load shows a moderate increase at low advance coefficient. However, for the same conditions the maximum observed out of plane bending moment is almost two times larger than the open water results. Similar trends are also seen in the plot of in plane bending moment, Figure 5-24(b), where the maximum loads have a magnitude that is approximately 2 to 4 times larger than the open water results. One noteworthy result that was observed is that while

the direction of the out of plane bending did not normally change from mean to maximum value, the maximum in plane bending moment in ice was often of different sign than that of the open water result.

At reduced pitch the out of plane bending moment maximums were observed to decrease from those measured at the design pitch. For example, at the same nominal cut depth of approximately 34mm, the out of plane bending moment at 24.07°, Figure 5-25(a), had a maximum of approximately 16Nm. At the design pitch, Figure 5-24(a), the maximum was observed to be approximately 25Nm. The maximum and mean in plane bending moments were observed to be approximately the same in both the design case and in the 24.07° case for the same depth of cut.

For the -20.93° pitch, Figure 5-29(a) and (b) the mean out of plane bending moments were slightly lower than the open water situation. The in plane bending moment was larger than the open water case, but only marginally so. The minimums, Figure 5-26(a) and (b) were observed to be approximately 5 times the open water results.

A summary of the maximum and minimum values for blade thrust, torque, and out of plane bending moment observed at each pitch is included in Table 5-4. The advance coefficient and depth of cut at which the maximum and minimum occurred are also included (in this table the depth of cut ( $h_i$ ) is measured in mm). For comparison the mean open water bollard values are also included.

**Table 5-4 Maximum and minimum blade load table**

Pitch (°)	Blade Load								
	Thrust [N]			Torque [Nm]			Out of Plane BM [Nm]		
	OW	Max	Min	OW	Max	Min	OW	Max	Min
31.30	82.8	338.2	0.7	3.80	29.59	-0.61	8.40	53.22	-13.18
settings	J=0	J=0.7, h <sub>i</sub> =46	J=0.8, h <sub>i</sub> =36	J=0	J=0.6, h <sub>i</sub> =60	J=0.7, h <sub>i</sub> =46	J=0	J=0.1, h <sub>i</sub> =60	J=0.1, h <sub>i</sub> =46
24.07	60.6	168.9	-67.6	2.10	12.20	-0.32	2.83	20.90	-6.70
settings	J=0	J=0.2, h <sub>i</sub> =51	J=0.6, h <sub>i</sub> =28	J=0	J=0.4, h <sub>i</sub> =51	J=0.6, h <sub>i</sub> =40	J=0	J=0.4, h <sub>i</sub> =50	J=0.1, h <sub>i</sub> =50
-20.97	-25.7	-140.7	7.1	1.51	7.87	-0.50	1.48	17.53	-0.33
settings	J=0	J=0.3, h <sub>i</sub> =28	J=0.2, h <sub>i</sub> =16	J=0	J=0.2, h <sub>i</sub> =28	J=0.3, h <sub>i</sub> =8	J=0	J=0.3, h <sub>i</sub> =28	J=0.3, h <sub>i</sub> =28

## 5.5 Conclusions

The results from a series of model propeller ice interaction tests have been presented. These detail the results from both a shaft dynamometer measuring shaft thrust and torque and a blade dynamometer measuring six components of load on an individual blade during the ice milling process. Using a highly skewed model propeller the thrust and torque loads were measured as the blade milled into a sheet of model ice at various pitch settings and depths of cut. The loads on the blade were observed to increase as a result of the propeller milling into the ice sheet.

The maximum thrust and torque loads on an individual blade, as well as the out of plane bending moment, were observed to reach values equal to or greater than the total propeller open water values in certain ice milling conditions. For example the maximum out of plane bending moment for an individual blade in the design condition was 53.22Nm while the bollard pull value for the same pitch was 8.40Nm. Maximum blade thrust in the design condition reached 338.2N as well, which was greater than the total

propeller design pitch bollard pull value of 331.2N (82.8N per blade). The cyclic nature of this extreme load on each blade (once per propeller revolution) indicates that allowances for fatigue should figure prominently in the design of propellers and propulsion systems used in ice navigation.

## **5.6 Acknowledgements**

This research was funded primarily through a joint project between Transport Canada, Lloyd's Register, and the National Research Council Canada. The first author acknowledges with gratitude the financial support of the Natural Sciences and Engineering Research Council (Canada) and the Government of Newfoundland & Labrador.

Thanks are due to the people from Oceanic Consulting Corporation, Art Bowker Inc, and Memorial University's Technical Services Department for their help in the experimental work. Special thanks are extended to the ice tank crew at IMD for their assistance in conducting the experiments. Finally, we acknowledge the valuable contribution that Mr. John Bell and Mr. Ed Kennedy made to the research, particularly their role in the blade dynamometer design, fabrication and calibration.

## **5.7 References**

- Bose, N., Veitch, B. and Doucet, M. 1998. A design approach for ice class propellers. *Transactions, Society of Naval Architects and Marine Engineers*, Vol. 106.
- Doucet, J.M., Bose, N., and Veitch, B. 1999. Selection of scantlings for an ice class propeller: A case study for the *MV Ikaluk*. *Proceedings, Offshore Mechanics and Arctic Engineering*, American Society of Mechanical Engineers, 8 pp.

- Doucet, J.M., Liu, P., Bose, N., and Veitch, B. 1998. Numerical prediction of ice-induced loads on ice-class screw propellers using a synthesized contact/hydrodynamic code, Ocean Engineering Research Centre Report No. OERC-1998-004.**
- Jones, S.J. 1987. Ice tank Test Procedures at the Institute for Marine Dynamics. *Institute for Marine Dynamics Report No. LM-AVR-20.***
- Katsman, F.M., and Andruishin, A.V. 1997, *Strength Rates for Blades as Intended for the Propellers of Ice Breakers and Ice Ships*, Russian Maritime Register of Shipping.**
- Koskinen, P., Jussila, M. and Soinen, H., 1996, Propeller Ice Loads Models, Technical Research Centre of Finland, Research Notes 1739.**
- Liu, P., Doucet, M., Veitch, B., Robbins, I., and Bose, N. 2000. Numerical prediction of ice induced hydrodynamic loads on propellers due to blockage. *Oceanic Engineering International*, Vol.4, No.1, pp.31-38.**
- Searle, S., Veitch, B., and Bose, N., 1999, Ice-Class Propeller Performance in Extreme Conditions, *Transactions, Society of Naval Architects and Marine Engineers Vol 107.***
- Timco, G.W. 1986. EG/AD/S: A New Type of Model Ice for Refrigerated Towing Tanks. *Cold Regions Science and Technology*. Vol. 12: pages 175-195.**

## 5.8 Figures

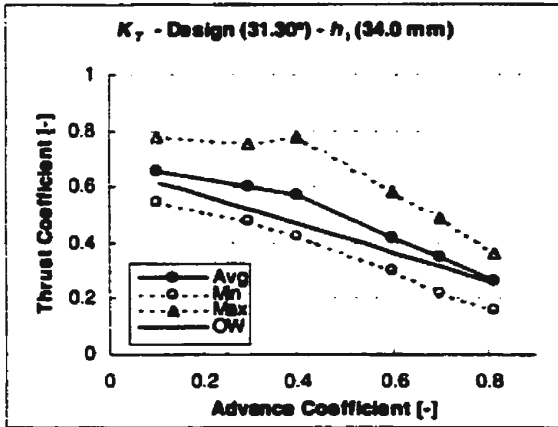
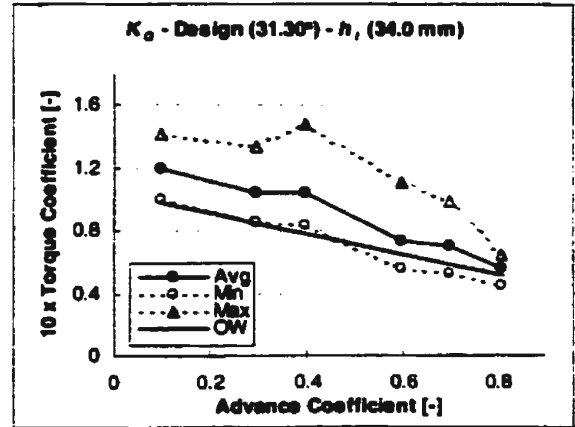


Figure 5-6 a)  $K_T - \phi = 31.30^\circ - h_i = 34.0 \text{ mm}$



b)  $K_Q - \phi = 31.30^\circ - h_i = 34.0 \text{ mm}$

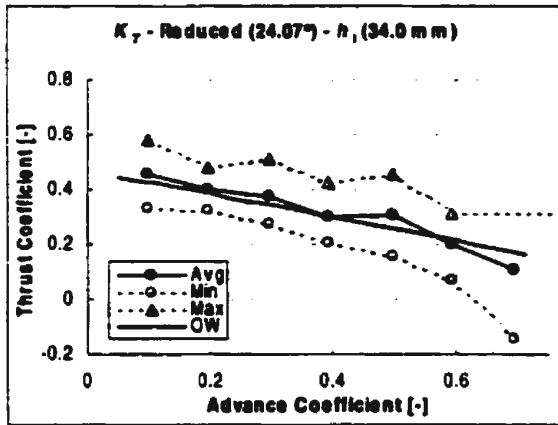
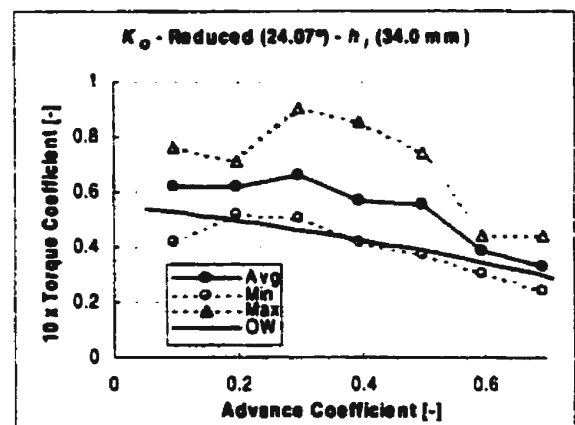


Figure 5-7 a)  $K_T - \phi = 24.07^\circ - h_i = 34.0 \text{ mm}$



b)  $K_Q - \phi = 24.07^\circ - h_i = 34.0 \text{ mm}$

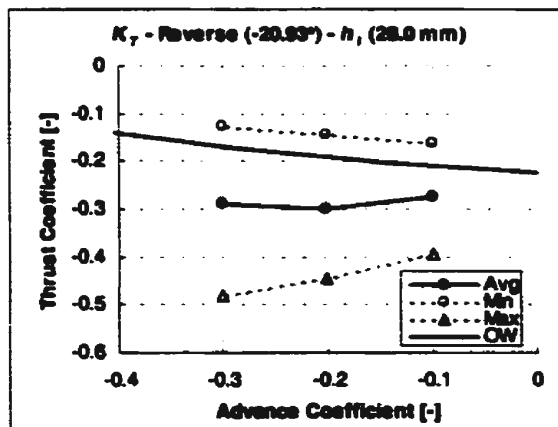
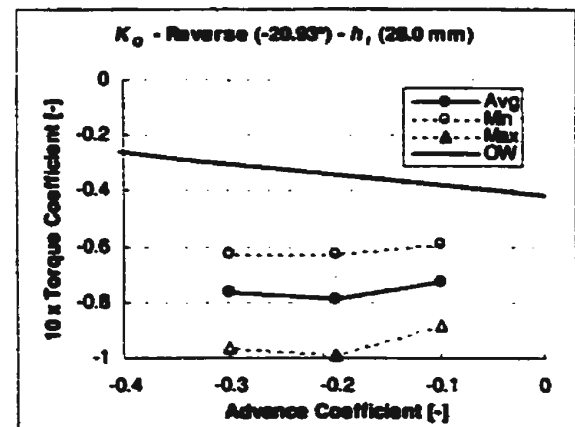


Figure 5-8 a)  $K_T - \phi = -20.93^\circ - h_i = 28.0 \text{ mm}$



b)  $K_Q - \phi = -20.93^\circ - h_i = 28.0 \text{ mm}$

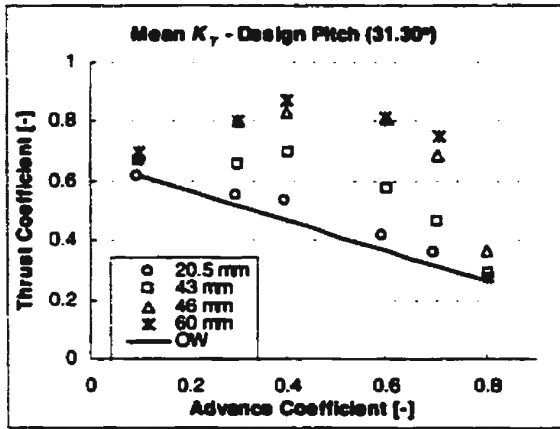
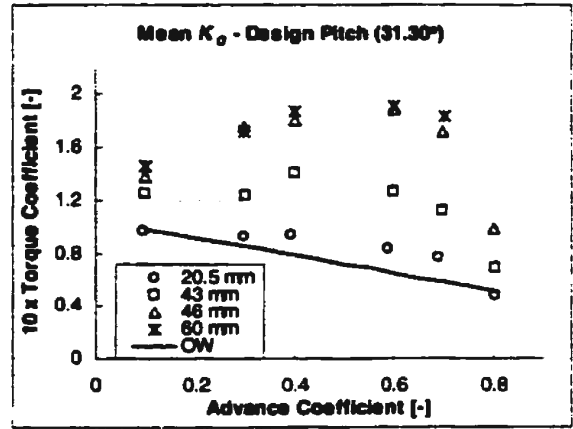


Figure 5-9 a)  $K_T - \phi = 31.30^\circ$  - Range of  $h_i$



b)  $K_Q - \phi = 31.30^\circ$  - Range of  $h_i$

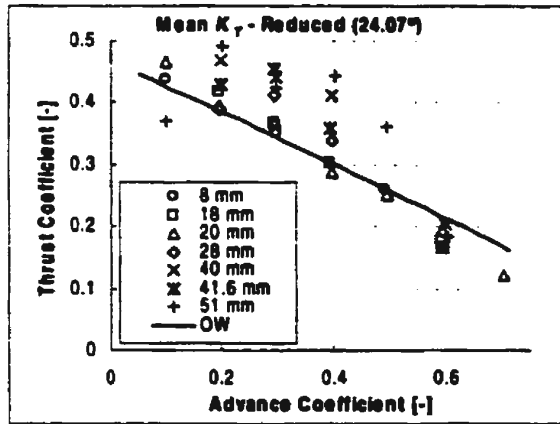
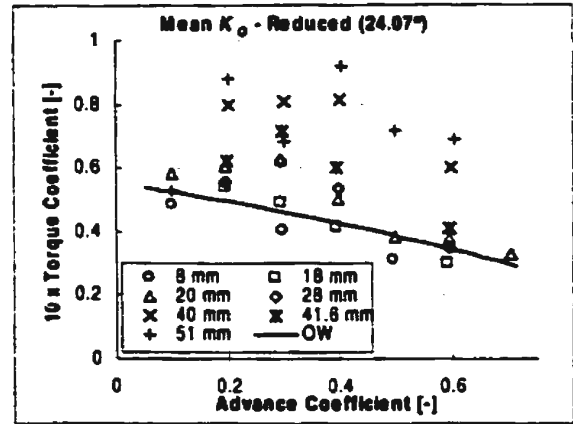


Figure 5-10 a)  $K_T - \phi = 24.07^\circ$  - Range of  $h_i$



b)  $K_Q - \phi = 24.07^\circ$  - Range of  $h_i$

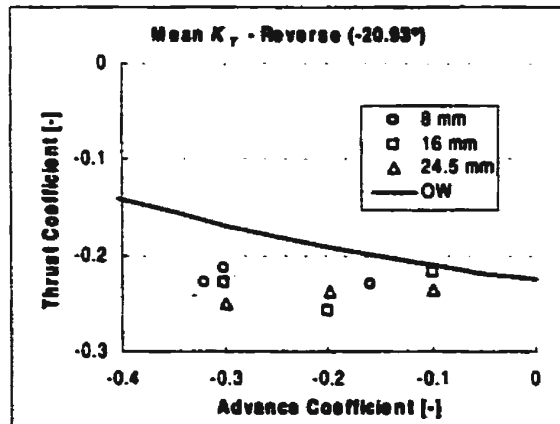
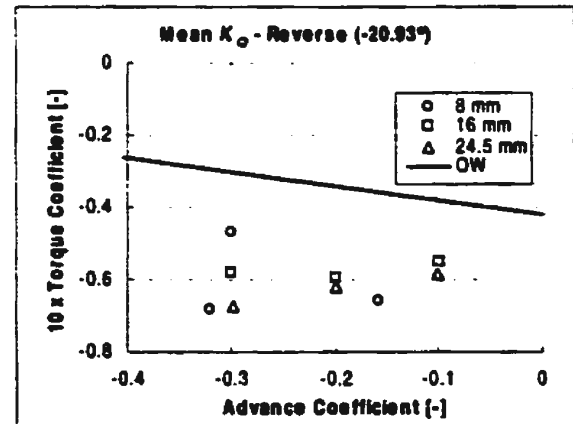


Figure 5-11 a)  $K_T - \phi = -20.93^\circ$  - Range of  $h_i$



b)  $K_Q - \phi = -20.93^\circ$  - Range of  $h_i$

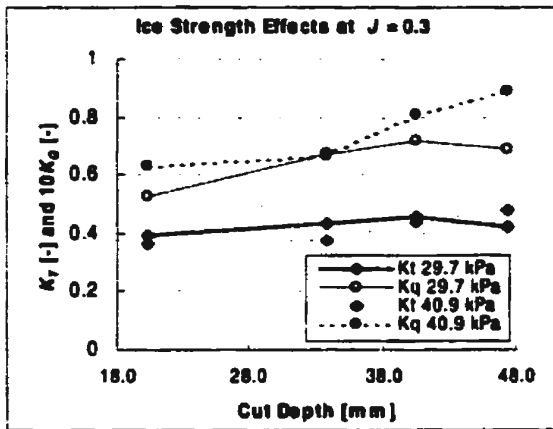


Figure 5-12 a) Effect of Ice Strength vs. Cut Depth

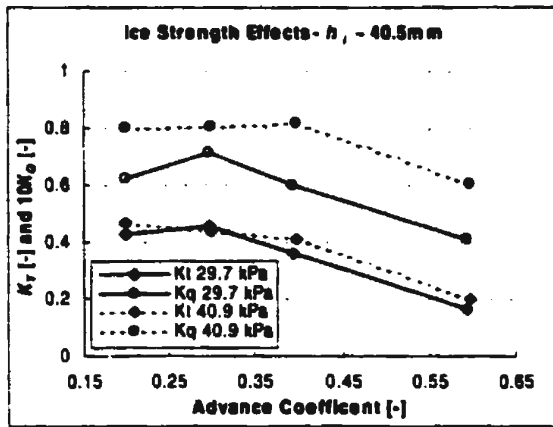


Figure 5-12 b) Effect of Ice Strength vs. Advance Coefficient

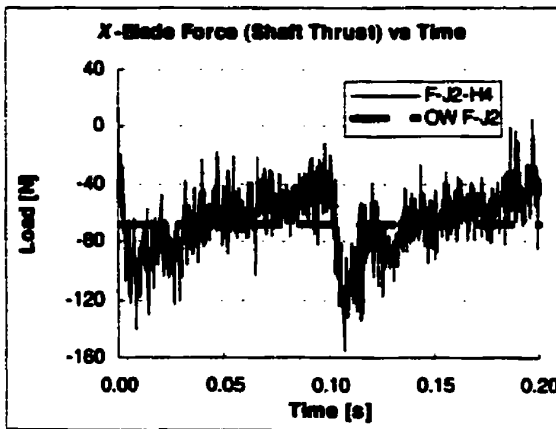
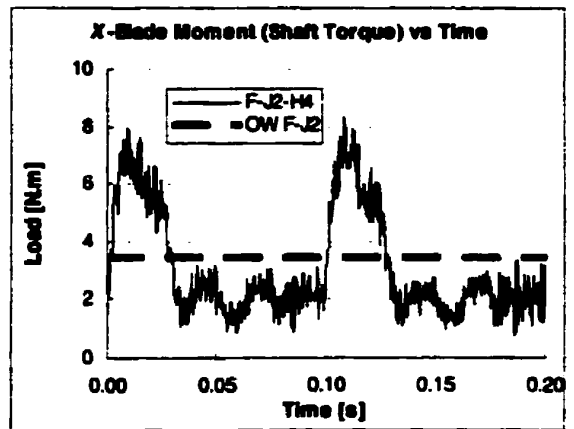


Figure 5-13 a) X-Force on Individual Blade



b) X-Moment on Individual Blade

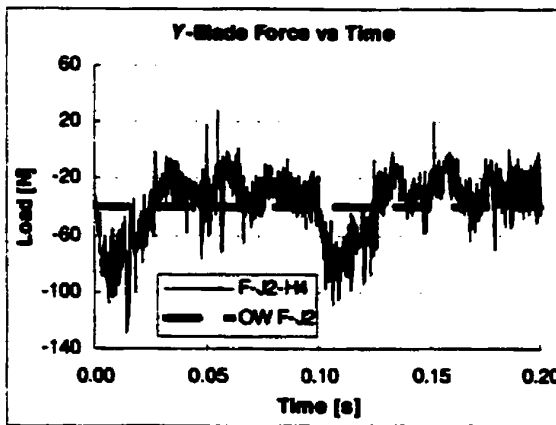
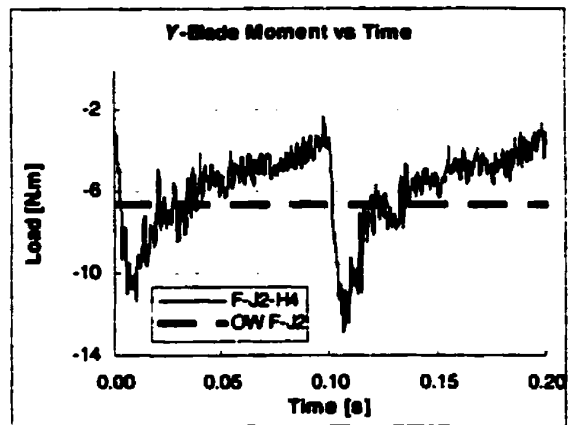


Figure 5-14 a) Y-Force on Individual Blade



b) Y-Moment on Individual Blade

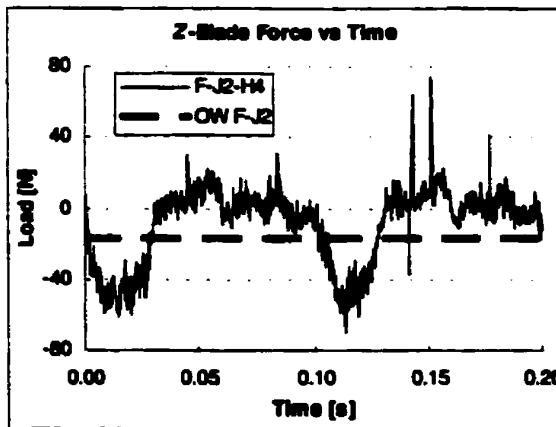
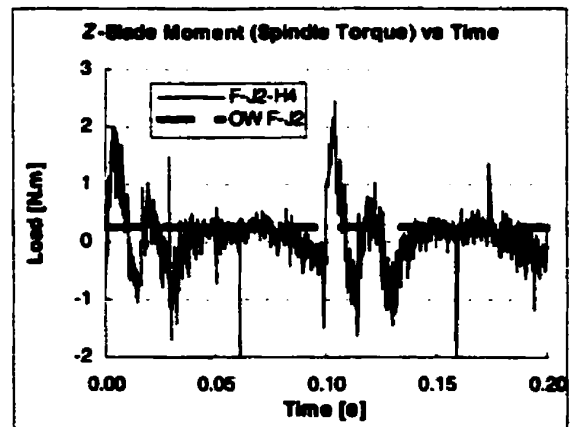


Figure 5-15 a) Z-Force on Individual Blade



b) Z-Moment on Individual Blade

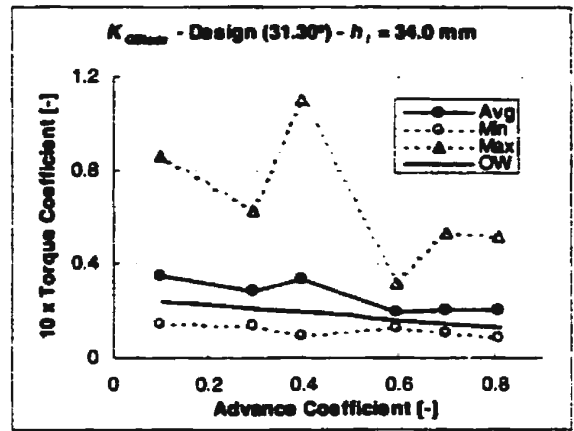
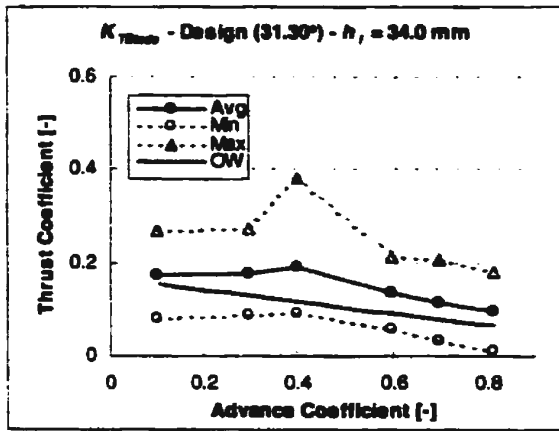


Figure 5-16 a)  $K_{T_{Blade}} - \Phi = 31.30^\circ - h_i = 34.0 \text{ mm}$  b)  $K_{Q_{Blade}} - \Phi = 31.30^\circ - h_i = 34.0 \text{ mm}$

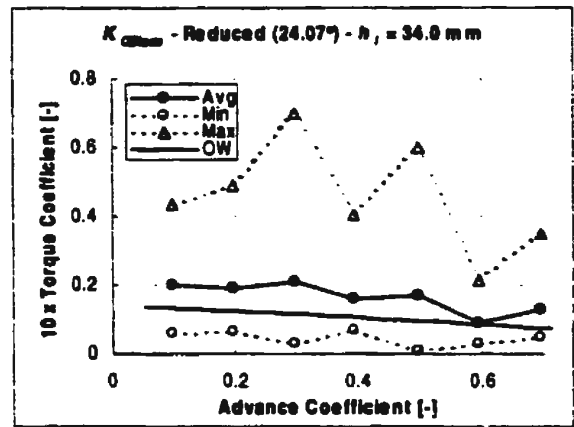
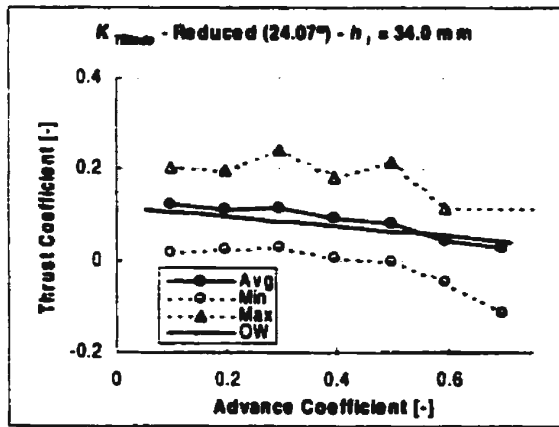


Figure 5-17 a)  $K_{T_{Blade}} - \Phi = 24.07^\circ - h_i = 34.0 \text{ mm}$  b)  $K_{Q_{Blade}} - \Phi = 24.07^\circ - h_i = 34.0 \text{ mm}$

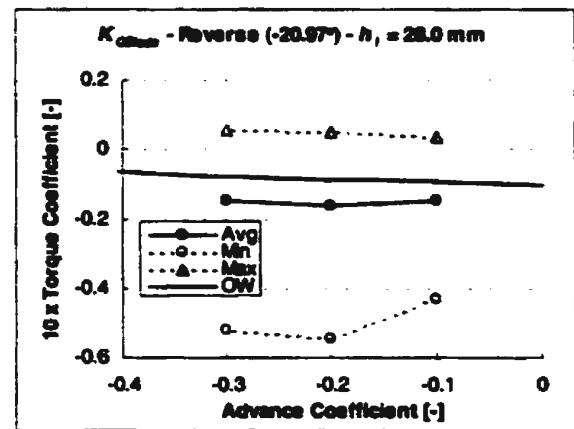
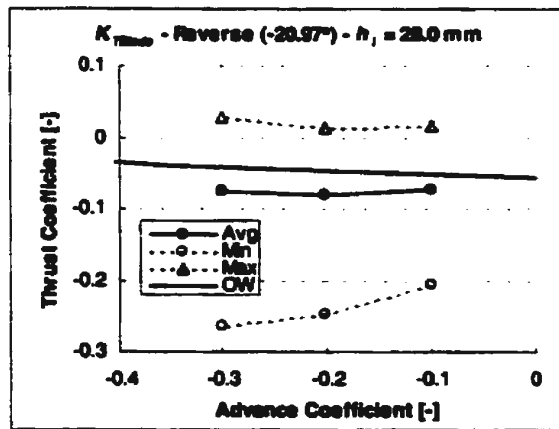


Figure 5-18 a)  $K_{T_{Blade}} - \Phi = -20.93^\circ - h_i = 28.0 \text{ mm}$  b)  $K_{Q_{Blade}} - \Phi = -20.93^\circ - h_i = 34.0 \text{ mm}$

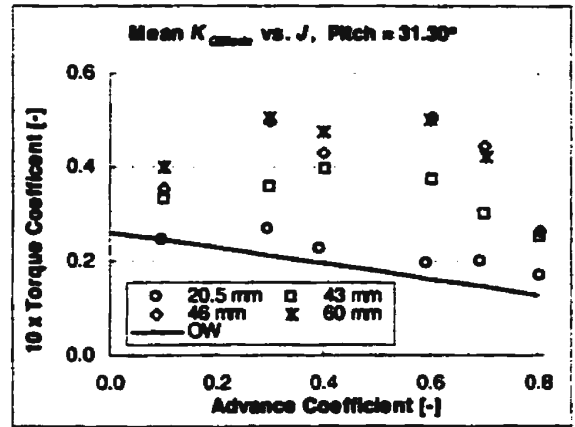
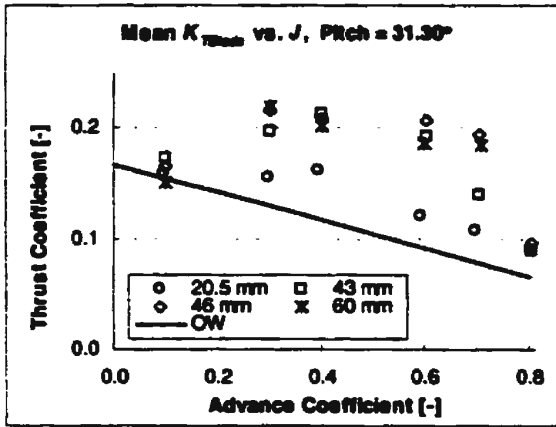


Figure 5-19 a)  $K_{TBlade} - \Phi = 31.30^\circ$  - Range of  $h_i$     b)  $K_{QBlade} - \Phi = 31.30^\circ$  - Range of  $h_i$

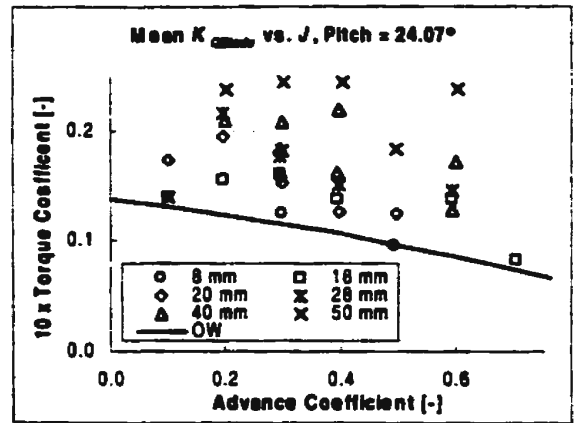
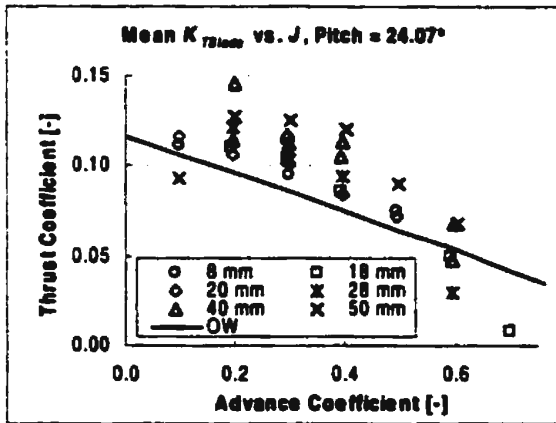


Figure 5-20 a)  $K_{TBlade} - \Phi = 24.07^\circ$  - Range of  $h_i$     b)  $K_{QBlade} - \Phi = 24.07^\circ$  - Range of  $h_i$

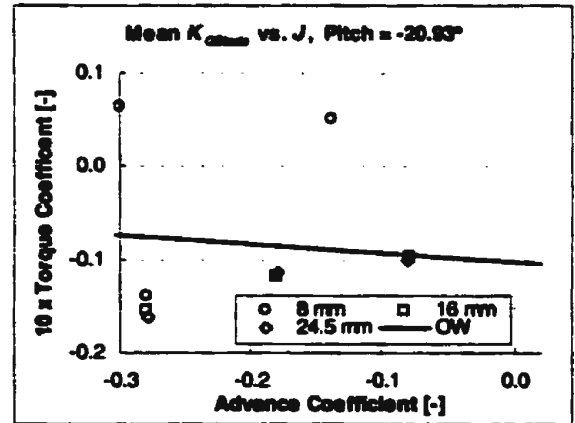
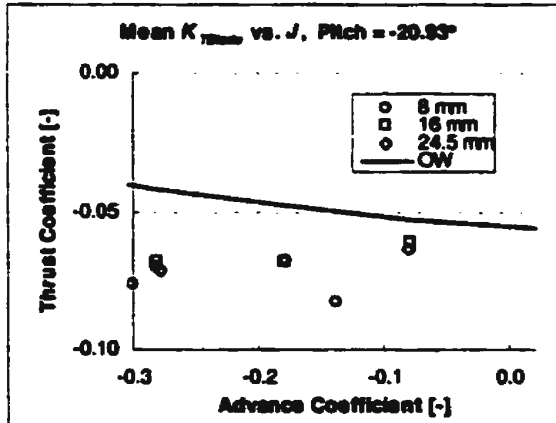


Figure 5-21 a)  $K_{TBlade} - \Phi = -20.93^\circ$  - Range of  $h_i$     b)  $K_{QBlade} - \Phi = -20.93^\circ$  - Range of  $h_i$

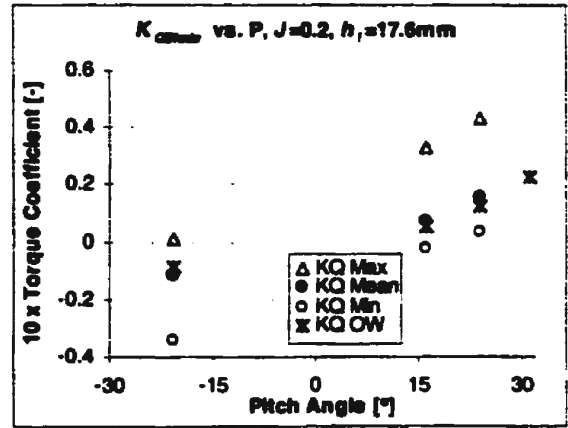
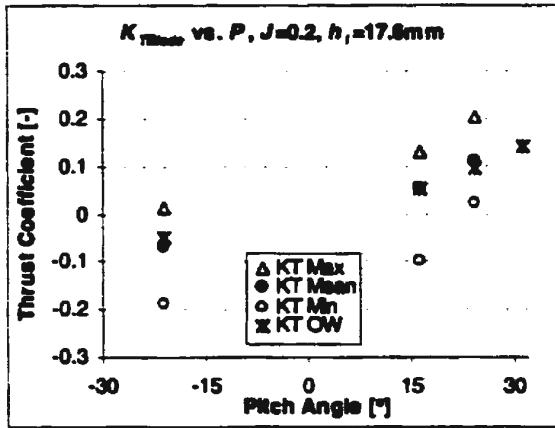


Figure 5-22 a)  $K_{Tblade}$  vs.  $\Phi$  (17.6 mm Mean Cut)      b)  $K_{Qblade}$  vs.  $\Phi$  (17.6 mm Mean Cut)

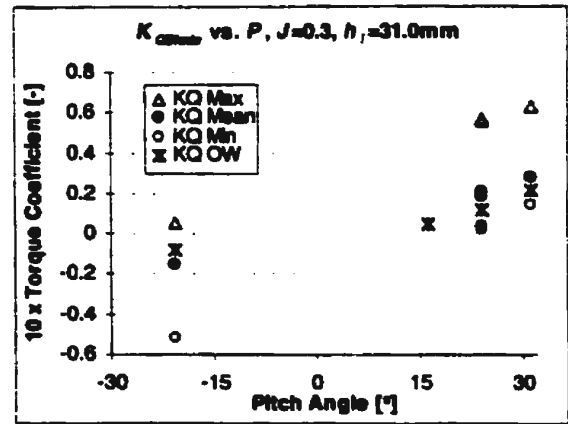
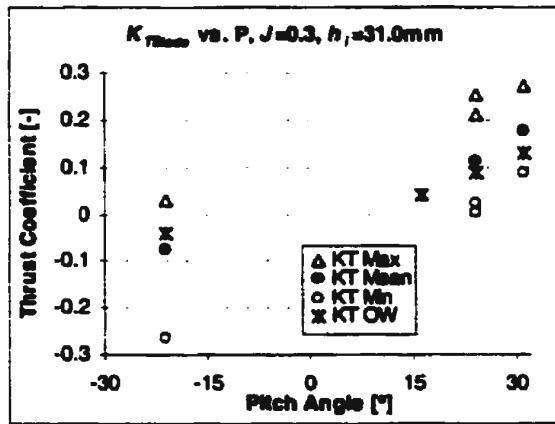


Figure 5-23 a)  $K_{Tblade}$  vs.  $\Phi$  (31.0 mm Mean Cut)      b)  $K_{Qblade}$  vs.  $\Phi$  (31.0 mm Mean Cut)

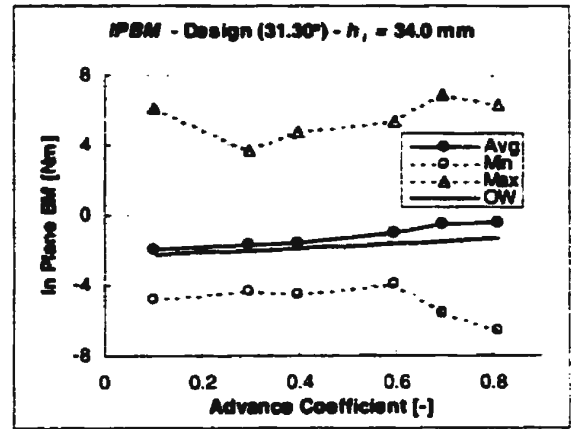
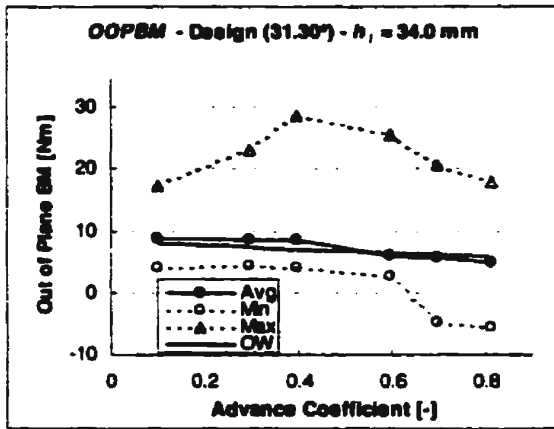


Figure 5-24 a) *OOPBM* -  $\Phi = 31.30^\circ$  -  $h_i = 34.0$  mm    b) *IPBM* -  $\Phi = 31.30^\circ$  -  $h_i = 34.0$  mm

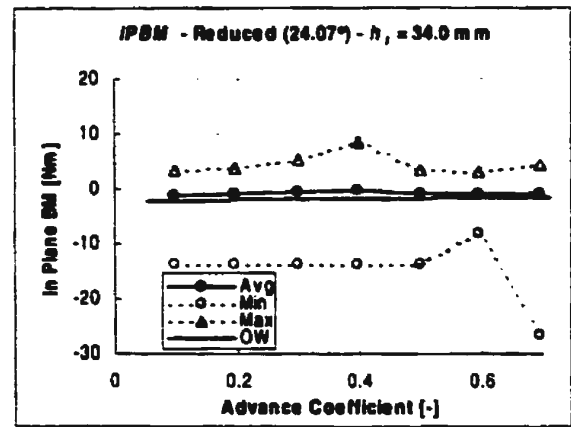
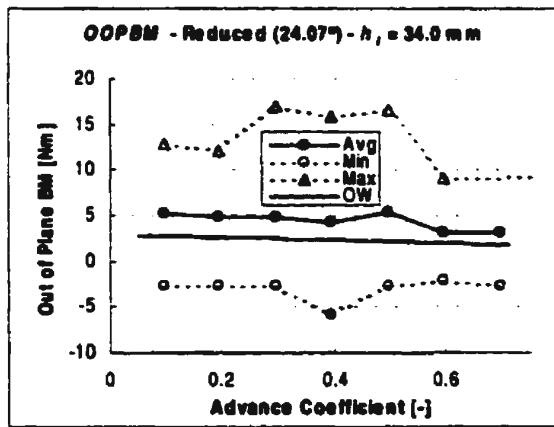


Figure 5-25 a) *OOPBM* -  $\Phi = 24.07^\circ$  -  $h_i = 34.0$  mm    b) *IPBM* -  $\Phi = 24.07^\circ$  -  $h_i = 34.0$  mm

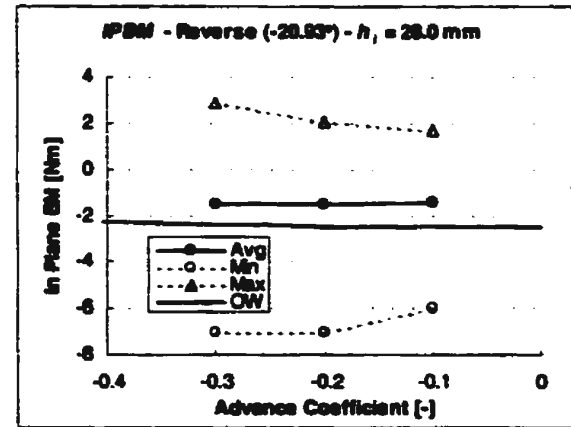
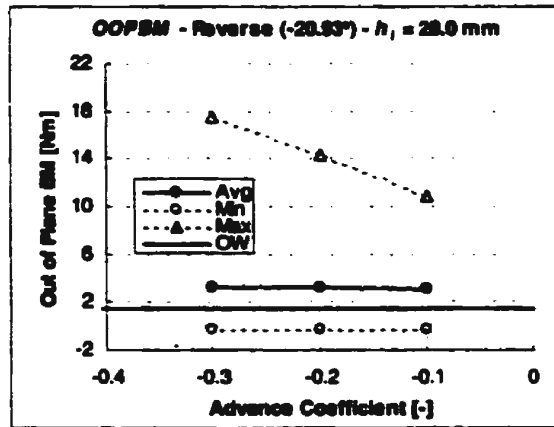


Figure 5-26 a) *OOPBM* -  $\Phi = -20.93^\circ$  -  $h_i = 28.0$  mm    b) *IPBM* -  $\Phi = -20.93^\circ$  -  $h_i = 28.0$  mm

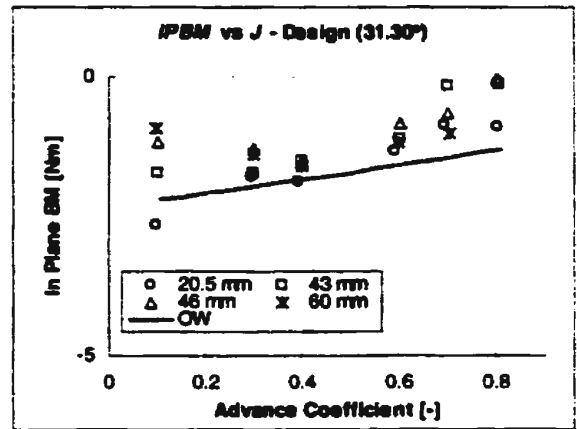
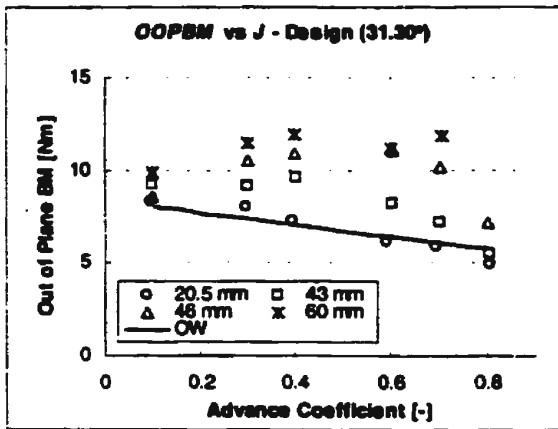


Figure 5-27 a) *OOPBM*-  $\phi = 31.30^\circ$ -Range of  $h_i$ ; b) *IPBM*-  $\phi = 31.30^\circ$  - Range of  $h_i$

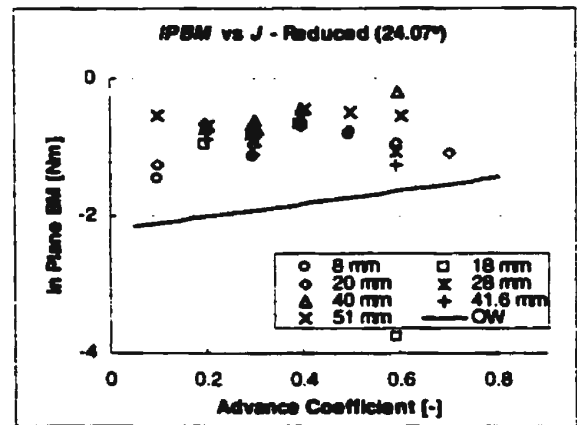
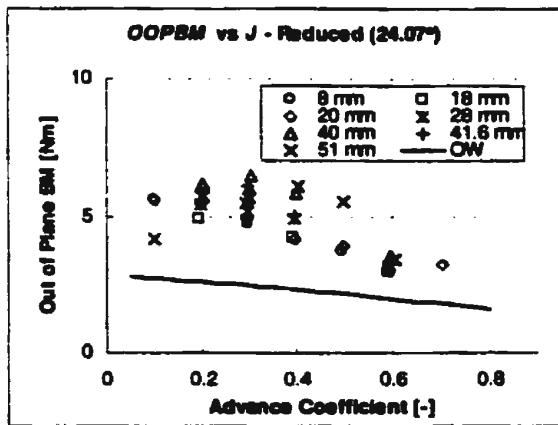


Figure 5-28 a) *OOPBM*-  $\phi = 24.07^\circ$ -Range of  $h_i$ ; b) *IPBM* -  $\phi = 24.07^\circ$  - Range of  $h_i$

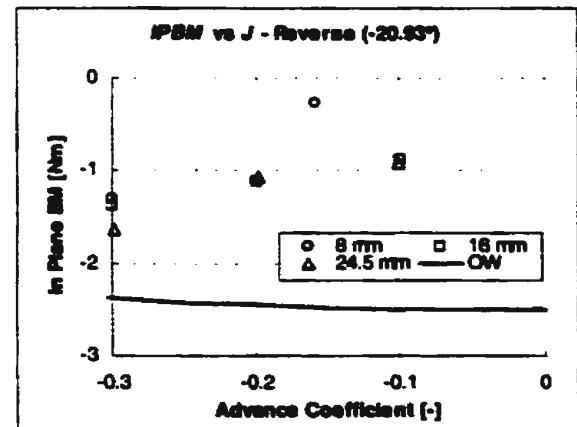
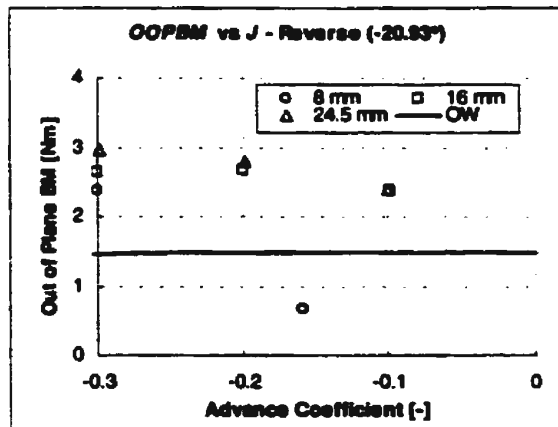


Figure 5-29 a) *OOPBM*-  $\phi = -20.93^\circ$ -Range of  $h_i$ ; b) *IPBM* -  $\phi = -20.93^\circ$  - Range of  $h_i$

## **Chapter 6**

### **Summary**

Damage to the propulsion systems of vessels due to navigation in ice can lead to serious risk to personnel and property. In an attempt to limit these risks, regulations such as the Finnish-Swedish Ice Class Rules and the Canadian Arctic Shipping Pollution Prevention Regulations set rules governing the design of propulsion systems used in ice. Most current ice class propeller design rules are based on the value of an ice torque dependent on the vessel's ice class. These ice torques and subsequent propeller design parameters have been developed and verified based on experience with conventional propeller geometry, i.e. low-skewed and low-rake designs, both with and without ducts. Consequently, use of these rules for highly skewed designs is not entirely accurate. However, highly skewed propellers have become common on some ice class passenger ferries, cruise ships and other vessels due to their low vibration and noise characteristics in open water.

This research has been completed to improve the understanding of highly skewed propellers behavior in ice. To accomplish this a series of model tests was completed comprised of various operating conditions for the controllable pitch propeller being modeled. The loads experienced by both the total propeller and the loads on an individual blade were recorded and examined.

In addition to the propeller-ice interaction tests, a series of model compression tests was conducted. The results from this series of tests presented a failure pattern dependent on the strain rate that can be used to estimate the compressive strength experienced by the propeller during the milling process. This strength, when combined with the geometric scale of the propeller, can be used to scale loads to the full scale propeller. This was not attempted in this thesis, however.

After performing the series of compression tests on EG/AD/S ice at three temperatures and a range of strain rates it has been concluded that EG/AD/S ice behaves in a manner similar to that of real fresh and salt water ice. That is, the model ice displays creep at the lower strain rates (below approximately  $10^{-3} \text{ s}^{-1}$ ), which proceeds to shear plane failure as the strain rate increases (between approximately  $10^{-3} \text{ s}^{-1}$  and  $10^0 \text{ s}^{-1}$ ). Increasing the strain rate above  $10^0 \text{ s}^{-1}$  causes the model ice to fail brittlely at an elevated peak stress as observed in polycrystalline fresh water ice and Baltic Sea ice. As expected the model ice became stronger as the temperature decreased.

Various operating conditions were investigated for the highly skewed propeller model, including four pitch settings, multiple advance ratios, and multiple depths of cut into the ice sheet. In addition to these controlled variables, the strength of the ice sheet varied over the course of testing as a result of the tempering process. After analyzing the results from all the tests the following conclusions have been drawn.

The maximum observed shaft thrust and torque loads occur during ice milling at the design pitch. The magnitude of these maximum loads was, in some cases, more than twice the propeller open water loads. In addition to the shaft loads experienced during the ice milling tests the loads measured on one instrumented blade also show relevant results. During the ice milling the individual blade experienced thrust loads approximately equal the open water bollard load recorded by the total propeller. The maximum thrust coefficient experienced by the individual blade was approximately 0.65, which corresponds to an individual blade thrust of approximately 340 N, or approximately equal the total open water bollard thrust for the same pitch setting. Blade torque loads were observed to be up to approximately 30 Nm, or twice the total open water bollard load. Similarly the maximum out of plane bending moment experienced by the blade during ice milling was approximately 55 Nm. The corresponding maximum open water value was 10 Nm.

At advance coefficients below 0.5 at the design pitch, the thrust and out of plane bending moment experienced a continual increase in load. These loads were in the direction for which the blade is designed to withstand its maximum load and as such should pose little risk. However, at advance ratios greater than 0.5 both the thrust and out of plane bending moment experienced a drop in load which continue on to the highest advance coefficient tested of 0.8. As this drop in load continued the out of plane bending moment became more negative. That is, ice loading is experienced more on the suction side of the blade, a situation that is of concern for two reasons. The first reason is propellers have been known to suffer more ice damage by being bent backwards, or the negative out of plane

direction. This is likely due to being designed for maximum loads in the forward ship direction, i.e. forward bending moment. Secondly, in highly skewed propellers the tip of the propeller is susceptible to suction side load deformation as illustrated in Figure 6-1 (a) and (b). In this figure pressure side loading (Figure 6-1 (a)) can be seen to act to bend the blade into the stronger part of the blade section. Figure 6-1 (b), shows how the suction side loading causes the blade section to deflect inward, a situation where the load can deform or even fail the blade as observed by Searle et al. (1999a) on both a model and full scale propeller.

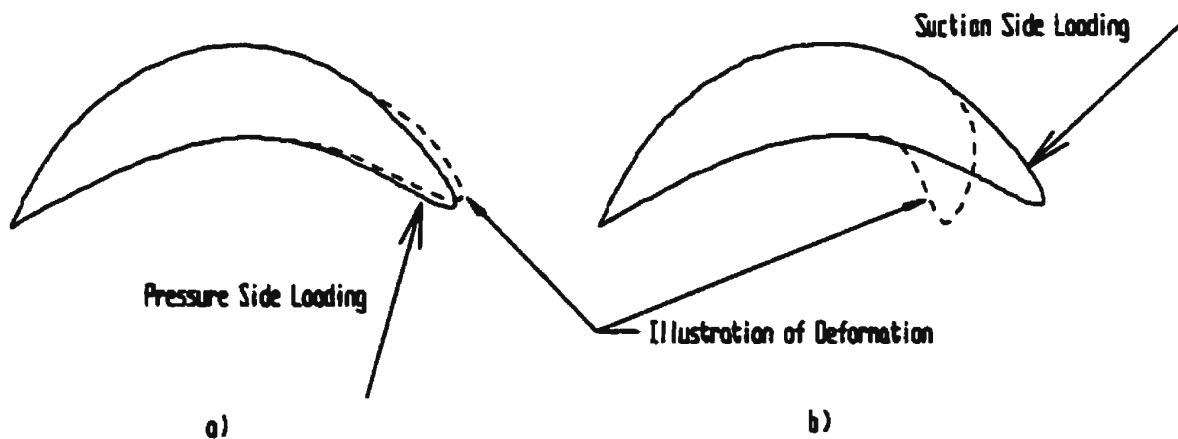


Figure 6-1 Illustration of Tip Loading

To prevent loads from reaching this negative thrust and out of plane bending moment conditions, and thus prevent the possibility of damage caused by such, it is advisable to operate the propeller at advance coefficients of less than 0.6 in ice covered waters. In the case of this propeller, operation at the design condition (point of highest efficiency at the

design pitch) would result in an advance coefficient of approximately 1.0. To drop this advance coefficient would require decreasing the ship speed by reducing the pitch on the blades and/or increasing the shaft rotational speed. Since increasing the shaft speed would normally result in increased thrust this would be counter productive. As such, operating the propeller at a reduced pitch in ice covered waters would be one possible solution.

When testing at the reduced pitch of  $24.07^\circ$  and advance ratios greater than 0.6, the propeller experienced a drop in thrust and out of plane bending moment similar to that observed at the design pitch. However, the peak open water efficiency observed for this pitch condition occurred at an advance coefficient of approximately 0.8. It would therefore be possible to operate the propeller at its peak efficiency for this reduced pitch condition without as much risk of damaging the propeller blades. The trade off in this situation is the increased transit time from operating at a reduced pitch and subsequently reduced thrust coefficient, (at peak efficiency for the design pitch the thrust coefficient is 0.2 while at the reduced pitch of  $24.07^\circ$  it is only approximately 0.13). However, this trade off may be justifiable if it prevents the damage or loss of an expensive highly skewed propeller blade.

A second option to reduce the risk of damage to the relatively weak tips of highly skewed propellers would be a limit on the amount of skew permitted in propellers for ice class vessels. By limiting the skew the section thickness at the blade tip can be increased, without major hydrodynamic penalties, thus reducing the possibility of damage.

**The results published here describe the first time individual blade load measurements of a highly skewed propeller model in ice were performed. Based on these tests it was concluded that during the ice milling event an individual blade experiences loads comparable in magnitude to the total propeller in open water. The out of plane direction of these loads at higher advance ratios results in loading that could result in tip and blade damage to the highly skewed blades. Based on these observations it is concluded that operation of highly skewed propellers for ice navigation should be at reduced speed, or limited to less extremely skewed designs.**

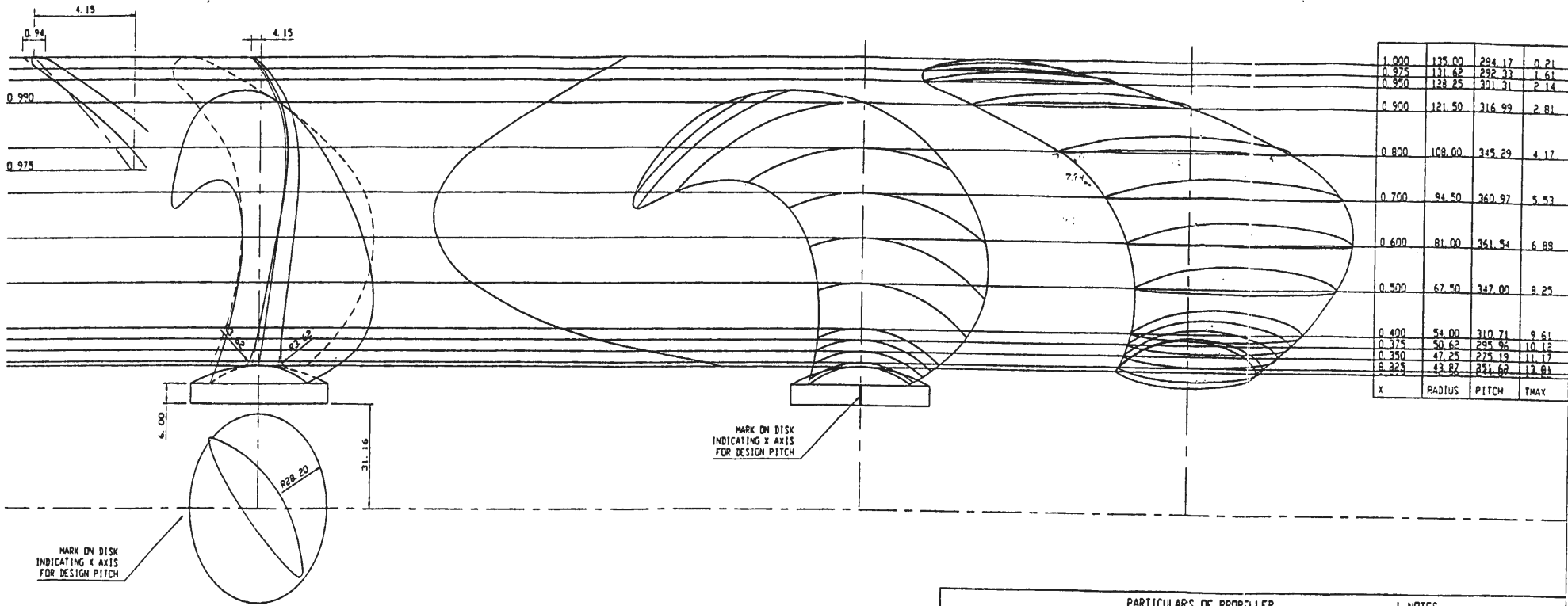
## **Bibliography and References**

- ASM Handbook, 2000. Volume 8, Mechanical Testing and Evaluation, Materials park, Ohio, p430-431.
- Bose, N., Veitch, B. and Doucet, M. 1998. A design approach for ice class propellers. *Transactions, Society of Naval Architects and Marine Engineers*, Vol. 106.
- Browne, R.P., Keinonen, A.J., and Semery, P., 1991, Ice Loading on Open and Ducted Propellers, *Proceedings of 1<sup>st</sup> ISOPE, Edinburgh*.
- Doucet, J.M., Bose, N., and Veitch, B. 1999. Selection of scantlings for an ice class propeller: A case study for the *MV Ikaluk*. *Proceedings, Offshore Mechanics and Arctic Engineering*, American Society of Mechanical Engineers, 8 pp.
- Doucet, J.M., Liu, P., Bose, N., and Veitch, B. 1998. Numerical prediction of ice-induced loads on ice-class screw propellers using a synthesized contact/hydrodynamic code, Ocean Engineering Research Centre Report No. OERC-1998-004.
- Jones, S.J., 1982. The confined compressive strength of polycrystalline ice. *J. Glaciol.* Vol. 28, No. 98, p.171- 177.
- Jones, S.J. 1987. Ice tank Test Procedures at the Institute for Marine Dynamics. *Institute for Marine Dynamics Report No. LM-AVR-20*.
- Jones, S.J., 1997. High strain rate compression tests on ice. *J. Physical Chemistry B*, Vol. 101, No. 32, p. 6099-6101.
- Katsman, F.M., and Andruishin, A.V. 1997, *Strength Rates for Blades as Intended for the Propellers of Ice Breakers and Ice Ships*, Russian Maritime Register of Shipping.
- Keinonen. A.J., and Browne, R.P. 1990. Ice Propeller Interaction Forces. *Transport Canada Publication 10401E Vol.1*.
- Koskinen, P., Jussila, M. and Soininen, H., 1996, Propeller Ice Loads Models, Technical Research Centre of Finland, Research Notes 1739.
- Liu, P., Doucet, M., Veitch, B., Robbins, I., and Bose, N. 2000. Numerical prediction of ice induced hydrodynamic loads on propellers due to blockage. *Oceanic Engineering International*, Vol.4, No.1, pp.31-38.
- Meglis, I., Melanson, P. and Jordaan, I., 1998. High speed testing of freshwater granular ice, NRC/IMD Report CR-1998-02.

- Minchev, D., Bose, N., Veitch, B., Atlar, I., Paterson, I., 2001, *Some analyses of propeller ice milling experiments*, Submitted, Canadian Marine Hydromechanics and Structures Conference '01.
- Searle, S. 1999, *Ice tank test of a highly skewed propeller and a conventional ice-class propeller in four quadrants*, Master of Engineering Thesis, Memorial University of Newfoundland, St. John's, Newfoundland
- Searle, S., Veitch, B., and Bose, N., 1999a, Ice-Class Propeller Performance in Extreme Conditions, *Transactions Society of Naval Architects and Marine Engineers Vol 107*.
- Searle, S., Veitch, B., and Bose, N., 1999b, Experimental Investigation of a Highly Skewed Propeller in Ice, *Proceedings, OMAE-99-1130*, 8pp.
- Spencer, D.S., Timco, G.W., 1990. CD model ice – A technique to produce controllable density model ice, *IAHR Ice Symposium 90*, Espoo, Finland.
- Tamura, K., Kato, H., and Yamaguchi, H., 1997, Experimental Approach to the Interaction between Nozzle-Propeller and Ice-Block, *Joint OMAE/POAC Conference, Yokohama, Japan*.
- Timco, G.W., 1986. EG/AD/S: A new type of model ice for refrigerated towing tanks, *Cold Science and Technology*, 12, p.175-195.
- Veitch, B., 1992, *Propeller-ice interaction*, Licentiate of Technology Thesis, Helsinki University of Technology, Espoo.
- Veitch, B., 1995, *Predictions of ice contact forces on a marine screw propeller during the propeller-ice cutting process*, Acta Polytechnica Scandinavica, Mechanical Engineering Series No. 118, Helsinki.
- Walker, D., Bose, N., and Yamaguchi, H. 1994, *Hydrodynamic Loads and Effects of Cavitation on Ice Class Propellers in Simulated Ice Blocked Flow*, Society of Naval Architects and Marine Engineers, Propellers/Shafting '94 Symposium, September 20-21, 1994.
- Woodford, C. 2000. Compressive strength of EGADS model ice over a range of strain rates. *OERC-2000-002*, Ocean Engineering Research Centre, Memorial University of Newfoundland.

## **Appendix I – Propeller Blade Geometry**

DETAIL BLADE TIP



PARTICULARS OF PROPELLER			NOTES
FULL SIZE		MODEL	
DIAMETER D	= 5200 mm	MATERIAL:	BRONZE
P AT ROOT PHUB	= 4716 mm	MATERIAL:	
P AT 0.7 R PO.7	= 6952 mm	DIAMETER	= 270.00 mm
P AT BL TIP P1.0	= 5473 mm	DHUB/D	= 0.316
DISC AREA AQ	= 21.237 m <sup>2</sup>	PO.7/D	= 1.337
EXP. BL. AREA AE	= 11.500 m <sup>2</sup>	PVIRT/D	= 1.454
PROJ. BL. AREA AP	= 9.543 m <sup>2</sup>	AE/AD	= 0.542
NO OF BLADES Z	= 4	AP/AQ	= 0.445

design p3 (Lloyd's)

PROPP. MODEL NO. 6503

SHIP MODEL NO.

SCALE 19.259

DRAWING NO. 15833-C02

Figure I-1 Propeller Blade Geometry

## **Appendix II – EG/AD/S Compression Test Error Analysis**

**Table II-1 Error Analysis Of EG/AD/S Compression Tests**

Variable		Y1	Y2	W1	W2	L	Vx	Fmax	T	W	A	SR	PS
<b>Strain Rate</b>													
4.6E-07	1/s	0.019	0.019	0.011	0.011	0.002	0.016	0.014	0.027	0.015	0.031	0.016	0.034
4.6E-03	1/s	0.019	0.019	0.011	0.011	0.002	0.026	0.014	0.027	0.015	0.031	0.026	0.034
4.6E-01	1/s	0.019	0.019	0.011	0.011	0.002	0.010	0.014	0.027	0.015	0.031	0.011	0.034
4.6E+00	1/s	0.019	0.019	0.011	0.011	0.002	0.048	0.400	0.027	0.015	0.031	0.048	0.401
<b>Strain Rate</b>		<b>Strain Rate</b>		<b>Peak Stress</b>									
4.6E-07	1/s	+- ratio error		0.016	0.034								
4.6E-03	1/s	+- ratio error		0.026	0.034								
4.6E-01	1/s	+- ratio error		0.011	0.034								
4.6E+00	1/s	+- ratio error		0.048	0.401								
<b>Strain Rate</b>		<b>Strain Rate</b>		<b>Peak Stress</b>									
				Error	Total	Error	Total						
4.6E-07	1/s	+- Units error		0.000	0.000	16636	496267						
4.6E-03	1/s	+- Units error		0.000	0.005	82279	2406302						
4.6E-01	1/s	+- Units error		0.005	0.460	93679	2748464						
4.6E+00	1/s	+- Units error		0.219	4.600	2711060	6753072						
<b>Strain Rate</b>		<b>Strain Rate</b>		<b>Peak Stress</b>									
4.6E-07	1/s	+- % error		1.3	3.4								
4.6E-03	1/s	+- % error		2.6	3.4								
4.6E-01	1/s	+- % error		1.1	3.4								
4.6E+00	1/s	+- % error		4.8	40.1								

**Error Analysis For EG/AD/S Ice Compression Tests**

**Formulae**

Thickness Formula	$T = (T1 - T2) / 2$
Width Formula	$W = (W1 - W2) / 2$
Length Formula	L
Area Formula	$A = T \times W$
Strain Rate Formula	$SR = Vx / L$
Peak Stress Formula	$PS = Fmax / A$

**Uncertainty in each Variables :**

---

**Thickness**

Since the thickness was not modified from the original thickness of the ice sheet it had some surface variation in it.

	Nominal Value for thickness		110.0	mm	
Bias Error	Error in the Calipers		+/-	0.1	mm
		+/- Ratio		0.0009	
					Assumed to be the scale division since the calipers were loose.
Precision Error	Surface Variation		+/-	2.1	mm
		+/- Ratio		0.019	
					Calculated from group of tests completed High as a result of surface variation.
	Total Error +/-				
	+/- Ratio			0.0193	

---

**Width**

Since the width was machined its surface variation is expected to be close to uniform Therefore the variation was not as sever as with the thickness.

	Nominal Value for width		110.0	m	
Bias Error	Error in the Calipers		+/-	0.1	mm
		+/- Ratio		0.0009	
					Assumed to be the scale division since the calipers were loose.
	Total Bias Error +/-			0.0009	
Precision Error			+/-	1.2	mm
		+/- Ratio		0.011	
					Calculated from group of tests completed
	Total Error +/-				
	+/- Ratio			0.0106	

---

<b>Length</b>	Length was measured with a steel ruler with 1mm divisions			
	Nominal Value for length		330.0	mm
<b>Bias Errors</b>	Error in the Ruler	+/-	0.5	mm
		+/- Ratio	0.0015	Assumed as 1/2 of the smallest scale
<b>Precision Error</b>		+/-	0.6	mm
		+/- Ratio	0.0020	Calculated from group of tests completed
	<b>Total Error +/-</b>			
		+/- Ratio	0.0025	

<b>Vx</b>	<b>Cross-Head Velocity</b>			
	<b>Desired Strain Rates</b>		<b>Cross-Head Speed</b>	
	4.6E-07 1/s		0.0002	mm/s
	4.6E-03 1/s		1.5180	mm/s
	4.6E-01 1/s		151.80	mm/s
	4.6E+00 1/s		1518.0	mm/s
<b>Bias Error</b>	Error in speed control	+/-	0.0000	mm/s
		+/-	0.0152	mm/s
		+/-	1.5180	mm/s
		+/-	15.1800	mm/s
				1% of cross head speed based on Factory Calibration Specification.
	4.6E-07 1/s	+/- Ratio	0.0100	
	4.6E-03 1/s	+/- Ratio	0.0100	
	4.6E-01 1/s	+/- Ratio	0.0100	
	4.6E+00 1/s	+/- Ratio	0.0100	
<b>Precision Error</b>		+/- Ratio	0.0127	Calculated from group of tests completed.
	4.6E-03 1/s	+/- Ratio	0.0243	
	4.6E-01 1/s	+/- Ratio	0.0032	
	4.6E+00 1/s	+/- Ratio	0.0466	

<b>Fmax</b>	<b>Peak Recorded Load.</b>			
	Error is based on calibration error in the load cells for the two lower strain rates.			
	At the highest strain rate a dynamic effect in the system is observed. The platen begins to vibrate prior to reaching full failure load. It is observed that at this speed the peak load is likely to be between 70 and 100 % of the recorded peak load. Giving an error of -30%			
<b>Bias Error</b>	Error in load cells	+/- Ratio	0.0100	Based on Factory Specifications.
	4.6E-07 1/s	+/- Ratio	0.0100	
	4.6E-03 1/s	+/- Ratio	0.0100	
	4.6E-01 1/s	+/- Ratio	0.0100	
	4.6E+00 1/s	+/- Ratio	0.0100	
	Dynamic Variation	- Ratio	0.4000	At highest strain rate only.
	<b>Total Bias Error</b>			
	4.6E-07 1/s	+/- Ratio	0.0100	
	4.6E-03 1/s	+/- Ratio	0.0100	
	4.6E-01 1/s	+/- Ratio	0.0100	
	4.6E+00 1/s	+/- Ratio	0.4001	

**Appendix III – Propeller-Ice Interaction Test Error Analysis**

Variable	T	To	Q	Qo	rho	n	D	Va	Xf	Xfo	P - Angle	Xm	Xmo	YM	Ymo
<b>Advance Coefficient</b>															
0.1	0.0056	0.0056	0.0068	0.0068	0.0001	0.0246	0.0045	0.0408	0.0353	0.0353	0.0163	0.0333	0.0333	0.0194	0.0194
0.3	0.0058	0.0058	0.0069	0.0069	0.0001	0.0246	0.0045	0.0181	0.0353	0.0353	0.0163	0.0333	0.0333	0.0194	0.0194
0.4	0.0072	0.0072	0.0077	0.0077	0.0001	0.0246	0.0045	0.0168	0.0353	0.0353	0.0163	0.0333	0.0333	0.0194	0.0194
0.6	0.0091	0.0091	0.0081	0.0081	0.0001	0.0246	0.0045	0.0138	0.0353	0.0353	0.0163	0.0333	0.0333	0.0194	0.0194
<b>Advance Coefficient</b>		<b>KT</b>		<b>KQ</b>		<b>J</b>		<b>KT (Blade)</b>		<b>KQ (Blade)</b>		<b>theta</b>	<b>Resultant</b>	<b>IPBM</b>	<b>OOPBM</b>
0.1	±/ ratio error	0.0368		0.0375		0.0479		0.0615		0.0594		0.0708	0.1094	0.1303	0.1303
0.3	±/ ratio error	0.0369		0.0375		0.0309		0.0615		0.0594		0.0708	0.1094	0.1303	0.1303
0.4	±/ ratio error	0.0374		0.0378		0.0302		0.0615		0.0594		0.0708	0.1094	0.1303	0.1303
0.6	±/ ratio error	0.0382		0.0380		0.0286		0.0615		0.0594		0.0708	0.1094	0.1303	0.1303
		<b>KT</b>		<b>KQ</b>		<b>J</b>		<b>KT (Blade)</b>		<b>KQ (Blade)</b>				<b>IPBM</b>	<b>OOPBM</b>
0.1	±/ Units error	Error	Total	Error	Total	Error	Total	Error	Total	Error	Total			Error	Total
0.1	±/ Units error	0.023	0.618	0.037	0.978	0.005	0.100	0.010	0.155	0.015	0.244			0.29	-2.21
0.3	±/ Units error	0.019	0.517	0.032	0.849	0.009	0.300	0.008	0.129	0.013	0.212			0.26	-1.97
0.4	±/ Units error	0.017	0.467	0.030	0.784	0.012	0.400	0.007	0.117	0.012	0.196			0.24	-1.84
0.6	±/ Units error	0.014	0.366	0.025	0.653	0.017	0.600	0.006	0.092	0.010	0.163			0.21	-1.59
<b>Advance Coefficient</b>		<b>KT</b>		<b>KQ</b>		<b>J</b>		<b>KT (Blade)</b>		<b>KQ (Blade)</b>				<b>IPBM</b>	<b>OOPBM</b>
0.1	±/ % error	37		37		4.8		6.2		5.9				13.0	13.0
0.3	±/ % error	37		38		3.1		6.2		5.9				13.0	13.0
0.4	±/ % error	37		38		3.0		6.2		5.9				13.0	13.0
0.6	±/ % error	38		38		2.9		6.2		5.9				13.0	13.0

Table III-1 Propeller-Ice Interaction Error Analysis

**Error Analysis For Propeller Ice Milling Tests**

**Formulae**

Thrust Coefficient Formula	$(T - T_0) / (\rho \times n^2 \times D^4)$
Torque Coefficient Formula	$(Q - Q_0) / (\rho \times n^2 \times D^5)$
Advance Coefficient Formula	$V_a / (n \times D)$
Thrust Coefficient (Blade Load)	$(X_l - X_{l0}) / (\rho \times n^2 \times D^4)$
Torque Coefficient (Blade Load)	$(X_m - X_{m0}) / (\rho \times n^2 \times D^5)$
theta formula	$\text{PitchAngle} - \text{atan}((X_m - X_{m0}) / (Y_m - Y_{m0}))$
Resultant Formula	$((X_m - X_{m0})^2 + (Y_m - Y_{m0})^2)^{1/2}$
IPBM Formula	$\sin(\theta) \times \text{Resultant}$
OOPBM Formula	$\cos(\theta) \times \text{Resultant}$

**Uncertainty in each Variables :**

<b>rho</b>	Tank Temperature was recorded using a digital thermometer with 0.02 degrees C divisions. Precision and calibration assumed to be within 0.02 degrees Celsius Tank Water Temperature varied over the course of the tests from 0.02 to 1.02 degrees				
	Nominal Value for used for density	0.9999	Mg/m <sup>3</sup>		
<b>Bias Error</b>	Calibration of Thermometer +/-	0.0200	degrees Celsius		
	Divisions on Tabled Data for Water +/- Ratio	0.0001 0.0001	Mg/m <sup>3</sup>	Per 2 Degrees near zero degrees C	
	<b>Precision Error</b>				
	Scale +/-	0.02	degrees Celsius		
	Position / Time +/-	0.50	degrees Celsius		
	Total "Fossilized" Error	0.50	degrees Celsius		
	Error in Density +/-	0.0000	Mg/m <sup>3</sup>		
	Total Precision Error +/- +/- Ratio	0.0000			
	Total Error +/- +/- Ratio	0.0001			
<b>D</b>	<b>Propeller Diameter</b> Outer Extent of each blade was recorded using a measurement block and touch probe.				
	Nominal Value for Blade Diameter	0.2700	m		
	<b>Bias Error</b>	hub +/-	0.0005	m	
		blade +/- (error in 2 blades)	0.001	m	
		measurement block +/-	0.0005	m	
	Total Bias Error +/-	0.0012	m		
	Total Error +/- +/- Ratio	0.0045			

<b>Va</b>	<b>Speed of the Carriage was recorded from the motor tachometer.</b>			
	J =	0.1	V =	0.270 m/s
	J =	0.3	V =	0.810 m/s
	J =	0.4	V =	1.080 m/s
	J =	0.6	V =	1.620 m/s
<b>Bias Errors</b>	<b>Calibration of Carriage Tachometer</b>			
	J = 0.1	+/- Ratio	0.0037	+/- 1 mm/s under 1.0 m/s
	J = 0.3	+/- Ratio	0.0012	
	J = 0.4	+/- Ratio	0.0011	+/- 0.1 % Over 1.0 m/s
	J = 0.6	+/- Ratio	0.0016	
	<b>Sampling Noise +/-</b>			
	J = 0.1	+/- Ratio	0.0019	Calculated from standard deviation using 2.83 x SD of Velocity / Mean Velocity
	J = 0.3	+/- Ratio	0.0006	
	J = 0.4	+/- Ratio	0.0022	
	J = 0.6	+/- Ratio	0.0005	
	<b>Tide +/-</b>			
	J = 0.1	+/- Ratio	0.0370	(Estimated 0.01 m/s tide)
	J = 0.3	+/- Ratio	0.0123	
	J = 0.4	+/- Ratio	0.0093	
	J = 0.6	+/- Ratio	0.0062	
	<b>Total Bias Error +/-</b>			
	J = 0.1	+/- Ratio	0.0373	
	J = 0.3	+/- Ratio	0.0124	
	J = 0.4	+/- Ratio	0.0096	
	J = 0.6	+/- Ratio	0.0064	
<b>Precision Error</b>	J = 0.1	+/- Ratio	0.003579	Calculated from Repeated tests at the same programmed velocity.
	J = 0.3	+/- Ratio	0.005700	
	J = 0.4	+/- Ratio	0.007278	
	J = 0.6	+/- Ratio	0.007393	
<b>n</b>	<b>Speed of Revolution</b>			
<b>Bias Error</b>	<b>Sampling Noise</b>			
	J = 0.1	+/- Ratio	0.000120	Calculated from standard deviation using 2.83 x SD of n / Mean n
	J = 0.3	+/- Ratio	0.000134	
	J = 0.4	+/- Ratio	0.000159	
	J = 0.6	+/- Ratio	0.000217	
<b>Precision Error</b>		+/- Ratio	0.02459584	Calculated from group of tests completed.
<b>Q</b>	<b>Torque</b>			
	Error is based on the error induced by 4 - 20 kg weights acting on the moment arm of 0.2159 m			
	Each Weight is assumed a bias error of 0.005 kg			
	Total Moment is therefore		169.4383	Nm
<b>Bias Error</b>	<b>Weights +/-</b>		0.02118	Nm
		+/- Ratio	0.00013	
	<b>Lever Arm +/-</b>		0.78480	Nm
		+/- Ratio	0.00483	
	<b>Sampling Noise</b>			
	J = 0.1	+/- Ratio	0.00316281	Calculated from standard deviation using 2.83 x SD of Q / Mean Q
	J = 0.3	+/- Ratio	0.00339981	
	J = 0.4	+/- Ratio	0.00478415	
	J = 0.6	+/- Ratio	0.00545152	
<b>Precision Error</b>		+/- Ratio	0.00388747	Calculated from group of trials.

<b>T</b>	<b>Thrust</b>	Error is based on the error induced by 4 - 20 kg weights. Each Weight is assumed a bias error of 0.005 kg Total Thrust is therefore 784.8000 N		
<b>Bias Error</b>	<b>Weights +/-</b>		0.1982 N	Error in maximum applied weights
		<b>+/- Ratio</b>	0.00025	
	<b>Sampling Noise +/-</b>			
	J = 0.1	<b>+/- Ratio</b>	0.00319182	Calculated from standard deviation using 2.83 x SD of T / Mean T
	J = 0.3	<b>+/- Ratio</b>	0.00348592	
	J = 0.4	<b>+/- Ratio</b>	0.00552053	
	J = 0.6	<b>+/- Ratio</b>	0.00790816	
<b>Precision Error</b>			0.00459528	Calculated from group of bollards.

<b>Xf</b>	<b>Thrust on individual blade</b>	Error is based on the error induced by 4 - 20 kg weights. Each Weight is assumed a bias error of 0.005 kg Total Thrust is therefore 784.8000 N		
<b>Bias Error</b>	<b>Weights +/-</b>		0.0981 N	Error in maximum applied weights
		<b>+/- Ratio</b>	0.000125	
	<b>Error in Matrix +/-</b>			
		<b>+/- Ratio</b>	0.03295086	Calculated from standard deviation using 2.83 x SD of Xf / Mean Xf
	<b>Total Bias Error +/-</b>		0.0330	
<b>Precision Error</b>			0.01264996	Calculated from group of bollards.
	<b>Total Error +/-</b>			
		<b>+/- Ratio</b>	0.0353	

<b>XM &amp; YM X and Y Moment in Blade Dyno.</b>				
Error is based on the error induced by 4 - 20 kg weights acting on the moment arm of 0.1626 m Each Weight is assumed a bias error of 0.005 kg Total Moment is therefore 127.6085 Nm				
<b>Biased Error</b>	<b>Weights +/-</b>		0.01595 Nm	
		<b>+/- Ratio</b>	0.000125	
	<b>Lever Arm +/-</b>		0.78480 Nm	
		<b>+/- Ratio</b>	0.00615006	
	<b>Error in Matrix +/-</b>			
		<b>+/- Ratio</b>	0.00999489	Calculated from standard deviation using 2.83 x SD of YM / Mean YM
	<b>Error in Matrix +/-</b>			
		<b>+/- Ratio</b>	0.0080372	2.83 x SD of XM / Mean XM
	<b>Total Bias Error +/-</b>		0.0117	YM
	<b>Total Bias Error +/-</b>		0.0101	XM
<b>Precision Error</b>			0.01548262	Based on YM from bollards
			0.03170269	Based on XM from bollards
	<b>Total Error +/-</b>			
		<b>+/- Ratio</b>	0.0194	YM
		<b>+/- Ratio</b>	0.0333	XM

<b>Pitch</b>				
Error is based on the error induced in pitch measurement. Design Pitch Measurement = 0.3941 m				
<b>Biased Error</b>	<b>Touch Probe +/-</b>		0.0005 m	
		<b>+/- Ratio</b>	0.00126871	

**Appendix IV - Shaft Thrust and Torque Coefficients versus  
Advance Coefficient Charts**

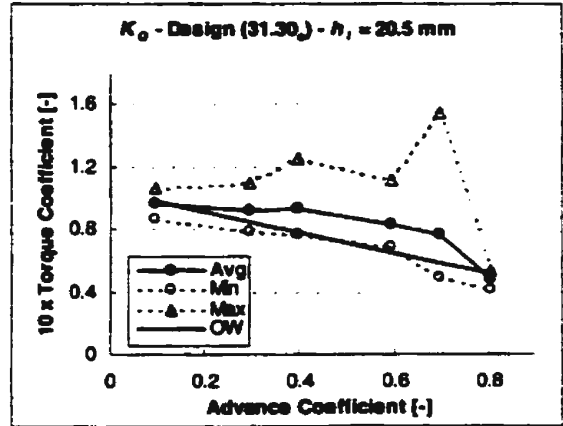
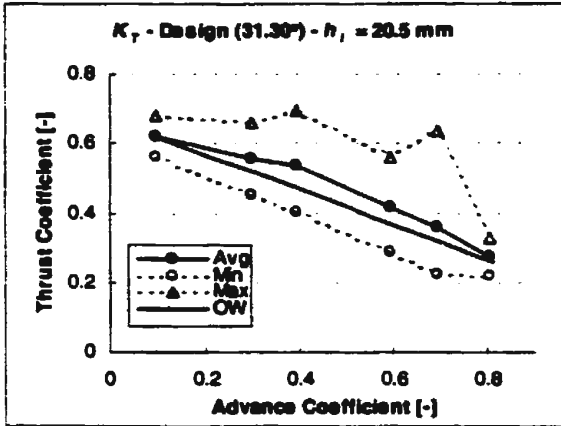


Figure IV-1 a)  $K_T$ :  $\Phi = 31.30^\circ$  -  $h_i = 20.5$  mm

b)  $K_Q$ :  $\Phi = 31.30^\circ$  -  $h_i = 20.5$  mm

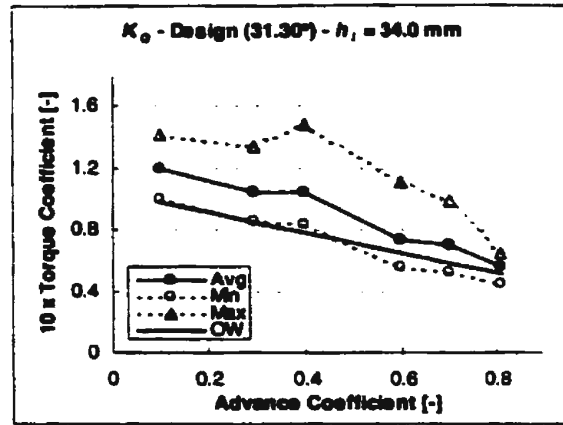
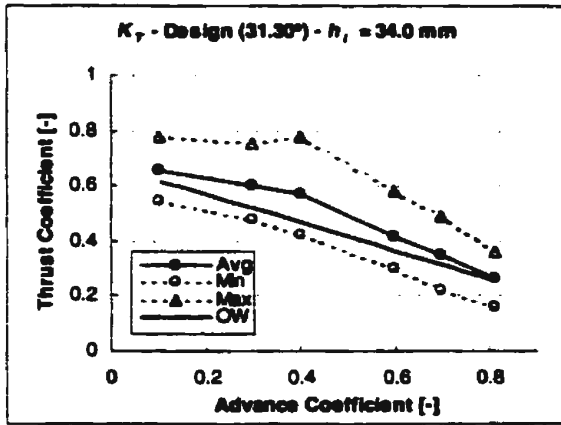


Figure IV-2 a)  $K_T$ :  $\Phi = 31.30^\circ$  -  $h_i = 34.0$  mm

b)  $K_Q$ :  $\Phi = 31.30^\circ$  -  $h_i = 34.0$  mm

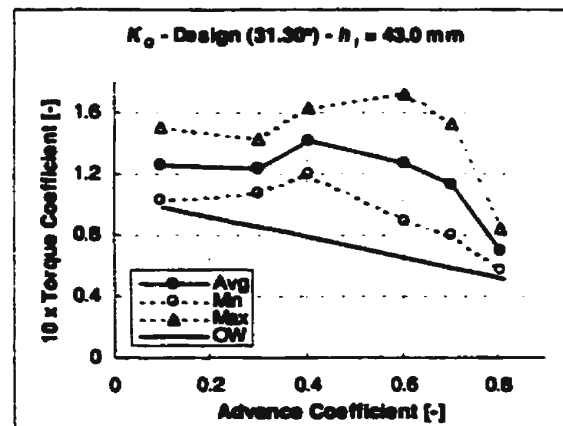
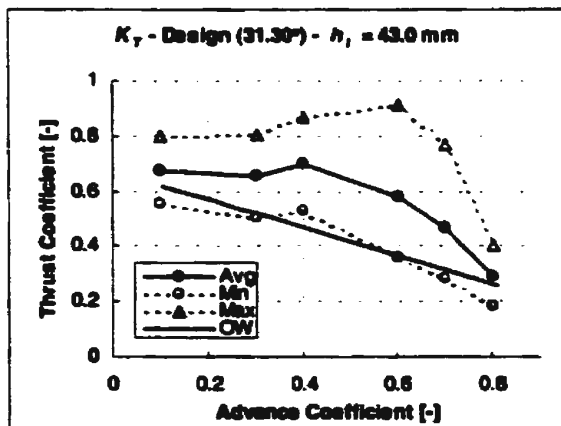


Figure IV-3 a)  $K_T$ :  $\Phi = 31.30^\circ$  -  $h_i = 43.0$  mm

b)  $K_Q$ :  $\Phi = 31.30^\circ$  -  $h_i = 43.0$  mm

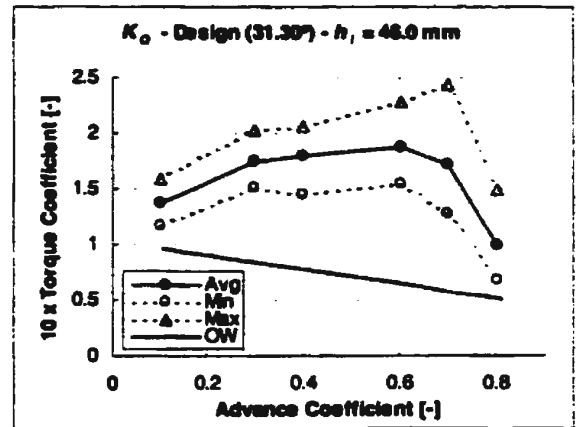
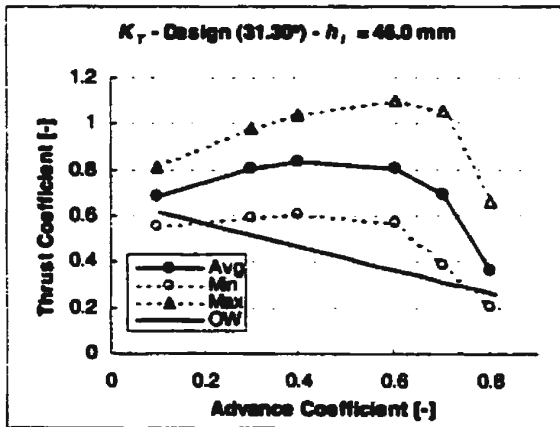


Figure IV-4 a)  $K_T$ :  $\Phi = 31.30^\circ - h_i = 46.0$  mm

b)  $K_Q$ :  $\Phi = 31.30^\circ - h_i = 46.0$  mm

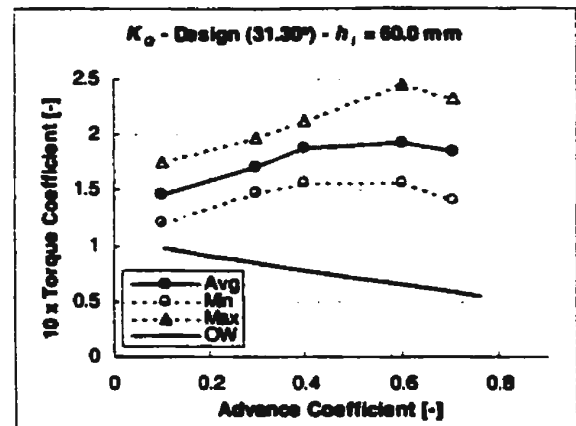
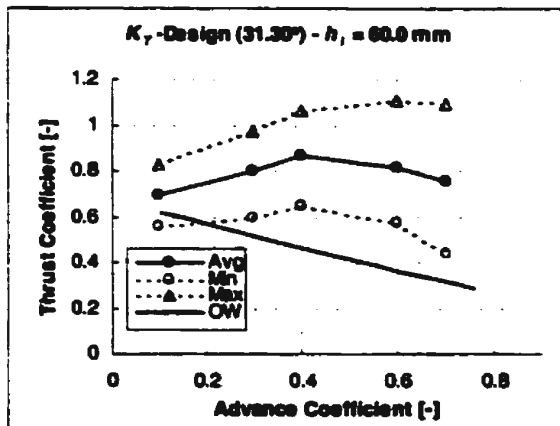


Figure IV-5 a)  $K_T$ :  $\Phi = 31.30^\circ - h_i = 60.0$  mm

b)  $K_Q$ :  $\Phi = 31.30^\circ - h_i = 60.0$  mm

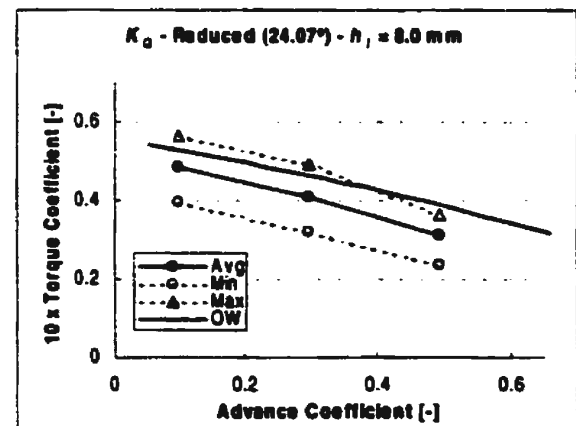
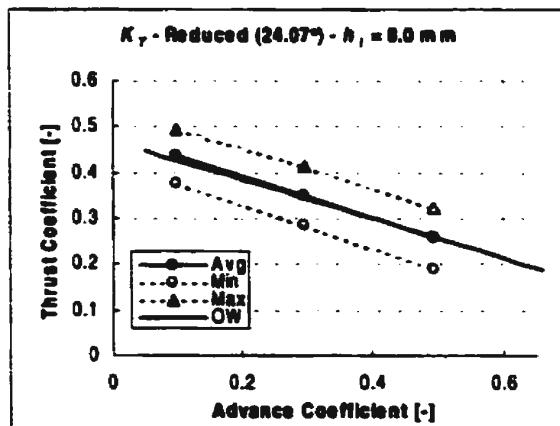


Figure IV-6 a)  $K_T$ :  $\Phi = 24.07^\circ - h_i = 8.0$  mm

b)  $K_Q$ :  $\Phi = 24.07^\circ - h_i = 8.0$  mm

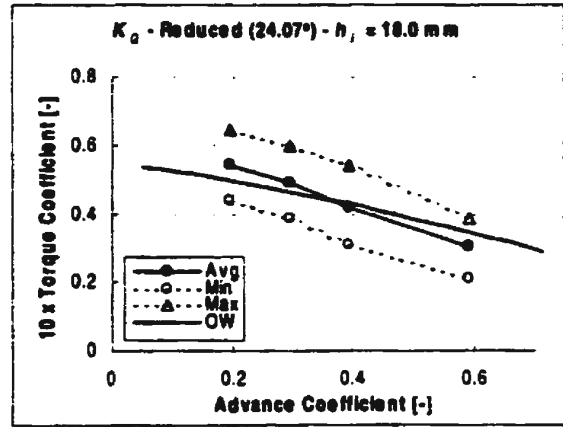
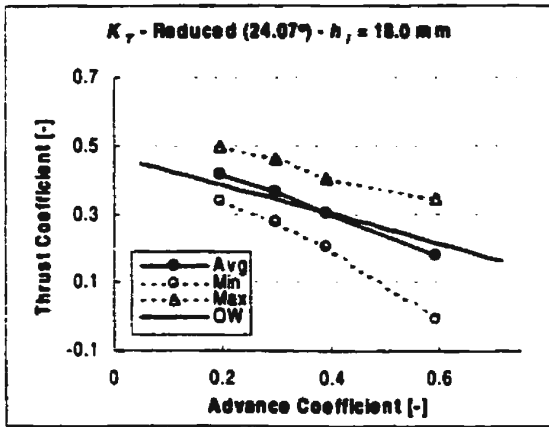


Figure IV-7 a)  $K_T$ :  $\Phi = 24.07^\circ$  -  $h_i = 18.0$  mm

b)  $K_Q$ :  $\Phi = 24.07^\circ$  -  $h_i = 18.0$  mm

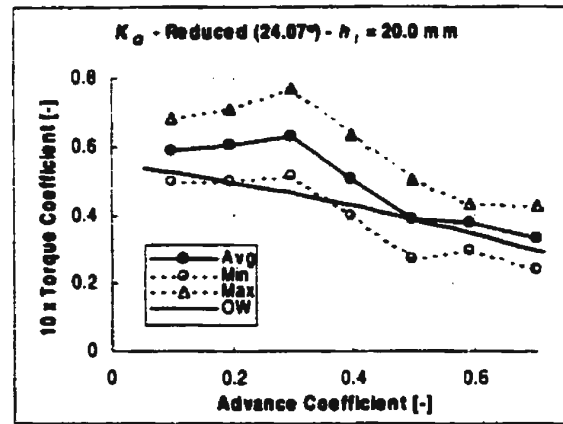
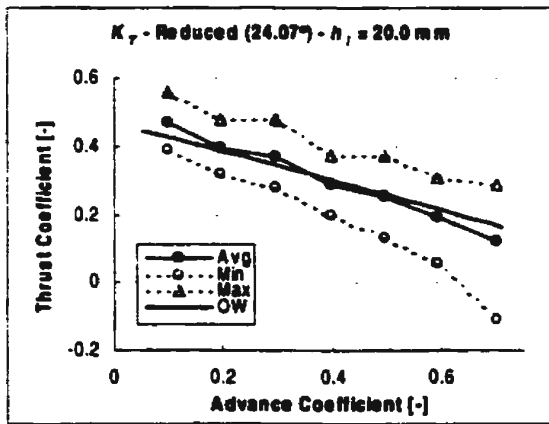


Figure IV-8 a)  $K_T$ :  $\Phi = 24.07^\circ$  -  $h_i = 20.0$  mm

b)  $K_Q$ :  $\Phi = 24.07^\circ$  -  $h_i = 20.0$  mm

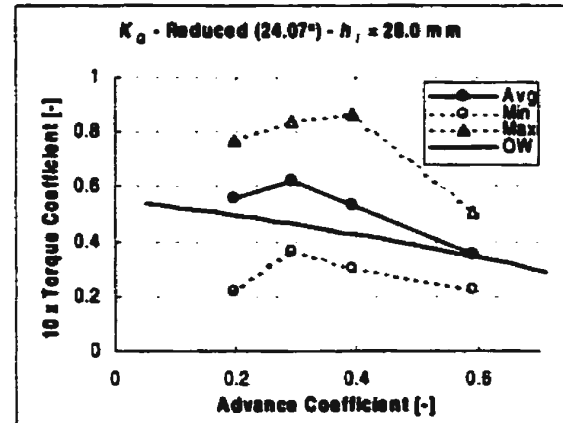
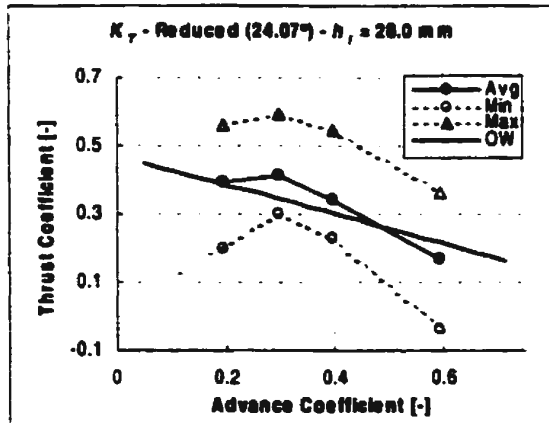


Figure IV-9 a)  $K_T$ :  $\Phi = 24.07^\circ$  -  $h_i = 28.0$  mm

b)  $K_Q$ :  $\Phi = 24.07^\circ$  -  $h_i = 28.0$  mm

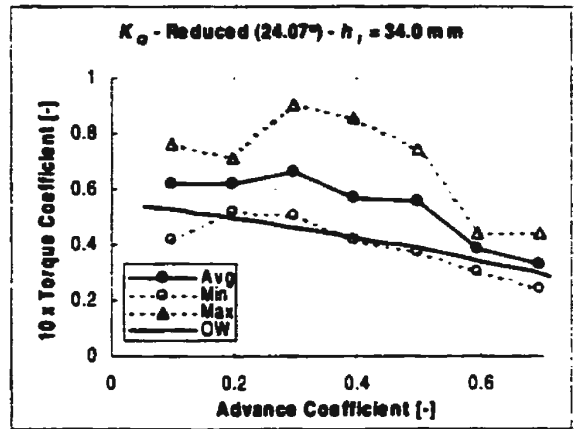
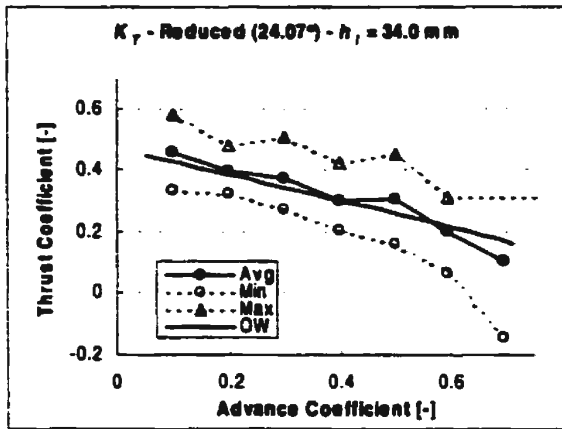


Figure IV-10 a)  $K_T$ :  $\Phi = 24.07^\circ$  -  $h_i = 34.0$  mm

b)  $K_Q$ :  $\Phi = 24.07^\circ$  -  $h_i = 34.0$  mm

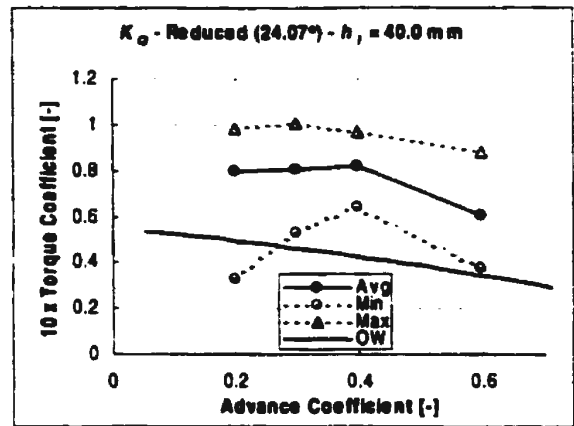
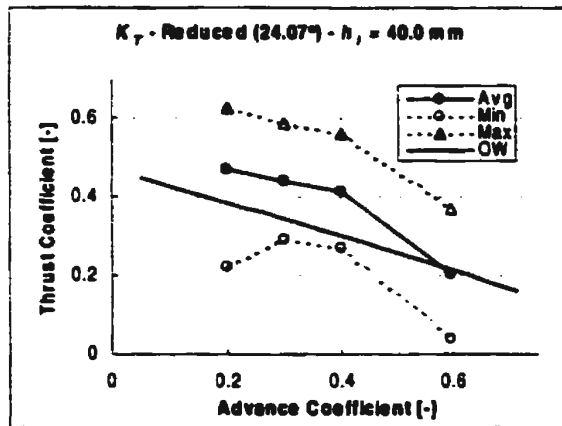


Figure IV-11 a)  $K_T$ :  $\Phi = 24.07^\circ$  -  $h_i = 40.0$  mm

b)  $K_Q$ :  $\Phi = 24.07^\circ$  -  $h_i = 40.0$  mm

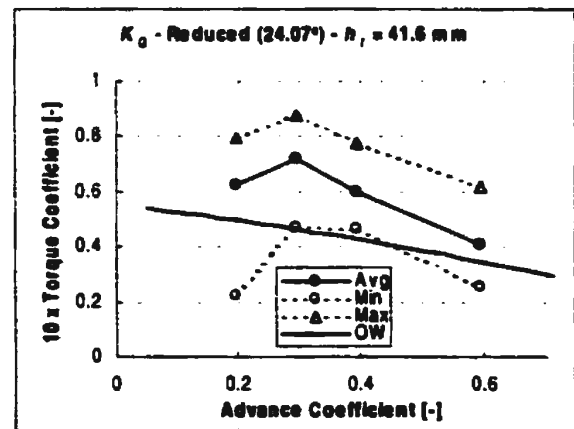
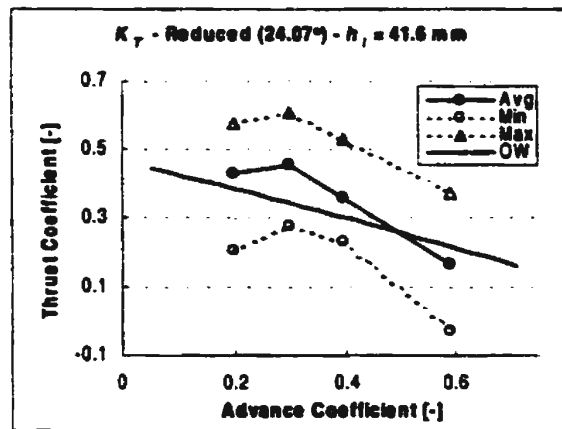


Figure IV-12 a)  $K_T$ :  $\Phi = 24.07^\circ$  -  $h_i = 41.6$  mm

b)  $K_Q$ :  $\Phi = 24.07^\circ$  -  $h_i = 41.6$  mm

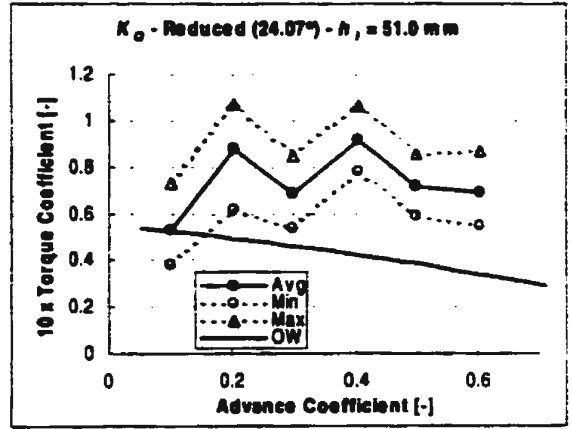
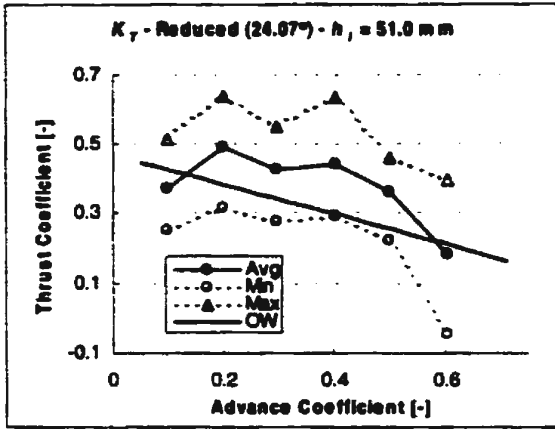


Figure IV-13 a)  $K_T$ :  $\Phi = 24.07^\circ$  -  $h_i = 51.0$  mm

b)  $K_Q$ :  $\Phi = 24.07^\circ$  -  $h_i = 51.0$  mm

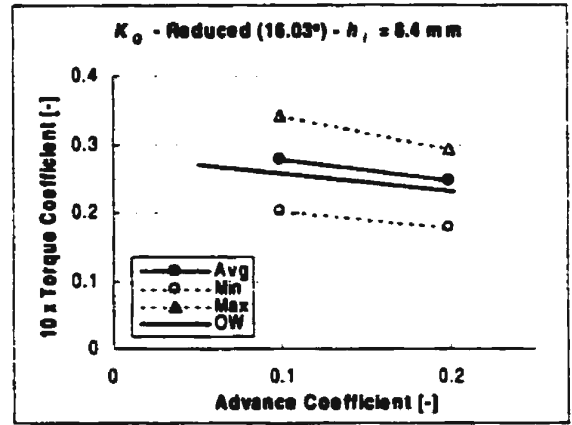
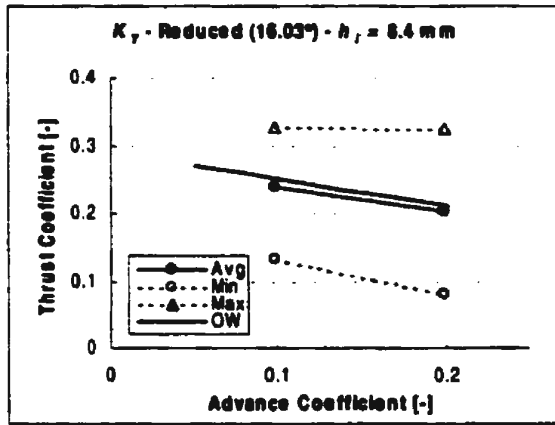


Figure IV-14 a)  $K_T$ :  $\Phi = 16.03^\circ$  -  $h_i = 8.4$  mm

b)  $K_Q$ :  $\Phi = 16.03^\circ$  -  $h_i = 8.4$  mm

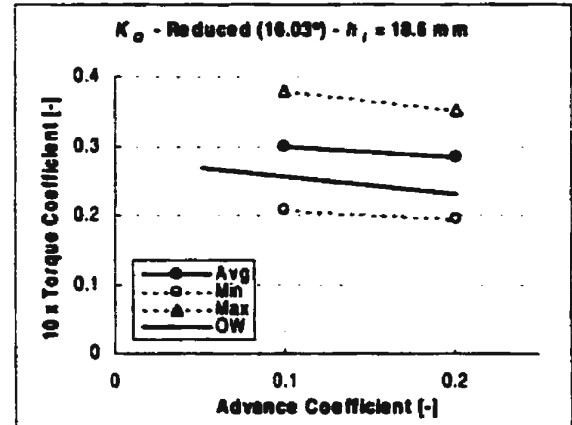
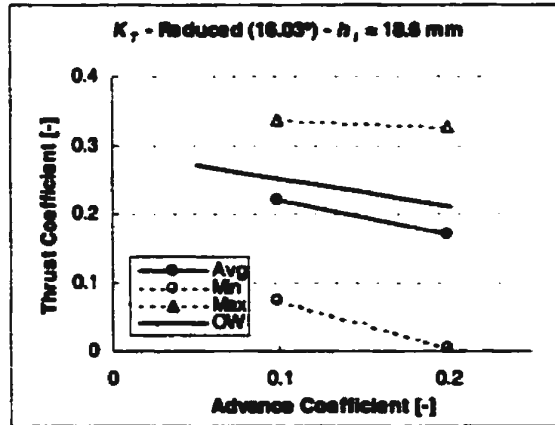


Figure IV-15 a)  $K_T$ :  $\Phi = 16.03^\circ$  -  $h_i = 18.6$  mm

b)  $K_Q$ :  $\Phi = 16.03^\circ$  -  $h_i = 18.6$  mm

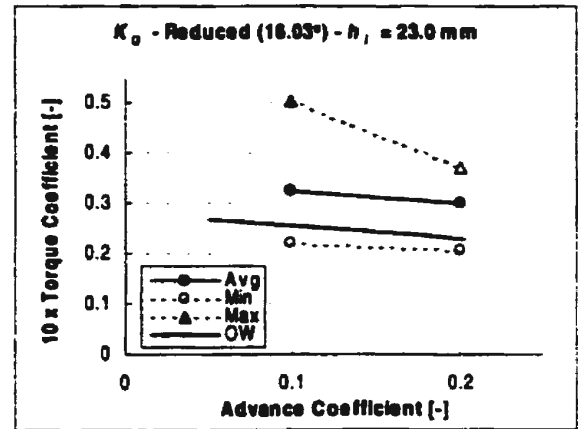
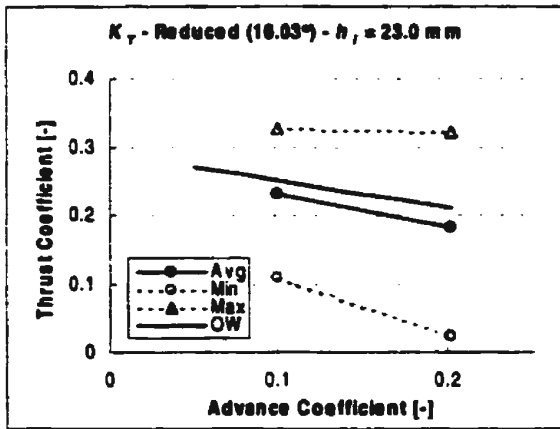


Figure IV-16 a)  $K_T$ :  $\Phi = 16.03^\circ$  -  $h_i = 23.0$  mm

b)  $K_Q$ :  $\Phi = 16.03^\circ$  -  $h_i = 23.0$  mm

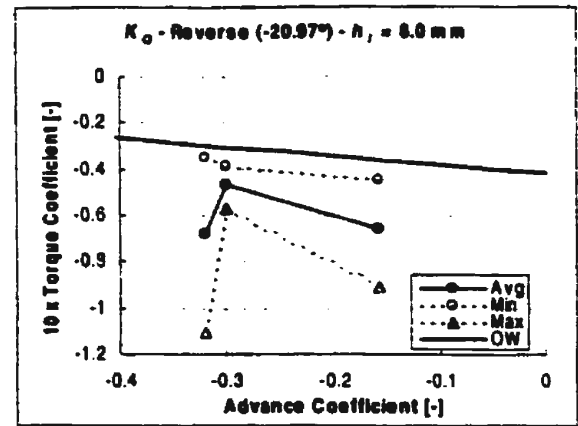
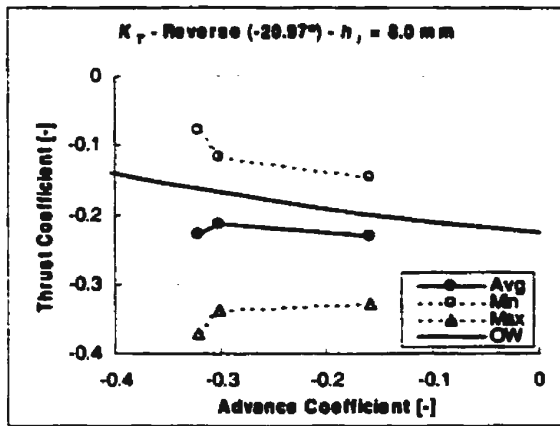


Figure IV-17 a)  $K_T$ :  $\Phi = -20.97^\circ$  -  $h_i = 8.0$  mm

b)  $K_Q$ :  $\Phi = -20.97^\circ$  -  $h_i = 8.0$  mm

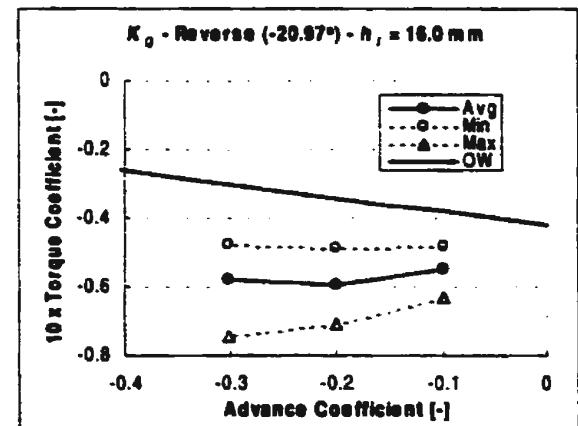
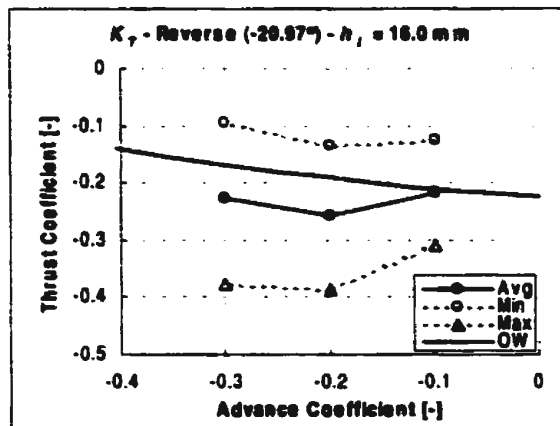


Figure IV-18 a)  $K_T$ :  $\Phi = -20.97^\circ$  -  $h_i = 16.0$  mm

b)  $K_Q$ :  $\Phi = -20.97^\circ$  -  $h_i = 16.0$  mm

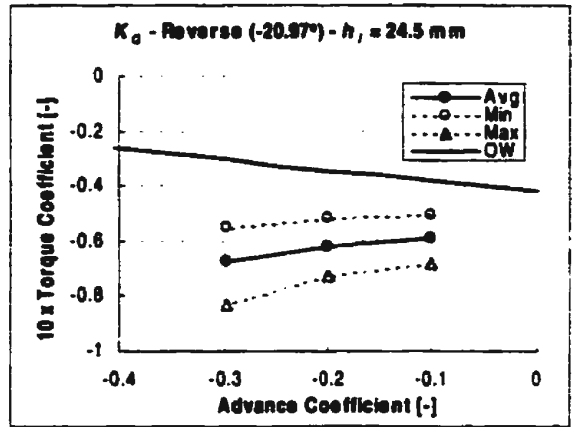
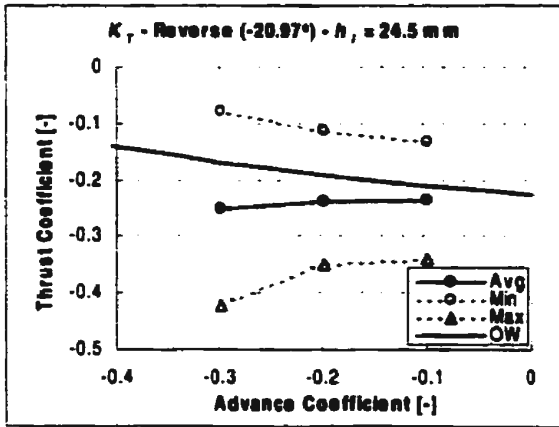


Figure IV-19 a)  $K_T$ :  $\Phi = -20.97^\circ - h_i = 24.5$  mm

b)  $K_Q$ :  $\Phi = -20.97^\circ - h_i = 24.5$  mm

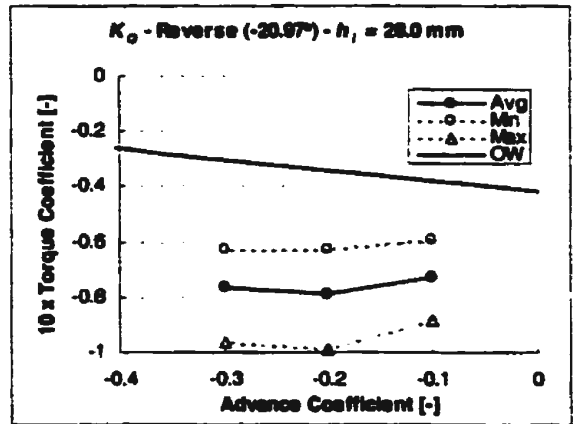
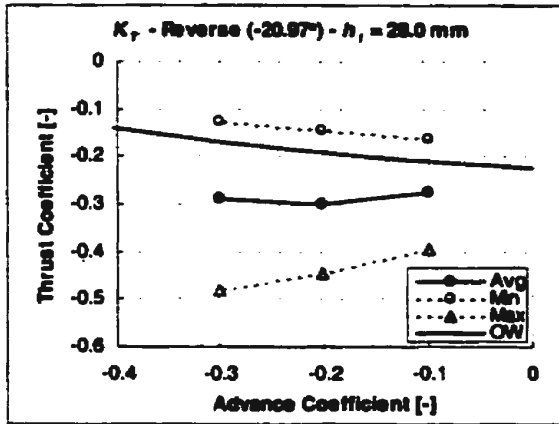


Figure IV-20 a)  $K_T$ :  $\Phi = -20.97^\circ - h_i = 28.0$  mm

b)  $K_Q$ :  $\Phi = -20.97^\circ - h_i = 28.0$  mm

**Appendix V - Blade Thrust and Torque Coefficients versus  
Advance Coefficient Charts**

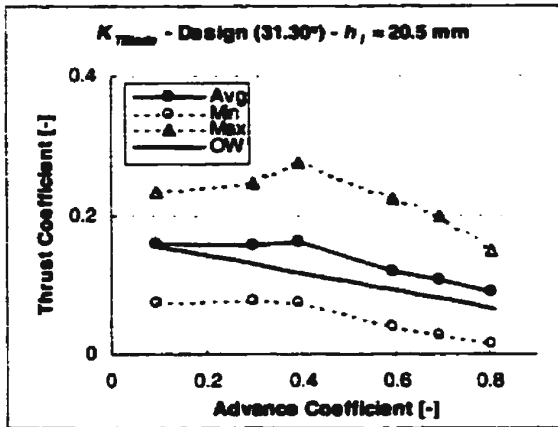
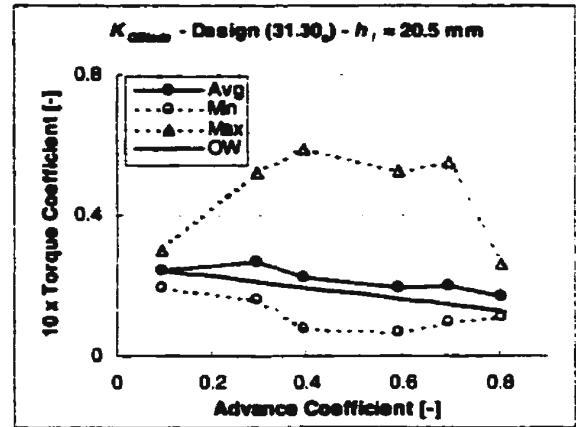


Figure V-1 a)  $K_{TBlade}$ :  $\Phi = 31.30^\circ - h_i = 20.5$  mm



b)  $K_{QBlade}$ :  $\Phi = 31.30^\circ - h_i = 20.5$  mm

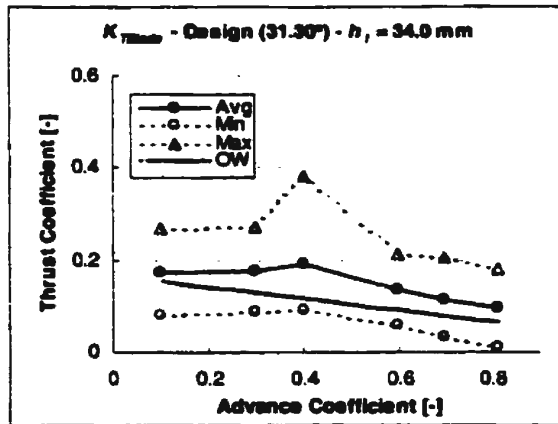
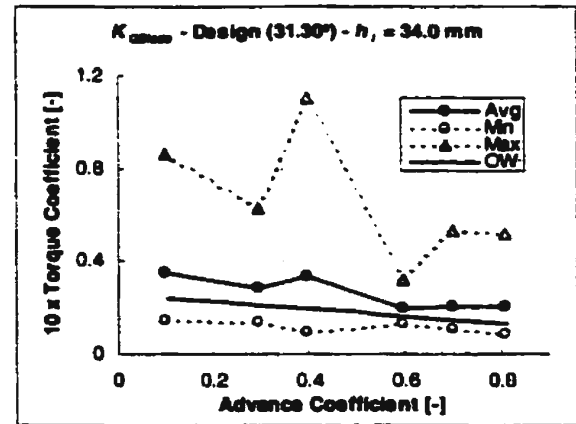


Figure V-2 a)  $K_{TBlade}$ :  $\Phi = 31.30^\circ - h_i = 34.0$  mm



b)  $K_{QBlade}$ :  $\Phi = 31.30^\circ - h_i = 34.0$  mm

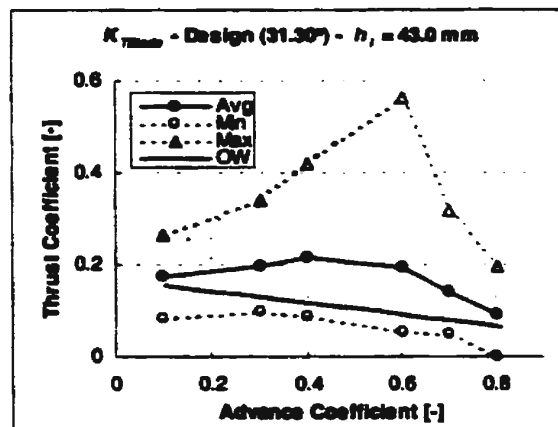
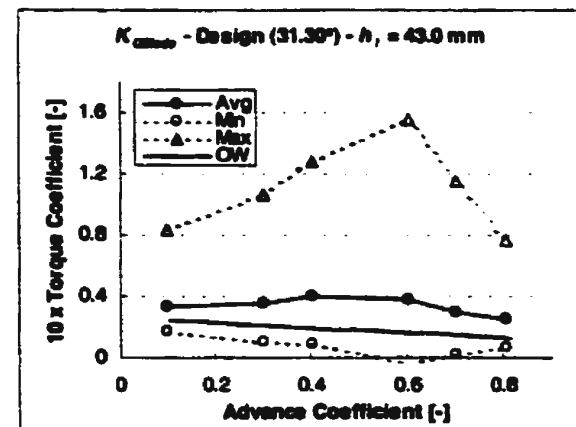


Figure V-3 a)  $K_{TBlade}$ :  $\Phi = 31.30^\circ - h_i = 43.0$  mm



b)  $K_{QBlade}$ :  $\Phi = 31.30^\circ - h_i = 43.0$  mm

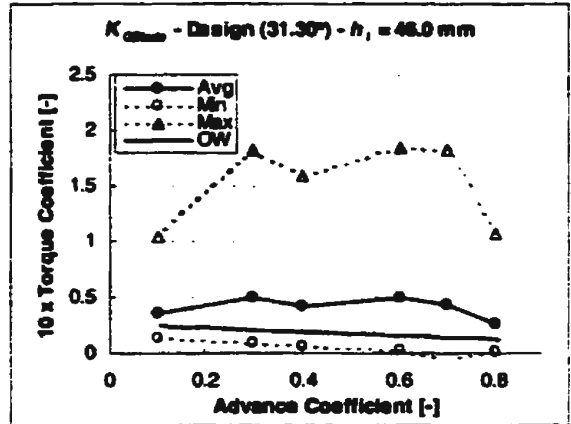
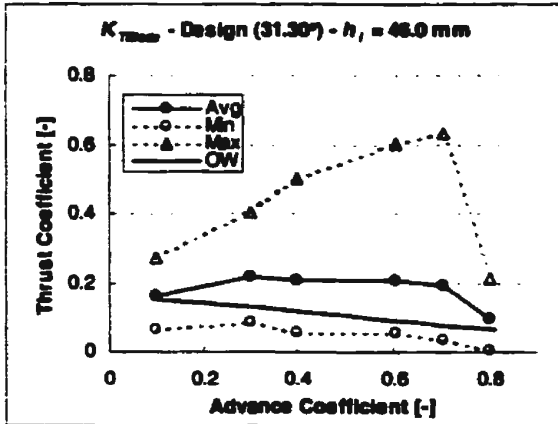


Figure V-4 a)  $K_{TBlade}$ :  $\Phi = 31.30^\circ - h_i = 46.0$  mm b)  $K_{QBlade}$ :  $\Phi = 31.30^\circ - h_i = 46.0$  mm

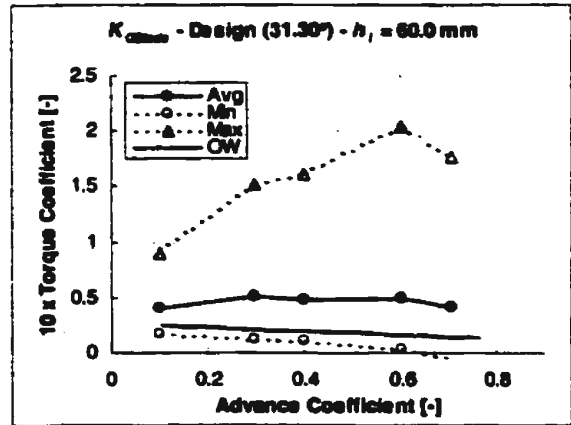
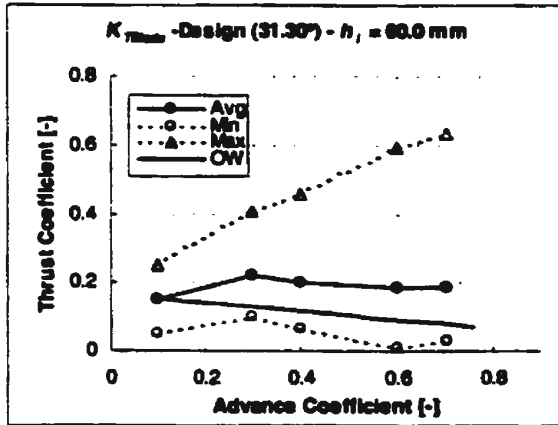


Figure V-5 a)  $K_{TBlade}$ :  $\Phi = 31.30^\circ - h_i = 60.0$  mm b)  $K_{QBlade}$ :  $\Phi = 31.30^\circ - h_i = 60.0$  mm

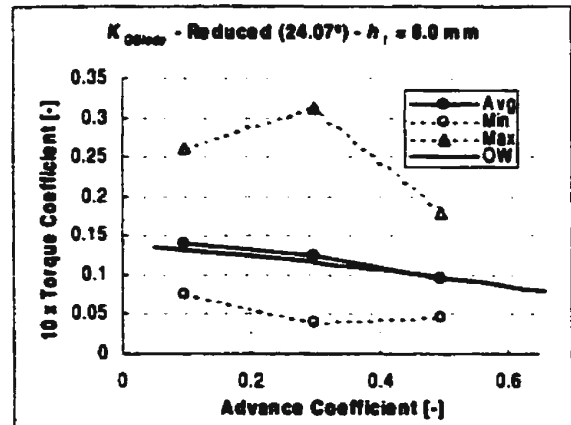
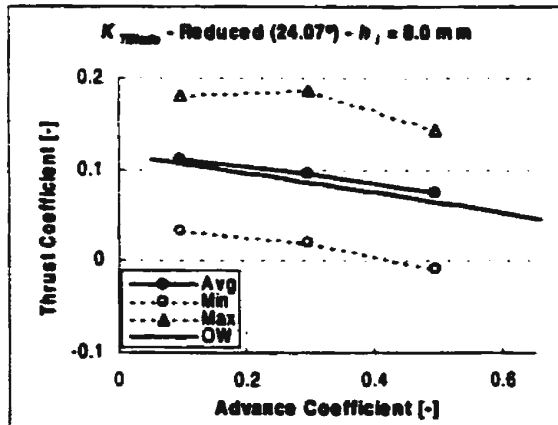


Figure V-6 a)  $K_{TBlade}$ :  $\Phi = 24.07^\circ - h_i = 8.0$  mm

b)  $K_{QBlade}$ :  $\Phi = 24.07^\circ - h_i = 8.0$  mm

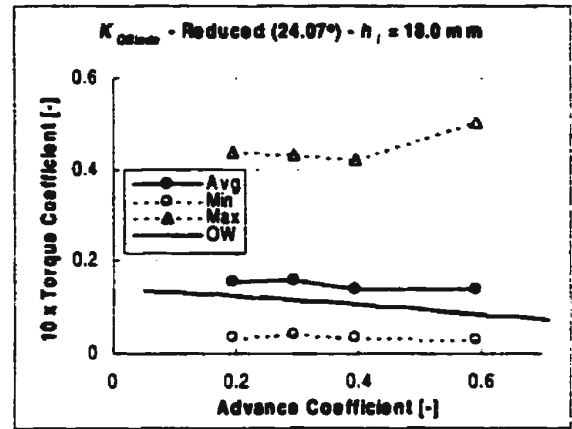
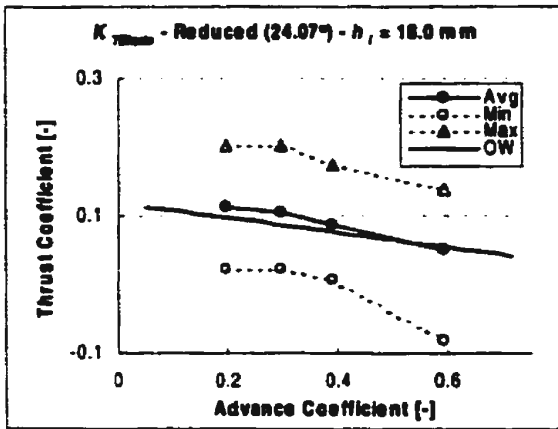


Figure V-7 a)  $K_{TBlade}$ :  $\Phi = 24.07^\circ - h_i = 18.0$  mm

b)  $K_{QBlade}$ :  $\Phi = 24.07^\circ - h_i = 18.0$  mm

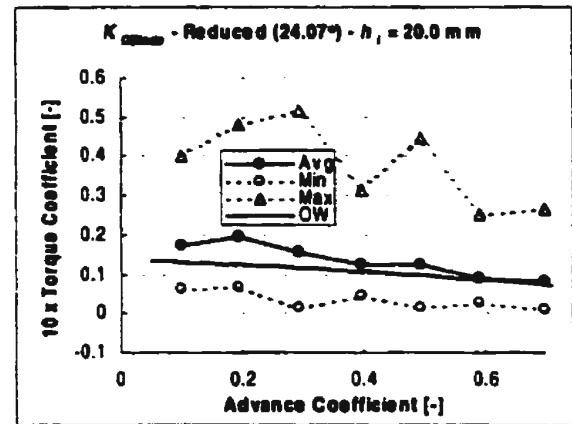
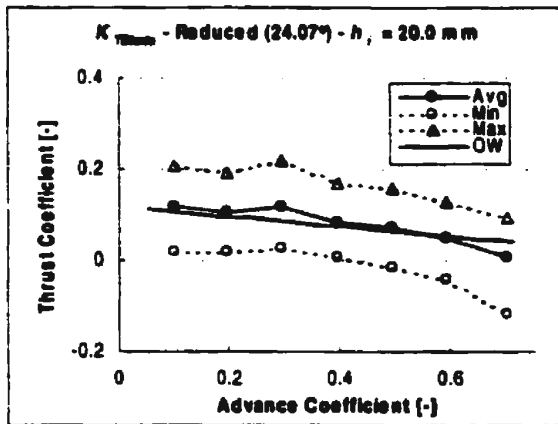


Figure V-8 a)  $K_{TBlade}$ :  $\Phi = 24.07^\circ - h_i = 20.0$  mm

b)  $K_{QBlade}$ :  $\Phi = 24.07^\circ - h_i = 20.0$  mm

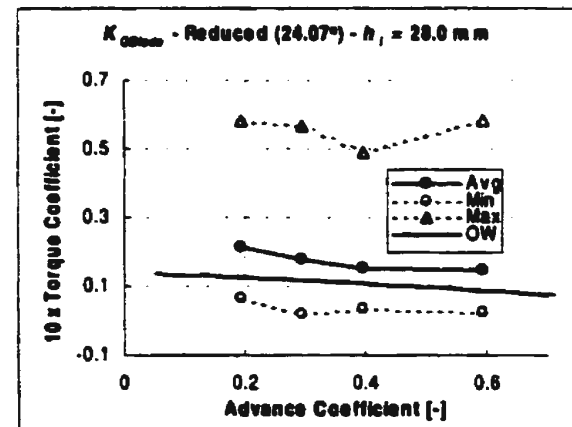
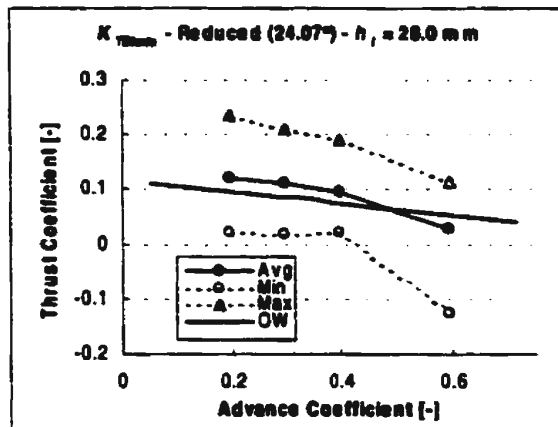


Figure V-9 a)  $K_{TBlade}$ :  $\Phi = 24.07^\circ - h_i = 28.0$  mm

b)  $K_{QBlade}$ :  $\Phi = 24.07^\circ - h_i = 28.0$  mm

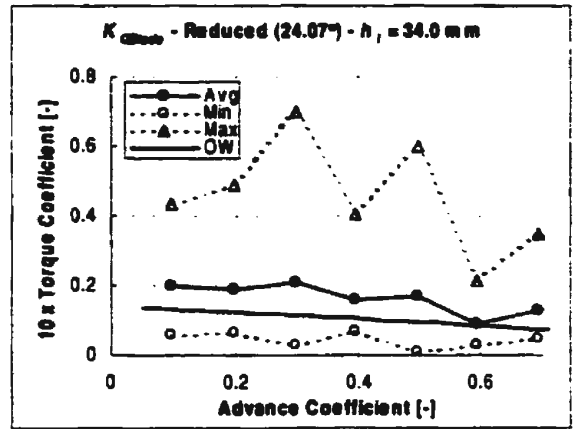
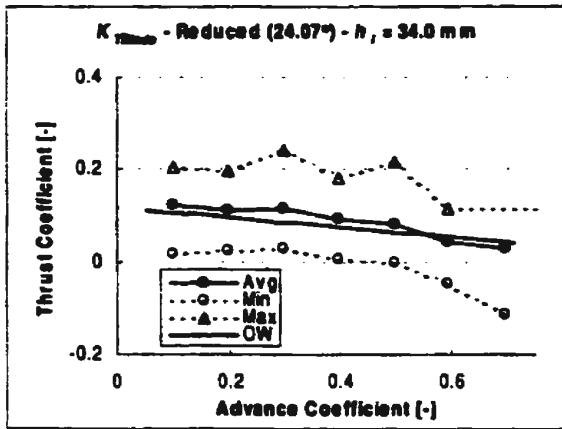


Figure V-10 a)  $K_{T_{Blade}}$ :  $\Phi = 24.07^\circ$  -  $h_i = 34.0$  mm

b)  $K_{Q_{Blade}}$ :  $\Phi = 24.07^\circ$  -  $h_i = 34.0$  mm

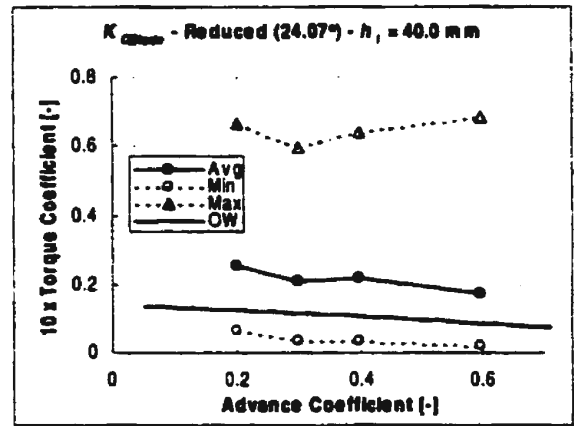
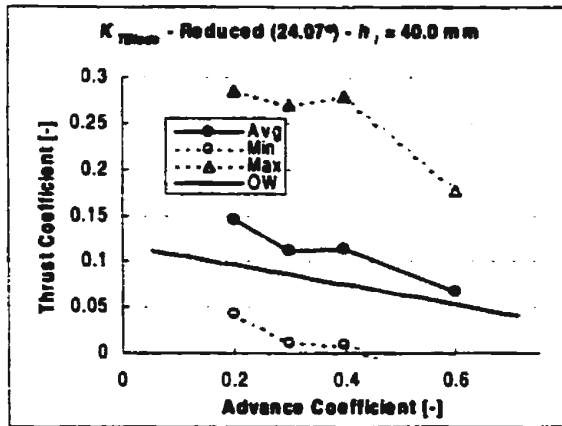


Figure V-11 a)  $K_{T_{Blade}}$ :  $\Phi = 24.07^\circ$  -  $h_i = 40.0$  mm

b)  $K_{Q_{Blade}}$ :  $\Phi = 24.07^\circ$  -  $h_i = 40.0$  mm

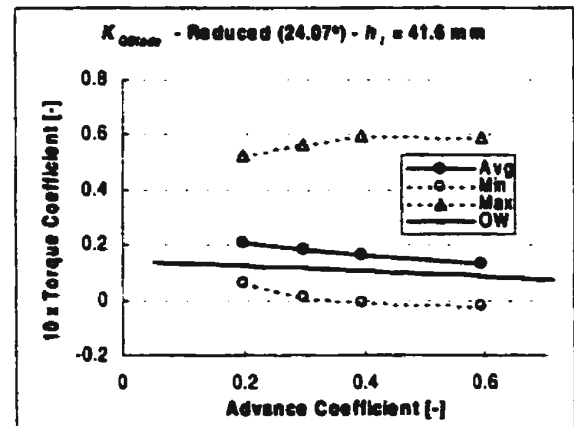
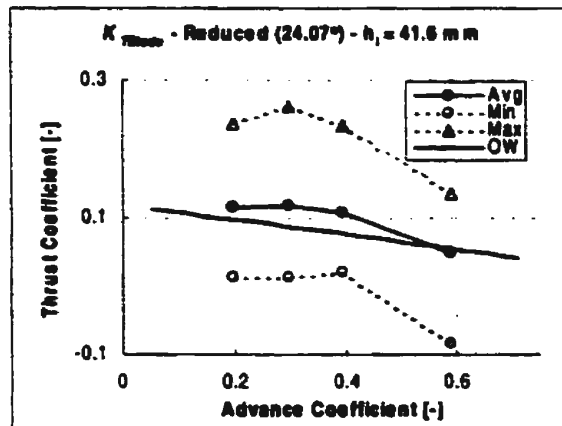


Figure V-12 a)  $K_{T_{Blade}}$ :  $\Phi = 24.07^\circ$  -  $h_i = 41.6$  mm

b)  $K_{Q_{Blade}}$ :  $\Phi = 24.07^\circ$  -  $h_i = 41.6$  mm

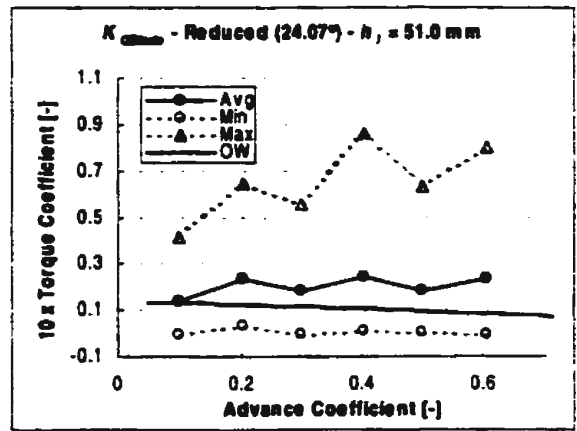
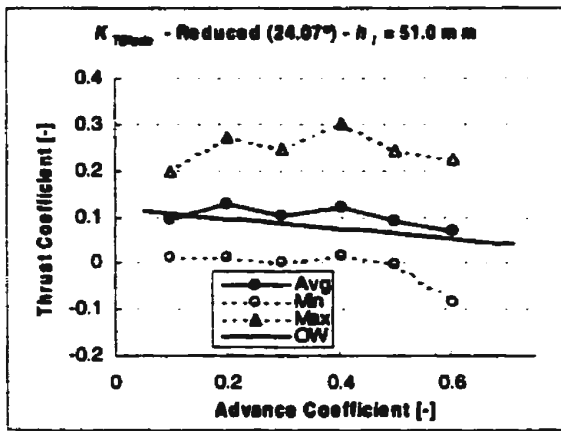


Figure V-13 a)  $K_{TBlade}$ :  $\Phi = 24.07^\circ - h_i = 51.0$  mm

b)  $K_{QBlade}$ :  $\Phi = 24.07^\circ - h_i = 51.0$  mm

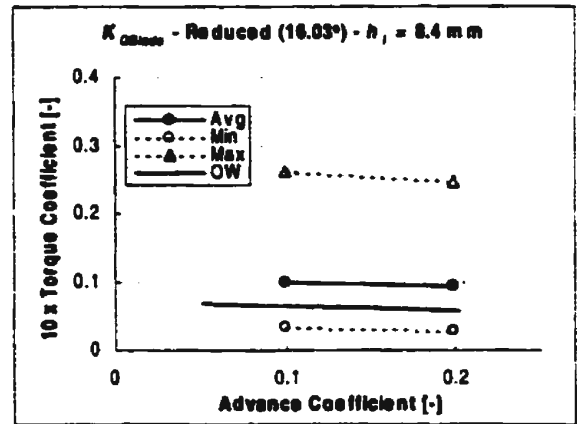
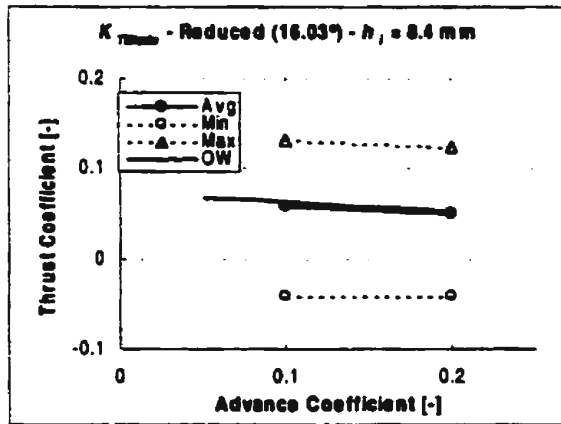


Figure V-14 a)  $K_{TBlade}$ :  $\Phi = 16.03^\circ - h_i = 8.4$  mm

b)  $K_{QBlade}$ :  $\Phi = 16.03^\circ - h_i = 8.4$  mm

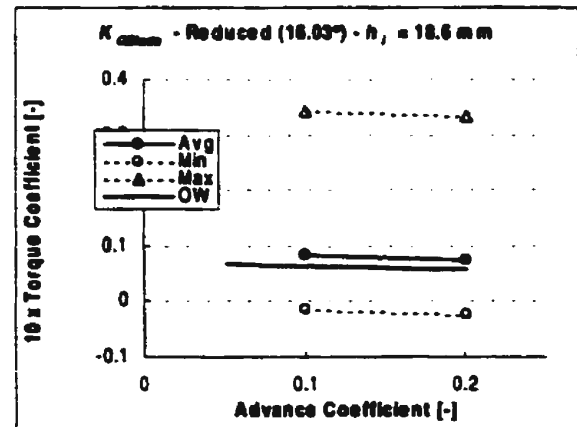
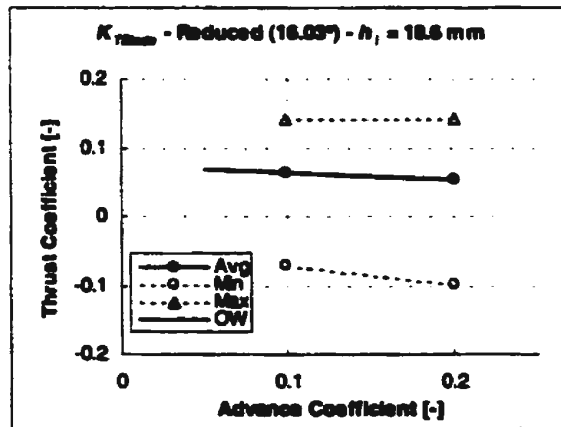


Figure V-15 a)  $K_{TBlade}$ :  $\Phi = 16.03^\circ - h_i = 18.6$  mm

b)  $K_{QBlade}$ :  $\Phi = 16.03^\circ - h_i = 18.6$  mm

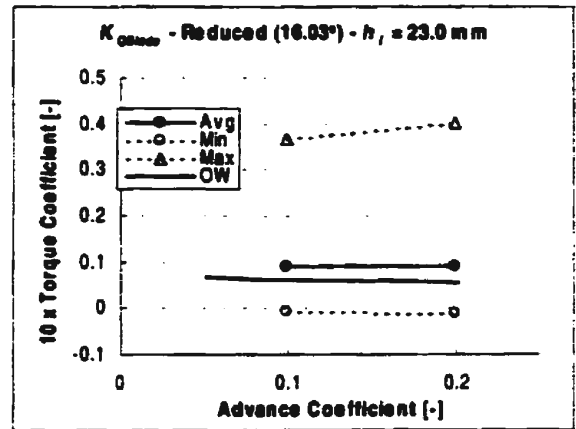
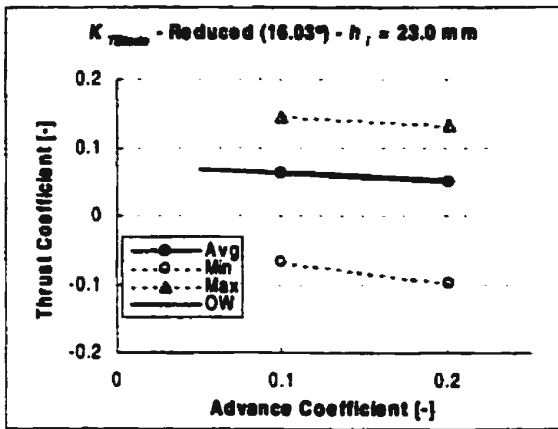


Figure V-16 a)  $K_{T\text{Blade}}$ :  $\Phi = 16.03^\circ - h_i = 23.0 \text{ mm}$

b)  $K_{Q\text{Blade}}$ :  $\Phi = 16.03^\circ - h_i = 23.0 \text{ mm}$

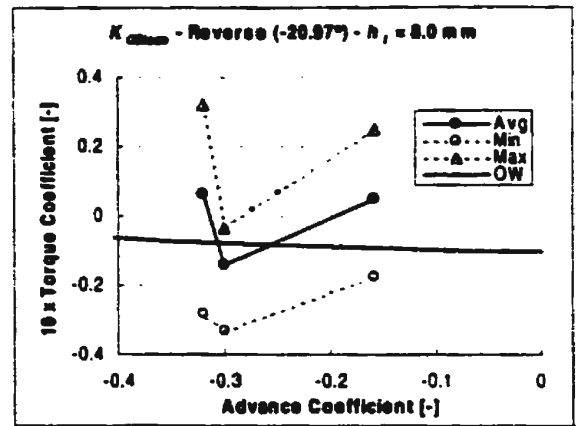
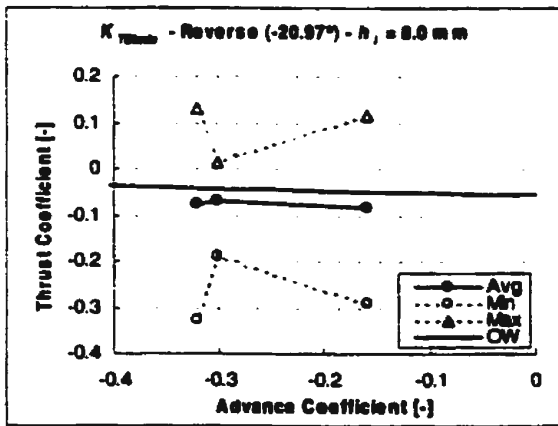


Figure V-17 a)  $K_{T\text{Blade}}$ :  $\Phi = -20.97^\circ - h_i = 8.0 \text{ mm}$

b)  $K_{Q\text{Blade}}$ :  $\Phi = -20.97^\circ - h_i = 8.0 \text{ mm}$

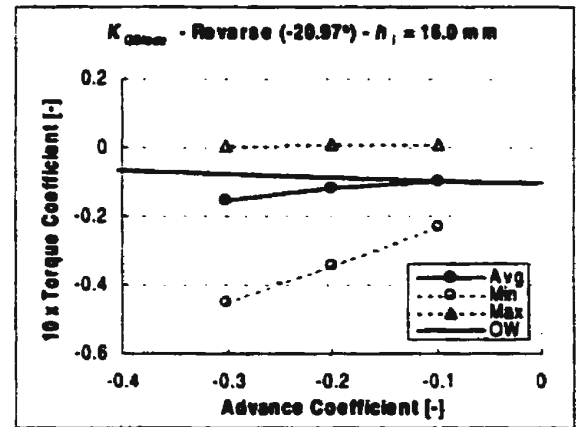
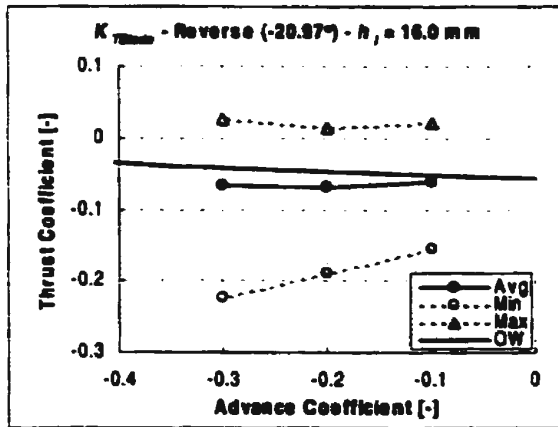


Figure V-18 a)  $K_{T\text{Blade}}$ :  $\Phi = -20.97^\circ - h_i = 16.0 \text{ mm}$

b)  $K_{Q\text{Blade}}$ :  $\Phi = -20.97^\circ - h_i = 16.0 \text{ mm}$

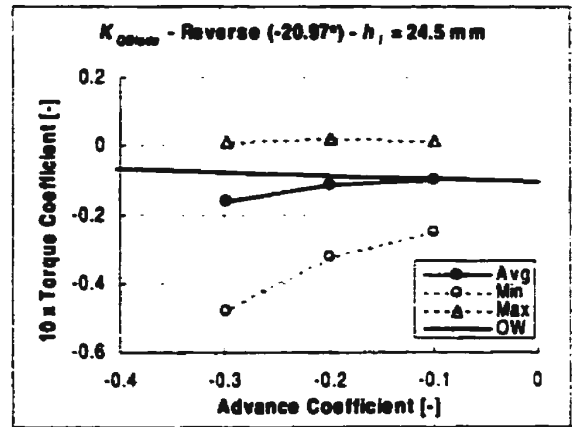
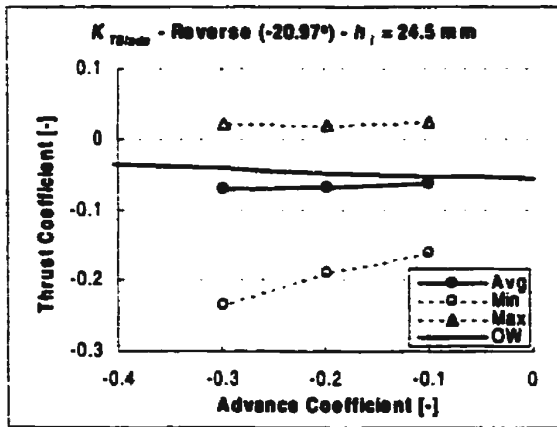


Figure V-19 a)  $K_{TB\text{Blade}}$ :  $\Phi = -20.97^\circ$  -  $h_i = 24.5$  mm      b)  $K_{QB\text{Blade}}$ :  $\Phi = -20.97^\circ$  -  $h_i = 24.5$  mm

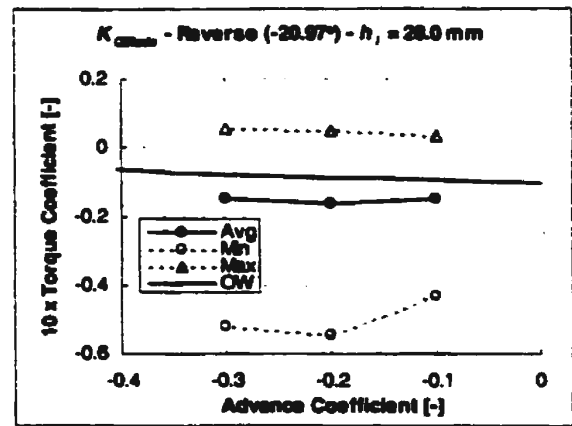
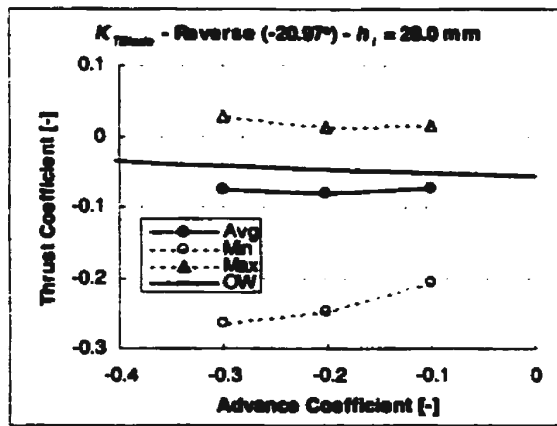


Figure V-20 a)  $K_{TB\text{Blade}}$ :  $\Phi = -20.97^\circ$  -  $h_i = 28.0$  mm      b)  $K_{QB\text{Blade}}$ :  $\Phi = -20.97^\circ$  -  $h_i = 28.0$  mm

## **Appendix VI - Blade Bending Moments versus Advance Coefficient Charts**

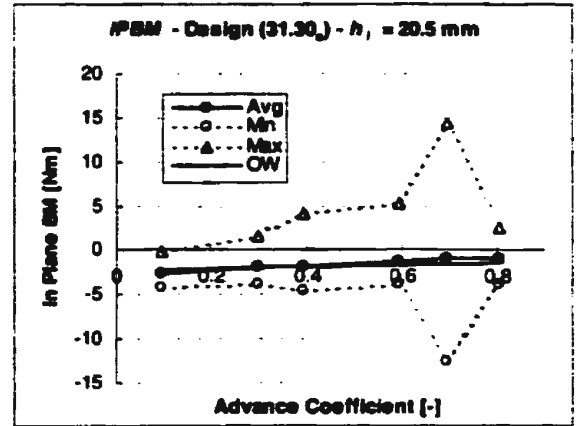
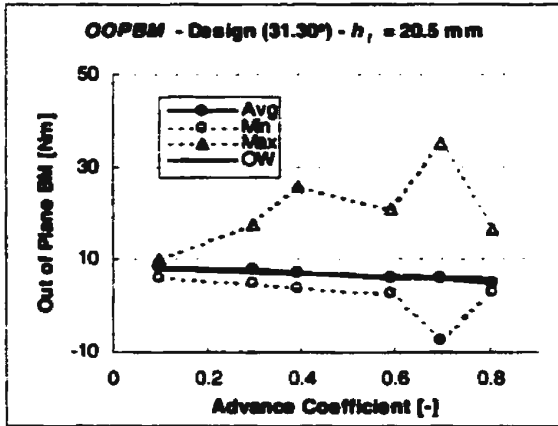


Figure VI-1 a) *OOPBM*:  $\Phi = 31.30^\circ - h_i = 20.5 \text{ mm}$  b) *IPBM*:  $\Phi = 31.30^\circ - h_i = 20.5 \text{ mm}$

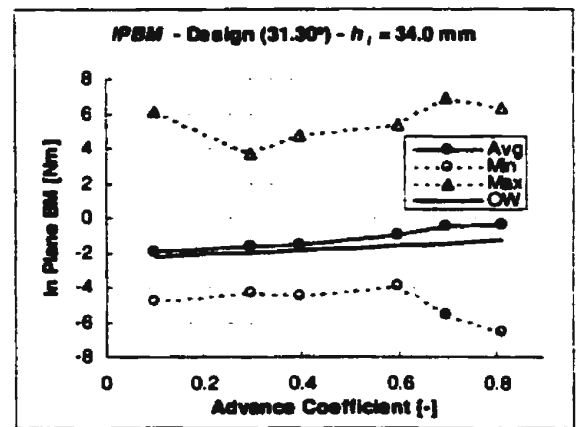
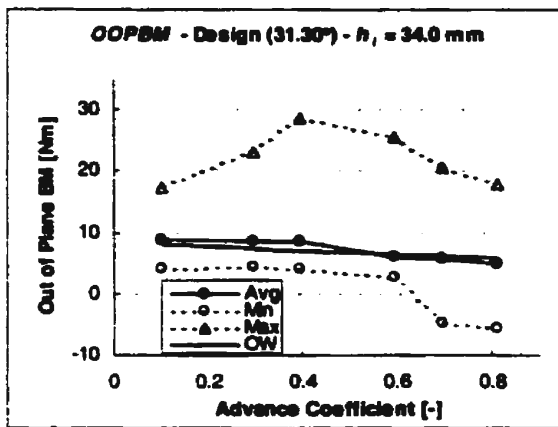


Figure VI-2 a) *OOPBM*:  $\Phi = 31.30^\circ - h_i = 34.0 \text{ mm}$  b) *IPBM*:  $\Phi = 31.30^\circ - h_i = 34.0 \text{ mm}$

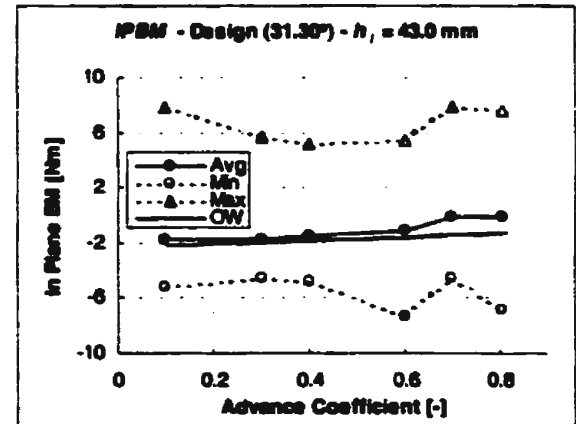
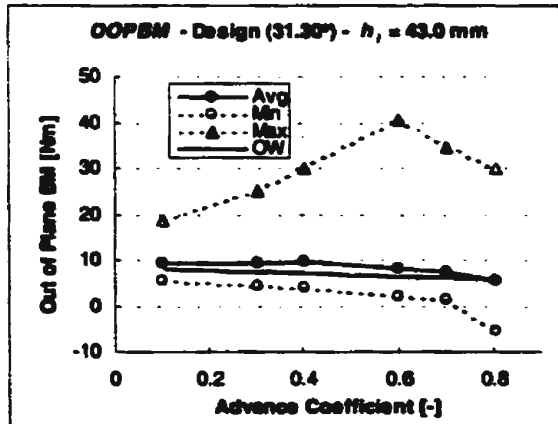


Figure VI-3 a) *OOPBM*:  $\Phi = 31.30^\circ - h_i = 43.0 \text{ mm}$  b) *IPBM*:  $\Phi = 31.30^\circ - h_i = 43.0 \text{ mm}$

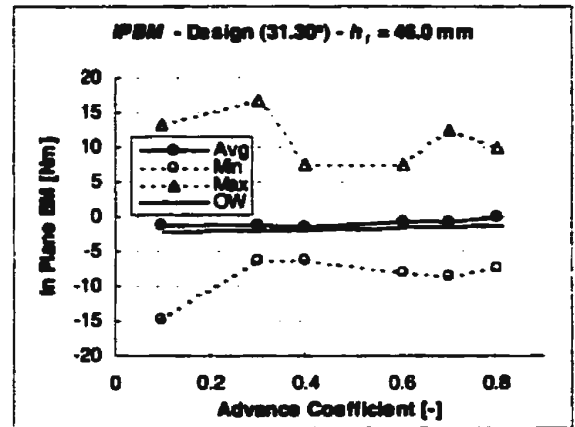
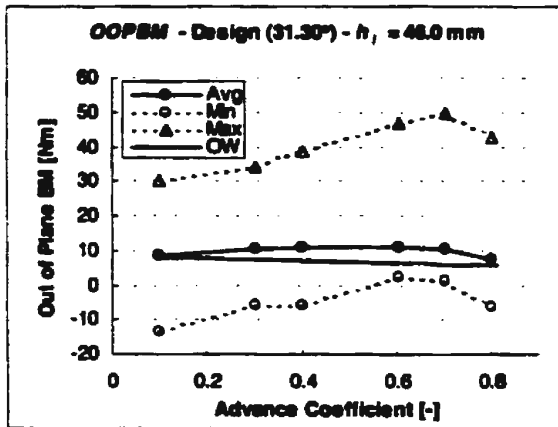


Figure VI-4 a) *OOPBM*:  $\Phi = 31.30^\circ - h_i = 46.0$  mm b) *IPBM*:  $\Phi = 31.30^\circ - h_i = 46.0$  mm

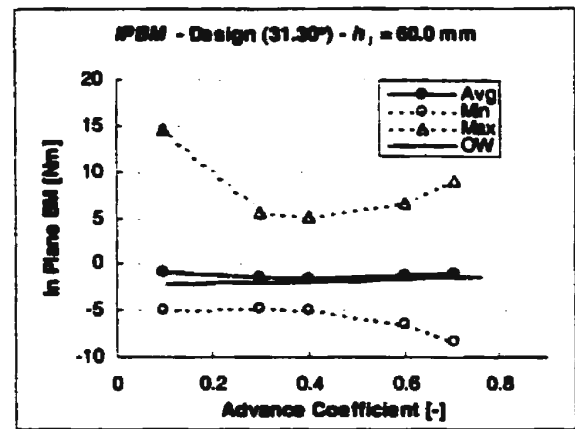
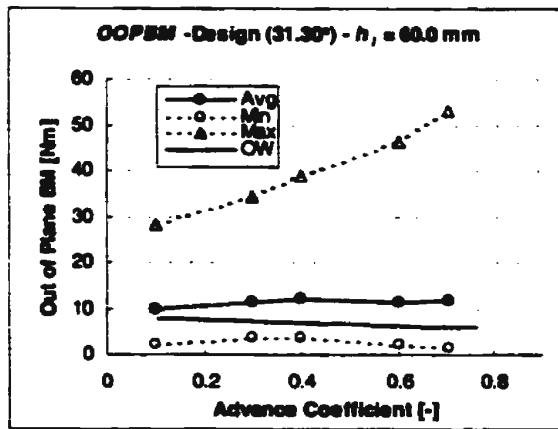


Figure VI-5 a) *OOPBM*:  $\Phi = 31.30^\circ - h_i = 60.0$  mm b) *IPBM*:  $\Phi = 31.30^\circ - h_i = 60.0$  mm

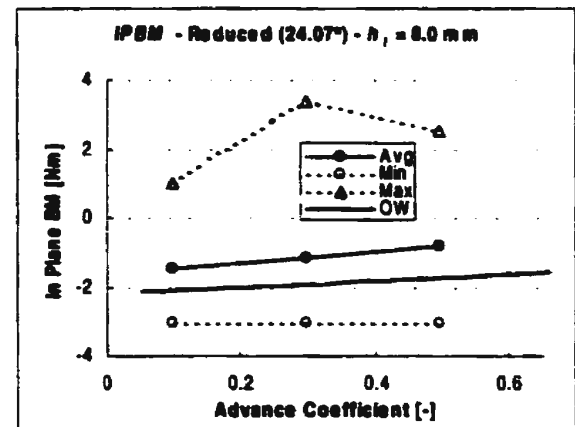
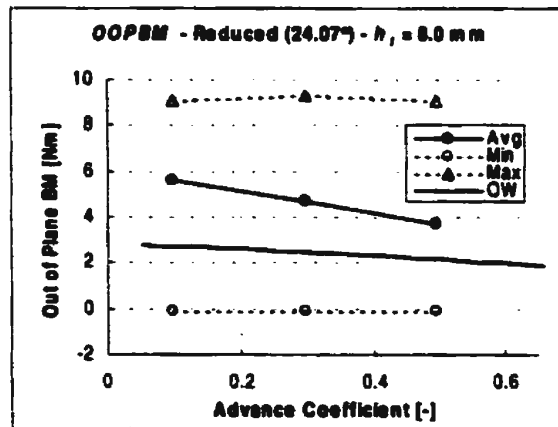


Figure VI-6 a) *OOPBM*:  $\Phi = 24.07^\circ - h_i = 8.0$  mm b) *IPBM*:  $\Phi = 24.07^\circ - h_i = 8.0$  mm

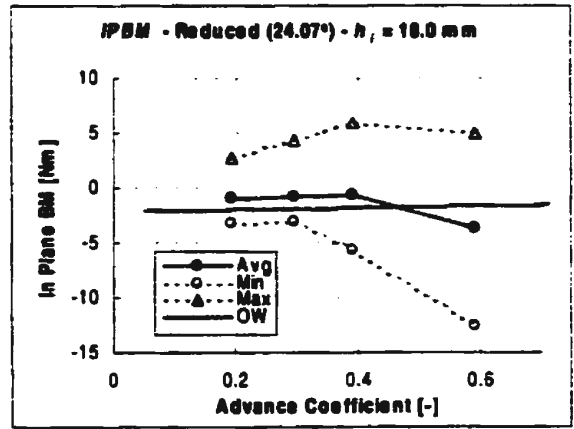
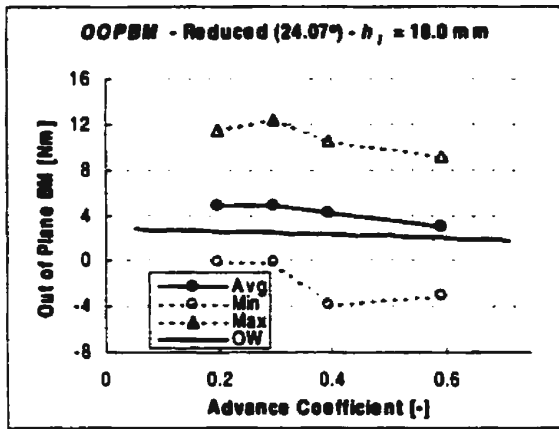


Figure VI-7 a) *OOPBM*:  $\Phi = 24.07^\circ - h_i = 18.0$  mm b) *IPBM*:  $\Phi = 24.07^\circ - h_i = 18.0$  mm

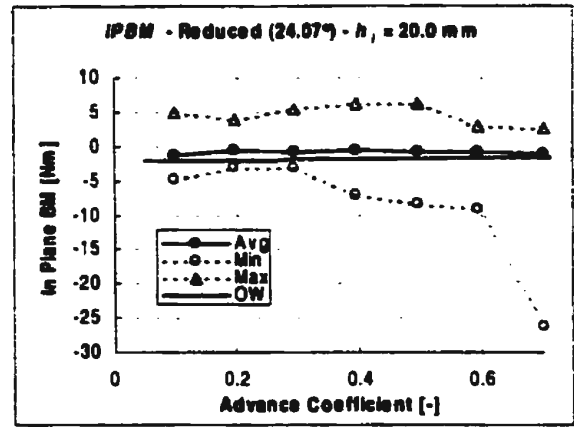
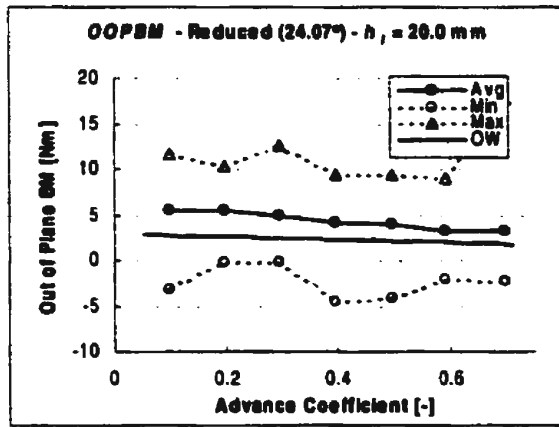


Figure VI-8 a) *OOPBM*:  $\Phi = 24.07^\circ - h_i = 20.0$  mm b) *IPBM*:  $\Phi = 24.07^\circ - h_i = 20.0$  mm

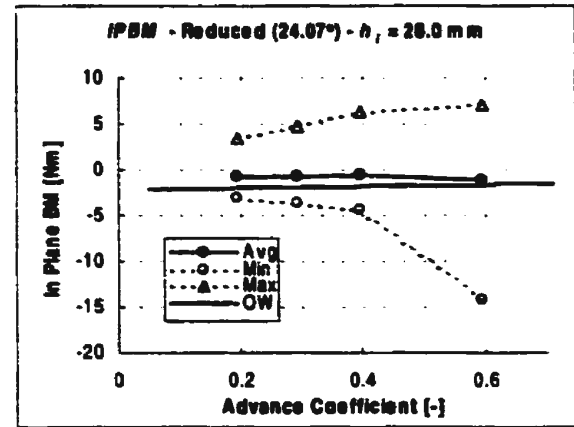
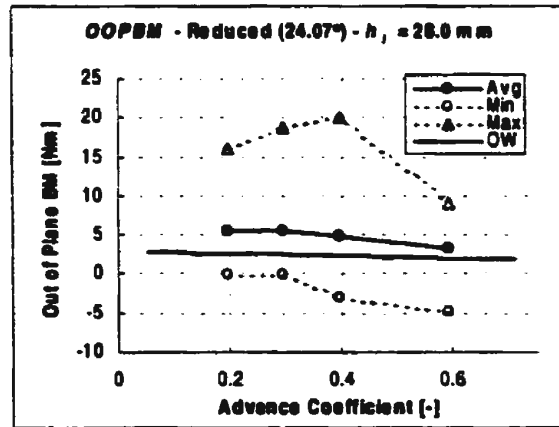


Figure VI-9 a) *OOPBM*:  $\Phi = 24.07^\circ - h_i = 28.0$  mm b) *IPBM*:  $\Phi = 24.07^\circ - h_i = 28.0$  mm

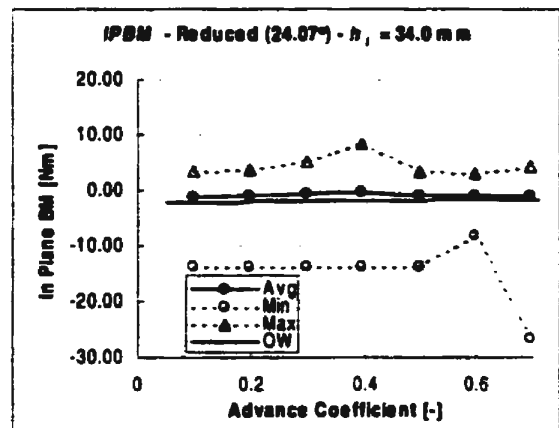
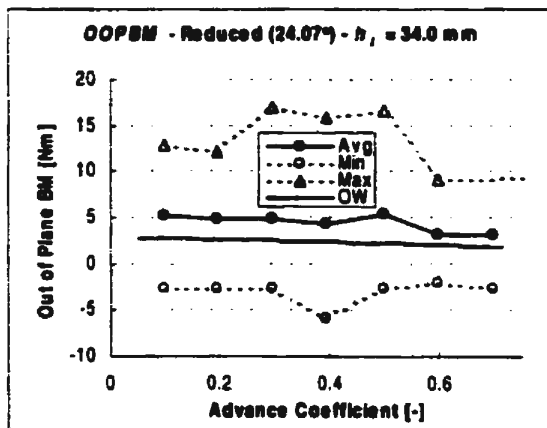


Figure VI-10 a) OOPBM:  $\Phi = 24.07^\circ - h_i = 34.0$  mm b) IPBM:  $\Phi = 24.07^\circ - h_i = 34.0$  mm

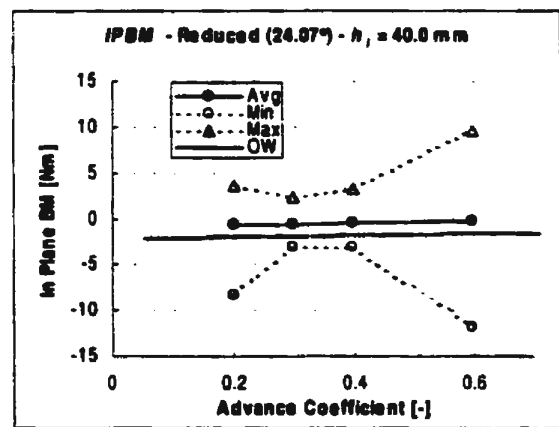
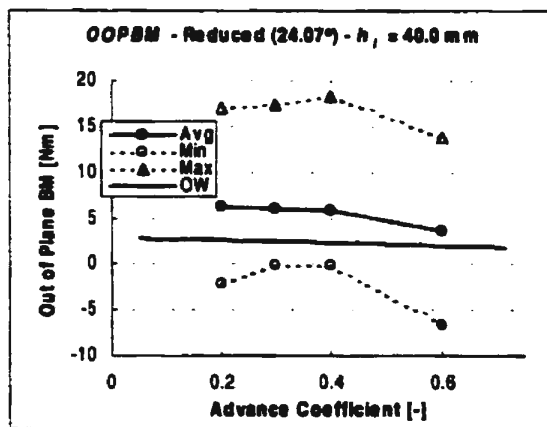


Figure V-11 a) OOPBM:  $\Phi = 24.07^\circ - h_i = 40.0$  mm b) IPBM:  $\Phi = 24.07^\circ - h_i = 40.0$  mm

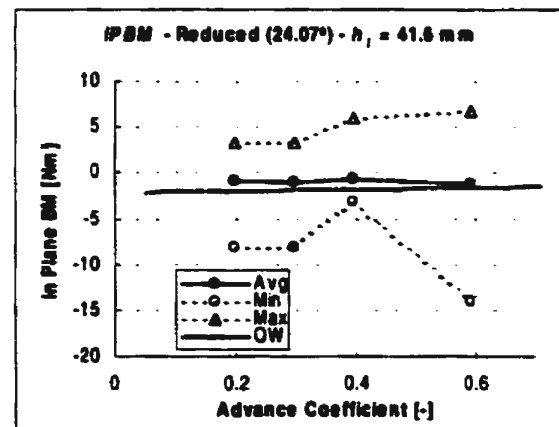
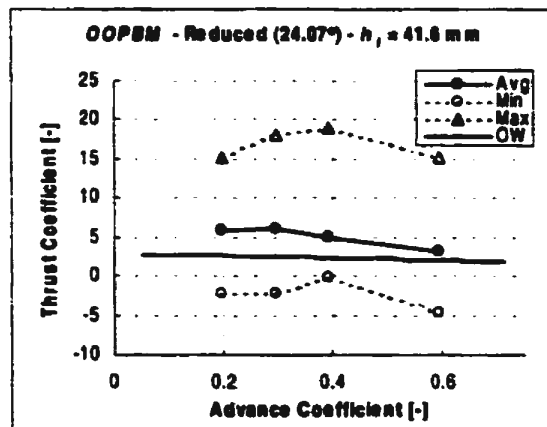


Figure VI-12 a) OOPBM:  $\Phi = 24.07^\circ - h_i = 41.6$  mm b) IPBM:  $\Phi = 24.07^\circ - h_i = 41.6$  mm

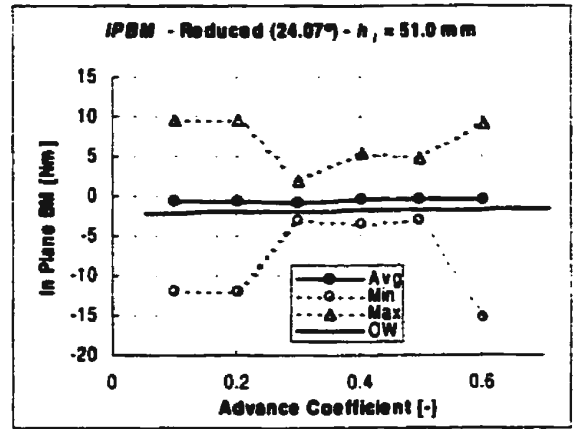
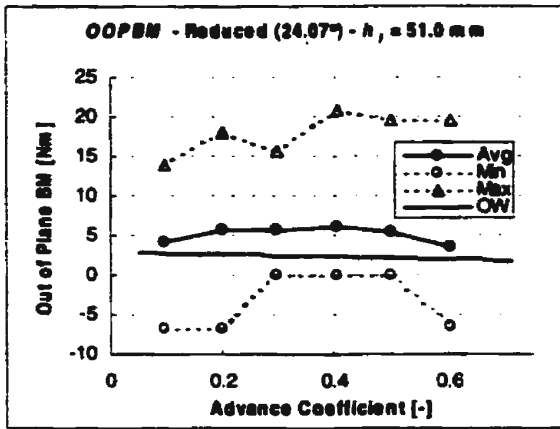


Figure VI-13 a) *OOPBM*:  $\Phi = 24.07^\circ$  -  $h_i = 51.0$  mm b) *IPBM*:  $\Phi = 24.07^\circ$  -  $h_i = 51.0$  mm

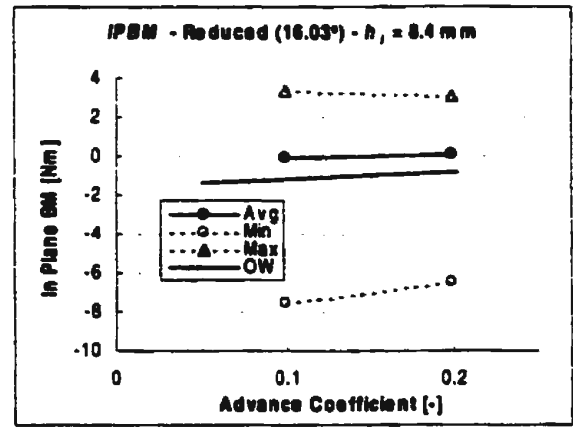
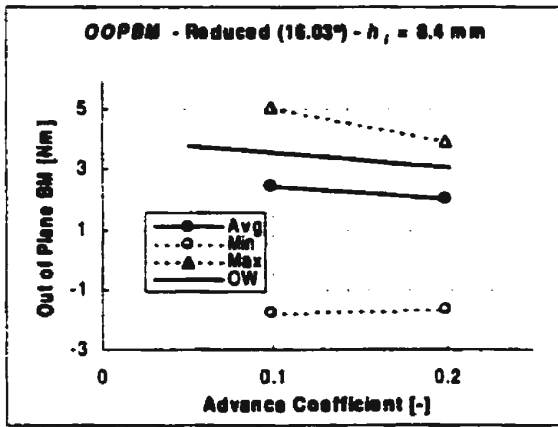


Figure VI-14 a) *OOPBM*:  $\Phi = 16.03^\circ$  -  $h_i = 8.4$  mm b) *IPBM*:  $\Phi = 16.03^\circ$  -  $h_i = 8.4$  mm

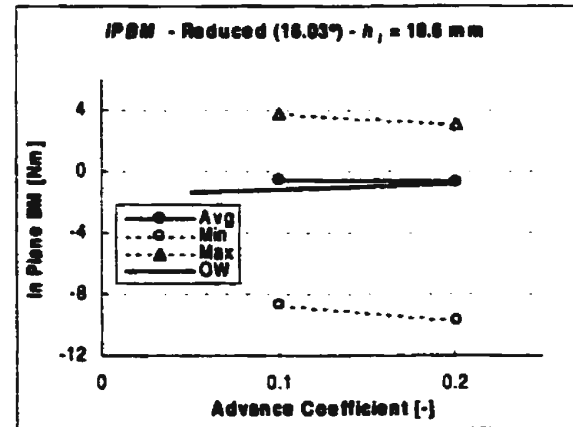
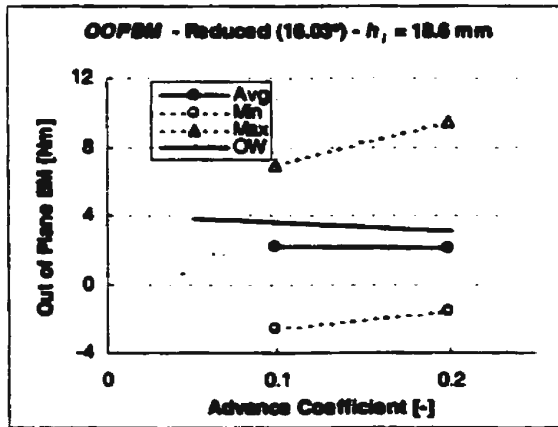


Figure VI-15 a) *OOPBM*:  $\Phi = 16.03^\circ$  -  $h_i = 18.6$  mm b) *IPBM*:  $\Phi = 16.03^\circ$  -  $h_i = 18.6$  mm

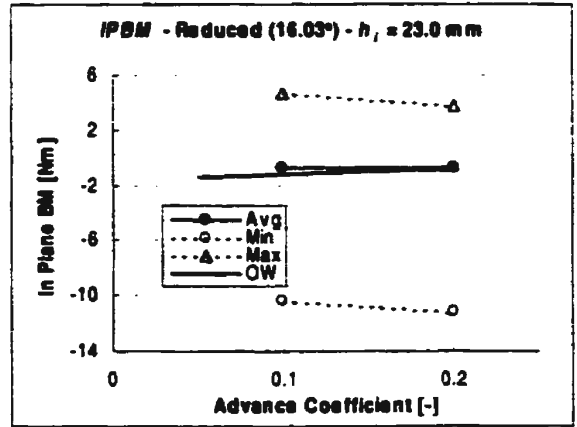
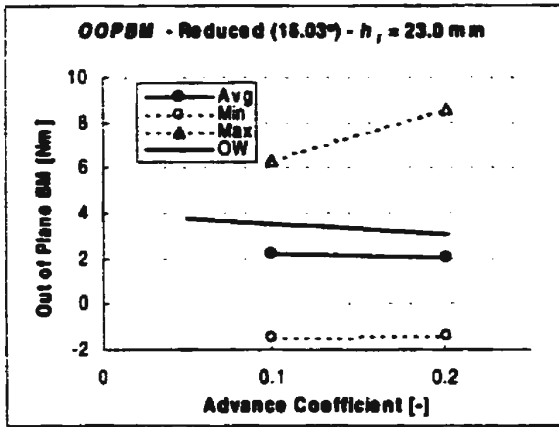


Figure VI-16 a) OOPBM:  $\Phi = 16.03^\circ - h_i = 23.0$  mm b) IPBM:  $\Phi = 16.03^\circ - h_i = 23.0$  mm

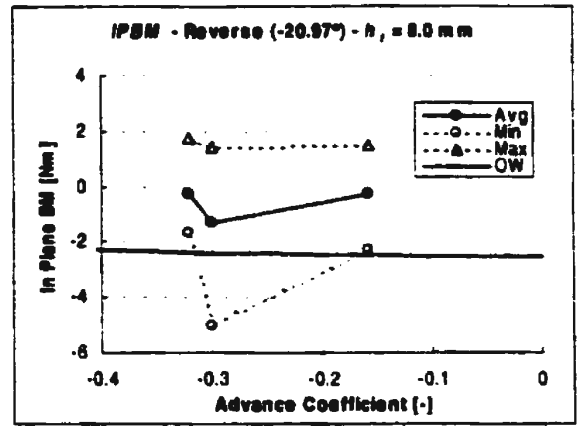
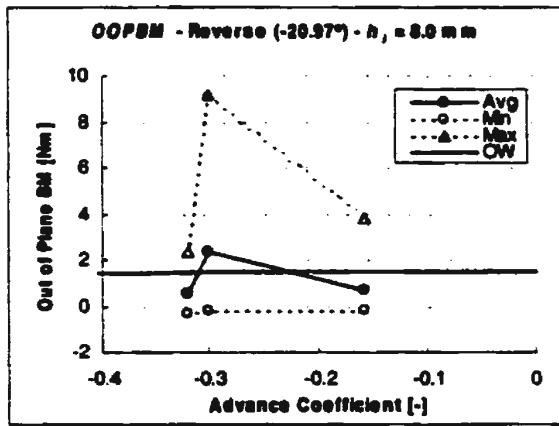


Figure VI-17 a) OOPBM:  $\Phi = -20.97^\circ - h_i = 8.0$  mm b) IPBM:  $\Phi = -20.97^\circ - h_i = 8.0$  mm

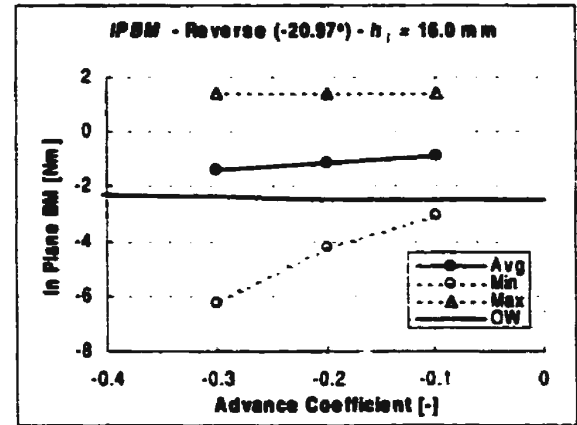
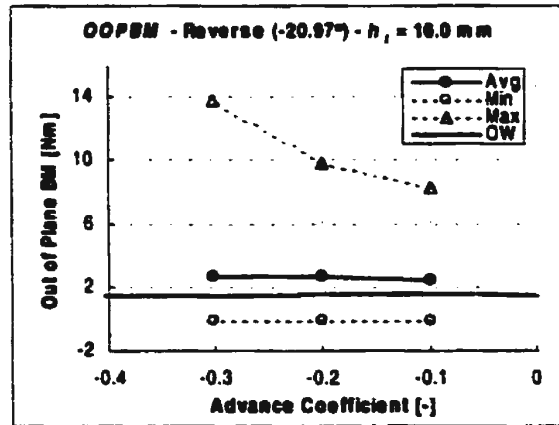


Figure VI-18 a) OOPBM:  $\Phi = -20.97^\circ - h_i = 16.0$  mm b) IPBM:  $\Phi = -20.97^\circ - h_i = 16.0$  mm

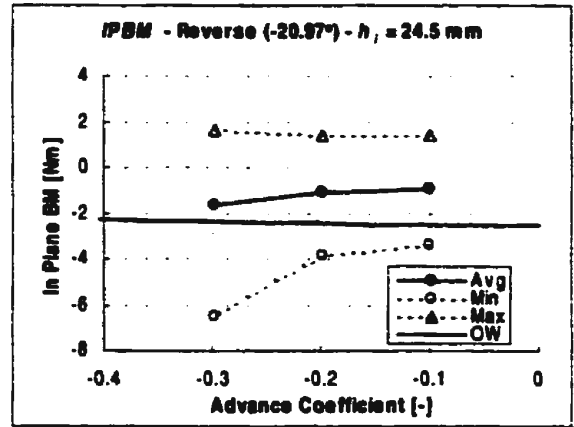
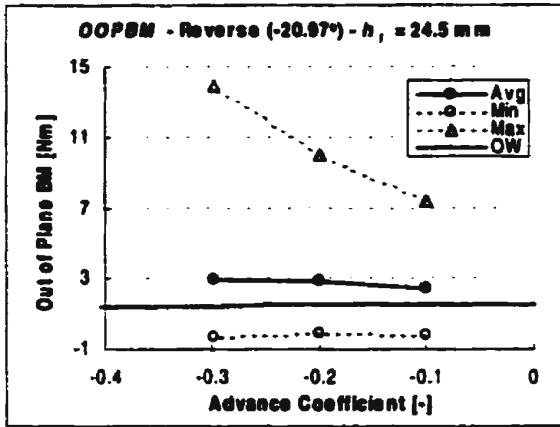


Figure VI-19 a) OOPBM:  $\phi = -20.97^\circ - h_i = 24.5$  mm b) IPBM:  $\phi = -20.97^\circ - h_i = 24.5$  mm

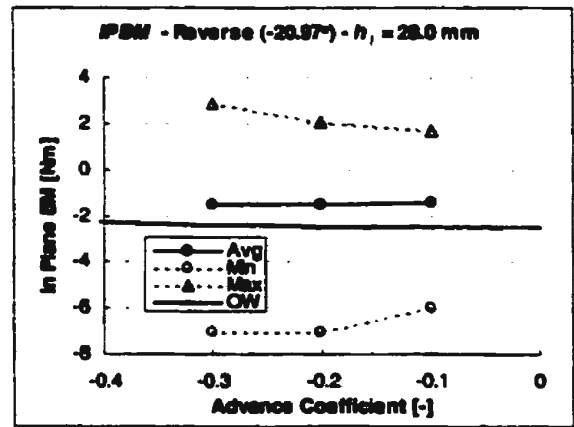
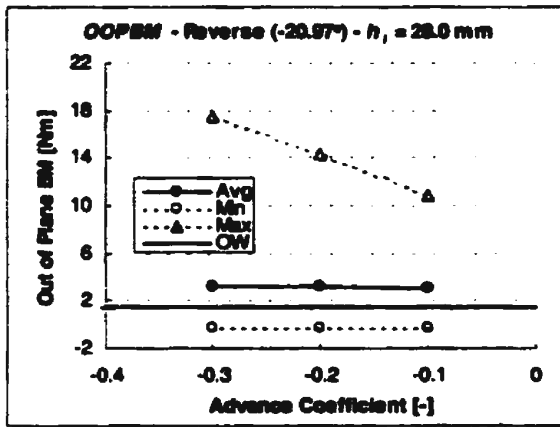


Figure VI-20 a) OOPBM:  $\phi = -20.97^\circ - h_i = 28.0$  mm b) IPBM:  $\phi = -20.97^\circ - h_i = 28.0$  mm







